Structure-Function Studies on *Vibrio cholerae* Cytolysin: a β-barrel Pore-Forming Toxin

A thesis

submitted by

Karan Paul

in partial fulfilment of

the requirements for the degree of

Doctor of Philosophy

Indian Institute of Science Education and Research (IISER)

Mohali

August, 2014

Declaration

The work presented in this thesis has been carried out by me under the guidance of Dr. Kausik Chattopadhyay at Indian Institute of Science Education and Research Mohali. This work has not been submitted in part or in full for a degree, diploma or a fellowship to any other University or Institute. Whenever contributions of others are involved, every effort has been made to indicate this clearly, with due acknowledgement of collaborative research and discussions. This thesis is a bonafide record of original work done by me and all sources listed within have been detailed in the bibliography.

Karan Paul
Place:
Date:

In my capacity as the supervisor of the candidate's PhD thesis work, I certify that the above statements by the candidate are true to the best of my knowledge.

Dr. Kausik Chattopadhyay
Assistant Professor,
Department of Biological Sciences,
Indian Institute of Science Education and Research Mohali.
Place:
Date:

Acknowledgement

I would like to thank my supervisor Dr. Kausik Chattopadhyay for his unwavering and creative guidance. His academic excellence and outstanding personality were the beacons during this journey.

My sincere gratitude to visionary Director Prof. N. Sathyamurthy for inspiration. I am thankful to Prof. Purnananda Guptasarma, Head, Department of Biological Sciences, for support and encouragement. I am grateful to my doctoral committee members, Dr. Arunika Mukhopadhaya and Prof. Purnananda Guptasarma for insightful suggestions and motivation. I thank my group members; Anand Kumar Rai and Kusum Lata for collaboration, Barkha Khilwani, Dr. Nidhi and Nidhi Kundu for encouragement and discussions in the group meetings. Also, I thank my friends Junaid Khan, Sanica, Shelly Gupta, Krishna, Aakansha, Sukhdeep Kumar, Ashutosh and Vinit Meshram for their help and support during these years.

I am grateful to IISER Mohali for providing advanced infrastructure and excellent research environment. I also thank IISER Mohali for financial support and hostel facility. I would like to acknowledge the Library facility of IISER Mohali and Dr. P Visakhi, Deputy Librarian, for providing subscription to various journals.

I also thank the Deans, faculty members, non-teaching staff, research scholars and BS-MS students of IISER Mohali for making the campus an excellent place to pursue research. My deepest gratitude to my parents and family members for their love and kindness.

Karan Paul

List of publications

1. **Paul, K.** and Chattopadhyay, K. (2011) Unfolding distinguishes the *Vibrio cholerae* cytolysin precursor from the mature form of the toxin. Biochemistry, 50 (19), 3936-3945.

2. **Paul, K.** and Chattopadhyay, K. (2012) Single point mutation in *Vibrio cholerae* cytolysin compromises membrane pore-formation mechanism of the toxin. FEBS Journal, 279 (21), 4039-4051.

3. Rai, A. K.*, **Paul, K.***, and Chattopadhyay, K. (2013) Functional mapping of the lectin activity site on the β-Prism domain of *Vibrio cholerae* cytolysin: implications for the membrane pore-formation mechanism of the toxin. J. Biol. Chem, 288 (3), 1665-1673. (*These authors contributed equally to this work)

4. **Paul, K.** and Chattopadhyay, K. (2014) Pre-pore oligomer formation by *Vibrio cholerae* cytolysin: Insights from a truncated variant lacking the pore-forming pre-stem loop. Biochem. Biophys. Res. Com., 443 (1), 189-193.

5. Lata, K, **Paul, K.**, and Chattopadhyay, K. (2014) Functional characterization of *Helicobacter pylori* TlyA: Pore-forming hemolytic activity and cytotoxic property of the protein. Biochem. Biophys. Res. Com., 444 (2), 153-157.

Contents

List of figures

List of Tables

Chapter 1: Introduction

1.1 Pore-forming toxins

Pathogenic bacteria have evolved a variety of ways to invade the host cellular systems and to disable the cells of the host immune system, in order to create a safe environment for their multiplication and dissemination. Pathogenic bacteria employ a battery of virulence factors and toxins to exert their pathogenesis mechanisms. Toxins produced by the pathogenic bacteria, in general, act distant from the site of infection (1). Bacterial toxin molecules are physically organized into distinct domains that recognize receptors on the host cell surface and activate a cascade of cellular pathways, thus leading to killing of the host cells (2). Bacterial toxins are most often protein molecules. A major class of toxins produced by the pathogenic bacteria are membrane-damaging toxins. Membrane-damaging toxins act by (i) ezymzymatically degrading the components of host cell membranes or cytoplasm, (ii) solubilising the cell membranes by detergent like actions, (iii) acting as pore-forming toxins (PFTs) (3). PFTs constitute 30% of all the toxins produced by the bacterial pathogens. PFTs act by forming pores in the host target cell membranes leading to colloid-osmotic lysis of the target cells (4-5) (Figure 1.1).

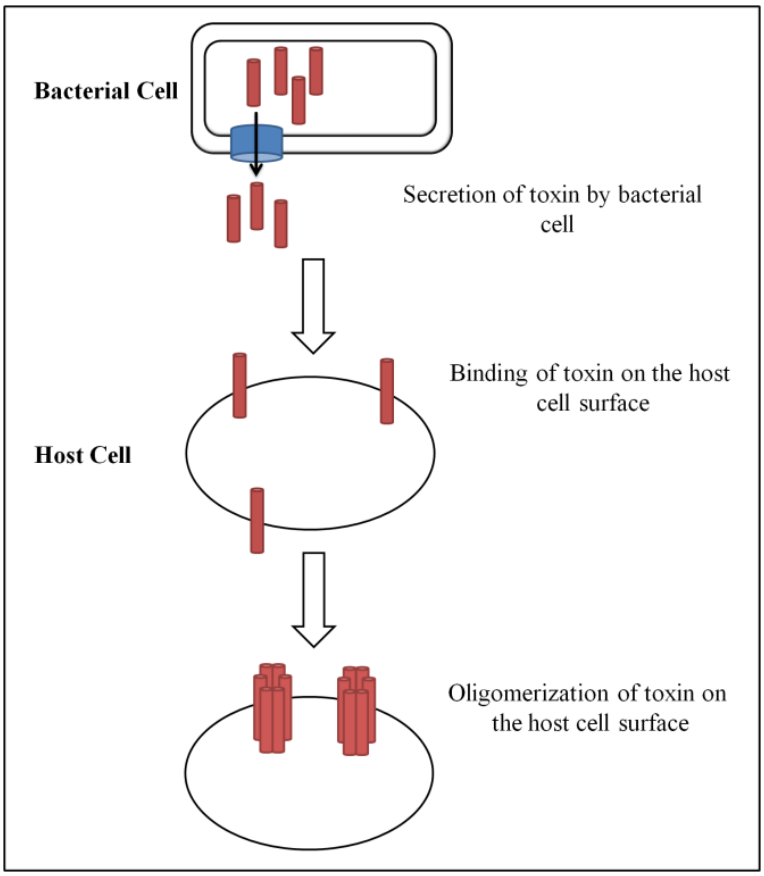

Figure 1.1: The general mechanism of the membrane pore-formation by PFTs.

1.2 Classification of the Pore-forming toxins

Pore-forming toxins (PFTs) can be classified based on their pore size formed on the target membranes. However, the widely accepted classification is based on the type of the secondary structures that the toxins employ to cross the host cell membranes. Based on this, PFTs are categorised as either α-helical or β-barrel PFTs (4).

α-PFTs form pores in the host cell membranes by using α-helices. (4). Based on the overall structural features, these toxin molecules consist mainly of α-helices. Pore-forming domains generally consist of a three-layer structure of up to ten α-helices entrapping a hydrophobic helical hairpin. This hairpin drives the initial steps of the membrane insertion process, and leads to the formation of the transmembrane pores (3, 6). Some examples of the members in this class are the pore-forming colicins produced by *Escherichia coli* (7), *Pseudomonas aeruginosa* exotoxin A (8), the insecticidal *Bacillus thuringiensis* δ-endotoxins (Cry) (9), Cytolysin A produced by pathogenic *E. coli* (10-11) and Diphtheria toxin produced by *Corynebacterium diphtheria* (12-13).

β-PFTs insert β-barrels into the target cell membranes to form a functional oligomeric pore structure. Each monomer contributes a β-hairpin structure toward pore formation. As observed in their structures, all β-PFTs consist mainly of β-structures (4, 14). The class includes *Aeromonas hydrophila* aerolysin (15-16), *Clostridium septicum* α-toxin (17-18), *Staphylococcus aureus* α-hemolysin (19), *Pseudomonas aeruginosa* cytotoxin (20), the protective antigen component of anthrax toxin produced by *Bacillus anthracis* (21), *Vibrio cholerae* cytolysin (22), and the members in the family of cholesterol-dependent cytolysins (23-24).

The oligomers formed by β-PFTs are highly stable, and remain intact even after solubilisation of the membranes with detergents. In contrast, oligomers of α-PFTs are far less stable and fall apart when the membranes are exposed to the detergents (4).

1.3 α-Pore-forming toxins

1.3.1 Colicins

Colicins belong to the α-PFT family of PFTs. These are secreted by *E. coli* and kill other related bacteria (7). The *E. coli* secreting these toxins also secretes an immunity protein that protects it against the actions of the colicins (7, 25-26). Once the toxin is secreted, it binds to the host cells via specific receptors on the bacterial outer membranes, and gets localized into the periplasmic space (27-29). In the periplasmic space, some colicins, like Colicin A form pores in the inner bacterial membranes, while other colicins are further

internalized into the cytoplasm where they perform various functions such as by acting as DNAse, RNAse, or by inhibiting the protein synthesis process (7, 25). Based on the structure (Figure 1.2), colicin molecules can be divided into three distinct domains (30): (i) the translocation domain, consisting of three α-helices, one of which extends into the receptor-binding domain, (ii) the receptor-binding domain, composed of three α-helices and a short β-hairpin, (iii) the pore-forming domain consisting of a bundle of 10 α-helices and a hydrophobic core composed an α-helical hairpin. The α-helical hairpin is exposed during pore formation through partial unfolding of the pore-forming domain triggered by low-pH environment at the membrane interface (27, 31).

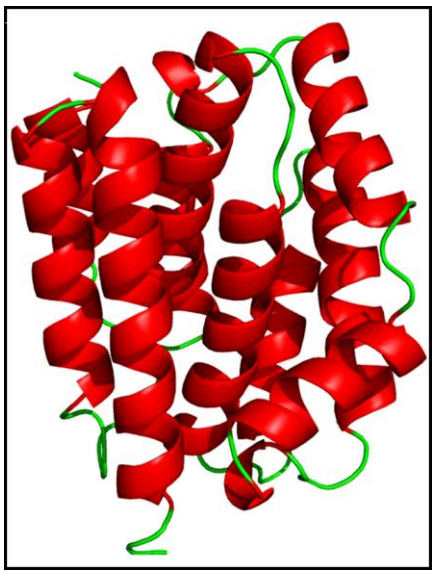

Figure 1.2: Crystal structure of α-PFT, Colicin A (PDB ID: 1CII)

1.4 β-Pore-forming toxins

β-barrel pore-forming toxins (β-PFTs) share a broadly similar mode of action (Figure 1.3). β-PFTs are secreted as water-soluble monomers; upon interaction with the host cell membranes, they convert into β-barrel transmembrane channels. The mode of action β-PFTs involves (i) secretion of the toxin as soluble monomers by the bacteria, (ii) binding of the toxin to specific cell-surface receptor, (iii) self-assembly of 6-7 monomers to form a non-functional pre-pore oligomer, (iv) conversion of the pre-pore oligomer into the functional transmembrane β-barrel pore (32). The following subsections will provide a brief overview of the representative β-PFTs.

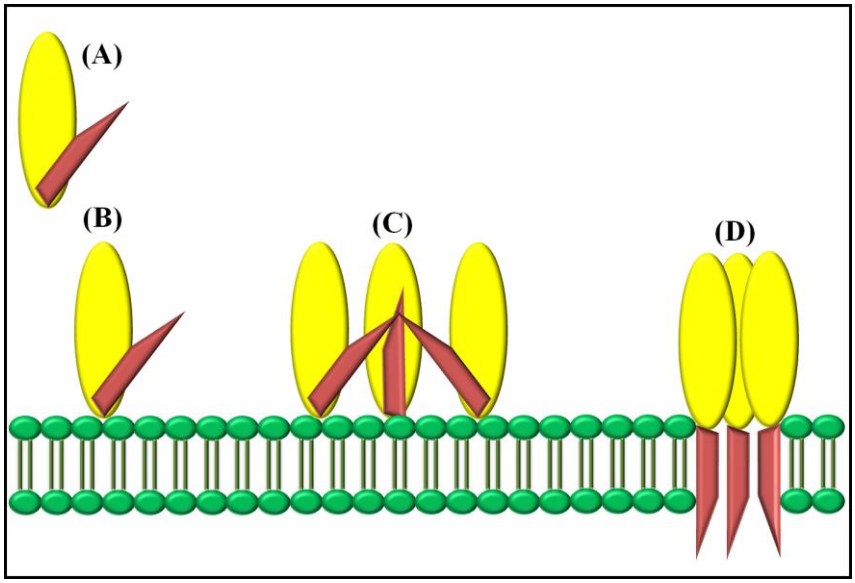

Figure 1.3: Sequential representation of β-PFT mode of action. (A) secretion of the toxin as soluble monomers by the bacteria, (B) binding of toxin to specific cell surface receptor, (C) self-assembly of 6-7 monomers to form a non-functional pre-pore oligomer, (D) conversion of pre-pore oligomer into functional transmembrane β-barrel.

1.4.1 Aerolysin

Aerolysin is seceted by the Gram-negative bacterium *Aeromonas hydrophilla* (33). It is secreted as a ~52 kDa inactive toxin known as Proaerolysin, through the type II secretion system. A signal peptide guides the translocation of proaerolysin across the inner membrane in an unfolded state. The molecule is subsequently folded and transported across the bacterial outer membrane into the extracellular space (3, 15). Upon secretion, proaerolysin is converted into active mature aerolysin after proteolytic removal of 41-43 amino acid residues from the C-terminal end (34). Eukaryotic proteases such as trypsin, α-chymotrypsin and cell-associated proteases such as furin and many proteases secreted by *A. hydrophilla* have been found to activate proaerolysin (35-36). Maturation of aerolysin is accompanied by conformational changes in the molecule, which result in the exposure of hydrophobic patches that might assist in protomer-protomer interactions and subsequent oligomerization (35).

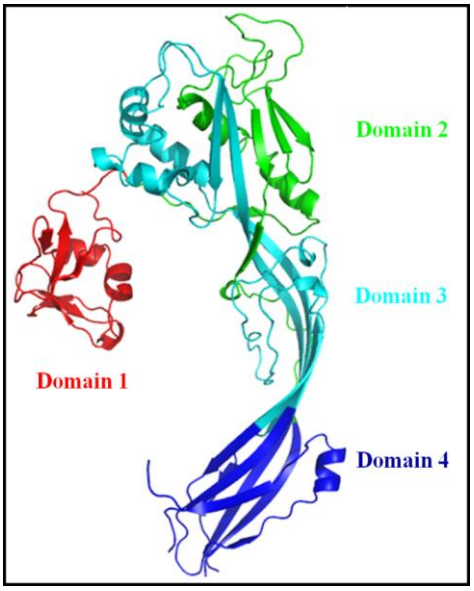

Figure 1.4: Structure of Proaerolysin (PDB ID: 1PRE)

Mature aerolysin monomers bind to specific receptors on the host cell surface, known as glycosyl-phophatidyl-inositol (GPI) anchored proteins (34). GPI-anchored proteins are mainly distributed in the lipid raft microdomains and perform diverse functions such as enzymes, adhesion molecules, antigens or receptors for various ligands. Aerolysin is known to mainly bind Thy-1 (37), contactin (38), CD14, arboxypeptidase M or NCAM (neural cell-adhesion molecule) (39) and surface glycoprotein of *Trypanosoma brucei* (34). Binding of aerolysin to the GPI-anchored proteins, which are mainly localized in the membrane microdomains or lipid rafts, helps in concentrating the toxin monomers, facilitating subsequent oligomerization (40).

The crystal structure for proaerolysin has been solved. Proaerolysin is an L-shaped molecule consisting of 4 domains (Figure 1.4) (41). Domain 1 and domain 2 of aerolysin are involved in the binding of aerolysin to specific receptor on the target cell membranes. Domain 2 and 3 are involved in the oligomer formation and stability. Domain 3 comprises of the characteristic channel forming transmembrane region. It consists of 20 amino acids forming two amphipathic β-sheets connected by a hydrophobic loop generating a β-hairpin-like structure. Domain 4 consists of the pro-peptide, which is proteolytically removed during the toxin activation. Toxin activation and receptor binding are the two events that trigger aerolysin oligomerization. This is followed by exposure of hydrophobic regions within domain 3, driving monomer-monomer interactions. Local conformational changes leading to unfolding drive β-hairpins from each monomer insert into the cell membrane leading to the

formation of a 14-stranded-β-barrel. The mushroom-shaped head is composed of domains 1 and 2, whereas the stem region is composed entirely of domains 3 and 4 (41).

Aerolysin forms heptameric transmembrane channels that are anion selective and lead to rapid loss of water and ions from the cell. This includes loss of K^+, influx of Ca^+ from endoplasmic reticulum and disruption of Na^+/K^+ gradient (42). This leads to activation of caspase-1, inflammasome and Nod-like receptors. Caspase-1 in turn activates cytokines IL18 and IL-1β, a characteristic of aerolysin-intoxicated cells (43). Pore formation by aerolysin also leads to the activation of Sterol Regulatory Element Binding Protein (SREBP) -1 and -2, responsible for membrane biogenesis and enhancement of cell survival (39).

1.4.2 Epsilon toxin

Epsilon toxin (ETX) belongs to the class of β-barrel PFTs. It is responsible for enterotoxemia, and accumulates in brain and kidneys. It is able to cross the blood-brain barrier. ETX is secreted by *Clostridium perfringens,* which is a spore-forming anaerobic, Gram-positive bacterium (44-46). ETX is secreted as an inactive pro-toxin of ~32.9kDa, which upon proteolytic removal of 11 N-terminal and 29 C-terminal residues converts into the active form of ~28.6 kDa. The removal of 29 amino acid residues from the C-terminal end results in the decrease in the pI value from 8.02 to 5.36 (47). Pro-toxin has been shown to bind to target eukaryotic cells but does not form oligomers. Therefore, the 29 C-terminal residues regulate the oligomerization of ETX on host cell membrane (48). ETX forms anion selective heptameric pores permeable to hydrophilic solutes of mass ~1 kDa (49).

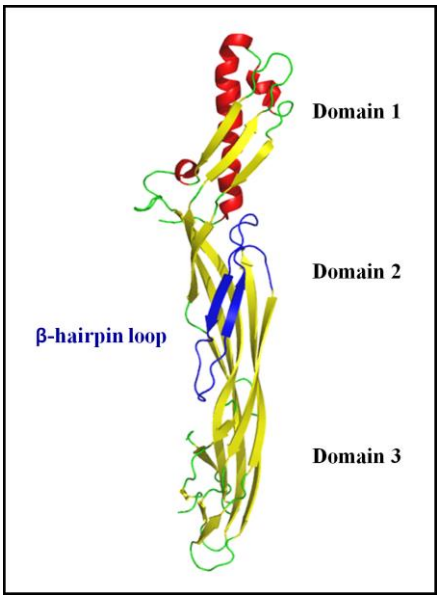

Figure 1.5: Structure of monomeric epsilon protoxin (PDB ID: 1UYJ)

The monomeric structure of ETX contains three distinct domains (Figure 1.5) composed mainly of β sheets (50). The domain 1 of ETX is composed mainly of α-helical structures and is implicated in the binding of ETX to specific receptors on the target cell surface through a cluster of aromatic residues: Tyr49, Tyr43, Tyr42, Tyr209 and Phe212. Domain 2 of ETX contains an amphipathic double stranded β-sheet structure implicated in the channel-forming activity. Each ETX monomer contributes two β-sheets in the formation of a functional heptameric channel. Site-directed mutagenesis studies have shown that the residues between His151-Ala181 in domain 2 contain alternative hydrophilic-hydrophobic residues, characteristic of channel forming β-hairpins in other β-PFTs (51). The domain 3 of ETX primarily contains the cleavage site for activation of the toxin.

ETX is secreted during the exponential growth phase of *C. Perfringen.* High level of ETX in the intestine is a characteristic feature of enterotoxemia. The toxin passes through the intestinal barrier and disseminates through circulation to several organs causing toxic shock (46). It has been argued that the ETX receptor is localized in the lipid raft microdomains. Disruption of lipid rafts by methyl-β-cyclodextrin treatment results in impairment of ETX binding and pore-formation (52). Moreover, the inactive pro-toxin and the active form of the toxin have been shown to preferentially bind lipid rafts (53). The initial steps in the mode of action of ETX following binding to specific receptors involve membrane blebbing and disruption (54-55). The cytotoxicity induced by ETX is characterised by rapid loss of intracellular K^+, ATP depletion, mitochondrial membrane permeabilization, increase in intracellular Ca^+ and Na^+ levels followed by cell death due to necrosis (49, 52).

1.4.3 *Staphylococcus aureus* α-Hemolysin (α-toxin)

Hemolysin (α-toxin) is secreted by *Staphylococcus aureus*, a facultatively anaerobic Gram-positive bacterium. It is known as hemolysin due of its ability to lyse red blood cells (erythrocytes). It has been established as a prominent factor in *S. aureus*-induced infections. Hemolysin is encoded by *hla* gene as a 293-amino acid long protein of molecular mass 33 kDa. It is secreted by the bacterium during the late log phase or stationary phase of growth. The expression of hemolysin is controlled by accessory gene regulator (*agr*) locus via regulatory RNA, RNA III (56-57). The mechanism of action of hemolysin involves (i) secretion of the toxin by *S. aureus,* (ii) binding to host cell surface, (iii) formation of heptameric non-toxic pre-pore oligomer, (iv) conversion of the pre-pore oligomer into a functional transmembrane pore.

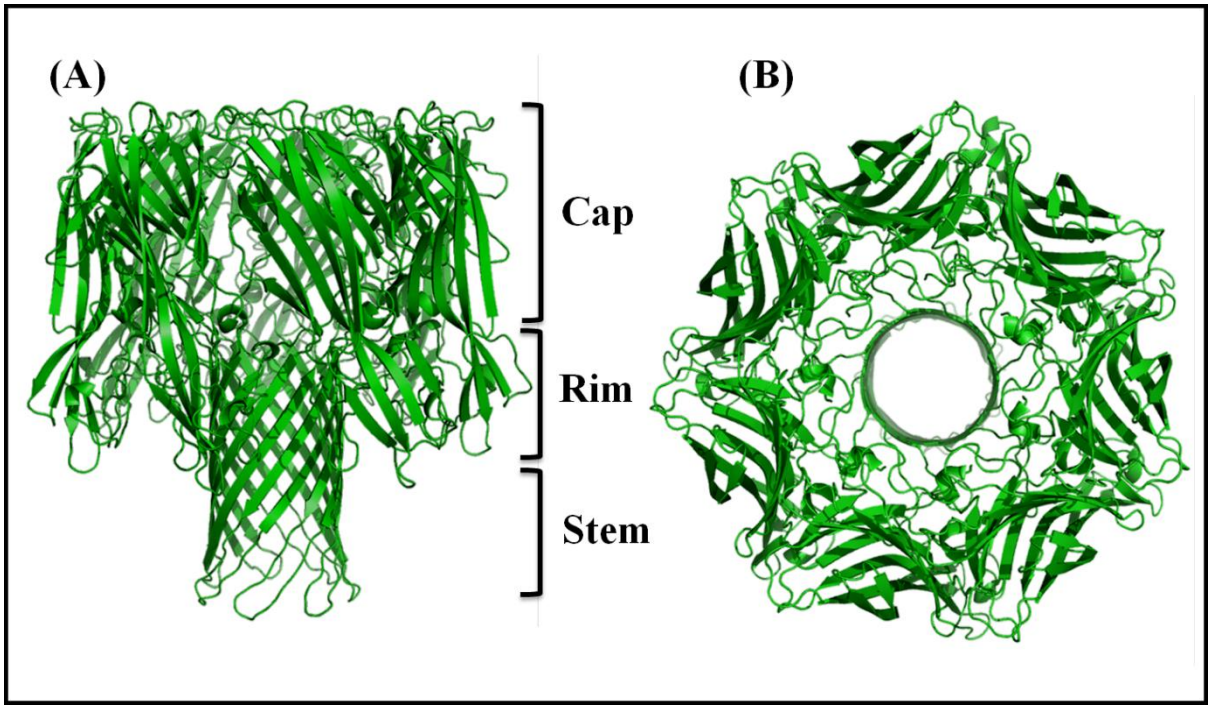

Figure 1.6: Structure of α-hemolysin heptamer (PDB ID: 7AHL). (A) Shows the Cap, Rim and the Stem domain of the transmembrane pore. (B) Shows the central pore.

Hemolysin binds to phosphocholine headgroups in the target cell membrane (58). Also the depletion of cholesterol from the host cells diminishes toxin binding. Recently, it was shown that A Disintegrin And Metalloprotease 10 (ADAM10) acts as the cell surface receptor for hemolysin (59). ADAM10 is a transmembrane zinc-dependent metalloprotease on the cell surface of host cells. The crystal structure for hemolysin heptamer has been solved (Figure 1.6). The hemolysin heptamer is composed of three domains. (i) The Cap domain forms the extracellular face of the toxin and defines entry of the pore while being exposed to the aqueous environment. (ii) The Rim domain is positioned on the outer leaflet of host plasma membrane. (iii) The Stem domain forms the transmembrane β-barrel structure (60). During the event of pore formation, N-terminal region of hemolysin undergoes a conformational change and interacts with the neighbouring protomer, stabilizing the heptameric pore structure. The Histidine residue at position 35 in the primary amino acid sequence of α-hemolysin has been shown to drive the insertion of stem into the membrane by moving into a hydrophobic environment during pre-pore to pore transition. Deletion mutations in the N-terminus or within the glycine rich stem region (residues 118-142) were shown to arrest the toxin in a pre-pore stage, indicating that these two regions are important in the pre-pore to pore transition (14). Hemolysin heptamer shows that the central glycine-rich stem region

from each monomer contributes a two-stranded antiparallel β-sheet to the β-barrel of the trans-membrane pore, which therefore comprises of 14 β-strands.

1.4.4 Anthrax toxin protective antigen (PA)

Anthrax toxin belongs to the family of binary toxins. It is produced by *Bacillus anthracis*, a rod-shaped, endospore forming, Gram-positive bacterium which is the causative agent of anthrax. Anthrax toxin is composed of three proteins, (i) Lethal factor (LF), a ~90 kDa Zinc-dependent protease that cleaves and inactivates MAP kinase kinase (61-62), (ii) Edema factor (EF), a ~89 kDa Calcium and calmodulin dependent adnylyl cyclase (63), (iii) Protective antigen (PA), a ~ 83 kDa (PA_{83}) β-pore-forming toxin that acts as the vehicle for delivery of LF and EF into the host cell cytoplasm. Protective antigen (PA) consists of 4 domains (Figure 1.7). Domain 1 is a β-sandwich with four α-helices. The 1-167 residues in the N-terminal of the protein known as PA_{20} inhibits monomer-monomer interactions required for heptamer formation; hence the PA_{20} is removed from the receptor-bound PA_{83} by cell-associated furin proteases, generating a truncated form of the protein known as PA_{63} (64-65). During proteolytic removal of PA_{20}, a β-sheet is ruptured, exposing a large hydrophobic region. Domain 1 of PA_{63}, the N-terminal segment left after removal of PA_{20} acts as the binding site for LF and EF in the oligomer.

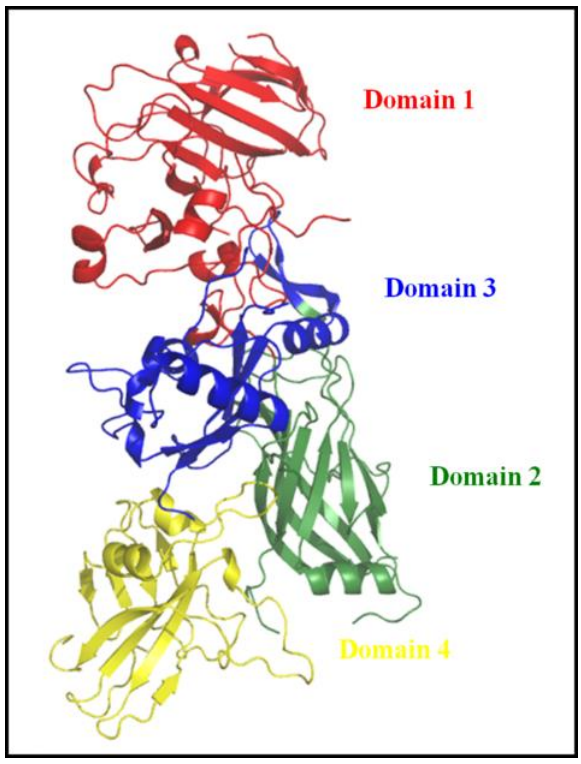

Figure 1.7: Structure of anthrax toxin Protective Antigen monomer (PDB ID: 1ACC)

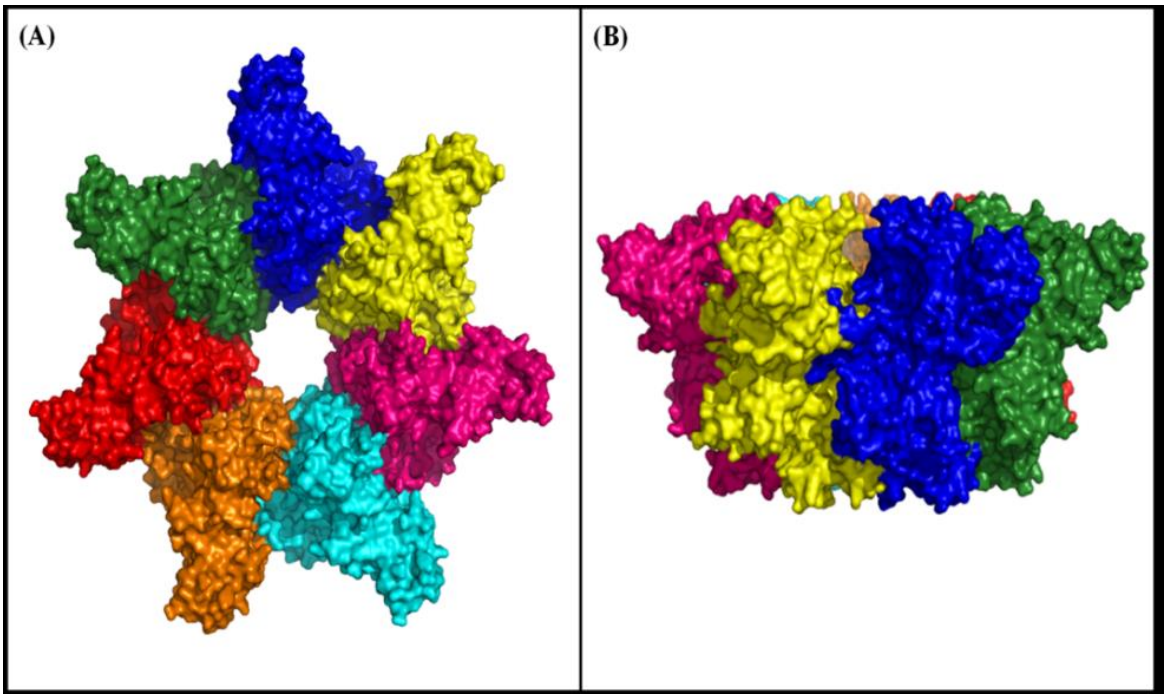

Figure 1.8: Heptameric pore structure of Protective Antigen (PDB ID: 1TZO).

Domain 2 is composed of a β-barrel core. After formation of the heptameric pre-pore oligomer by PA_{63}, domain 2 undergoes a major pH-dependent conformational rearrangement, allowing domain 2 from each monomer to contribute a 2 β-sheet hairpin, forming a 14 stranded-β-barrel transmembrane structure (66-67). Domain 3 consists of a ferridoxin-like fold. It mediates the interaction between monomers to allow for the self-association of PA_{63} leading to formation of a heptameric pore structure (Figure 1.8). Mutations in this domain have been shown to inhibit oligomerization of PA_{63} (68-69). Domain 4 of protective antigen is involved in the binding to specific cell receptors (70).

1.4.5 Cholesterol-dependent cytolysins

Cholesterol-dependent cytolysins (CDC) constitute the largest group among the family of β-PFTs. CDCs are mostly secreted by Gram-positive bacteria (24, 71). Some of the prominent members in the CDC family include Listeriolysin (LLO) from *Lysteria monocytogenes* (72), Pneumolysin (PLO) from *Streptococcus pneumonia* (73), Intermedilysin (ILY) from *Streptococcus intermedius* (74). CDC mode of action is critically dependent on the presence of cholesterol in the target cell membranes (71). Functionality of CDCs is also found to be pH-dependent (75). CDCs are known to make the largest pores in the β-PFT family, ranging from 25-30 nm size of pore diameter (24). The mode of action of CDCs

involves (i) cholesterol-dependent association of the soluble toxin monomers with host cell membranes, (ii) concentration of the monomers on the target membrane by lateral diffusion, (iii) formation of non-functional pre-pore oligomers, and (iv) insertion of the β-hairpin loop from the toxin protomers into the membrane leading to the formation of a functional pore (23, 71). The crystal structure of different CDCs revealed that a CDC protein is, in general, composed primarily of 4 domains. Domain 4 of the CDCs consists of a highly conserved 11 amino acid residue-long motif (ECTGLAWEWWR) known as the un-decapeptide or tryptophan-rich motif. This motif is responsible for the cholesterol-dependent membrane interactions of CDCs. The un-decapeptide partially inserts into the membrane to interact with the cholesterol leading to the lateral diffusion of the monomer on the membrane to interact with other monomers in order to form a functional β-barrel pore (76). Binding of Domain 4 to cholesterol initiates a conformational change in the Domain 3 exposing a β-strand. Hydrogen bonding between the Domain 3 β-strands of adjacent monomers leads to the formation of a non-functional pre-pore oligomer (defined as a completed ring complex on the membrane surface without insertion of the β-hairpin loops). After formation of the pre-pore oligomer, a second conformational change in the Domain 3 leads to the conversion of three α-helices into two β-sheets comprising the transmembrane β-hairpin (TMH) structure for each of the monomers. During the insertion, each monomer contributes two β-sheets in the form of a transmembrane β-hairpin leading to the functional pore-formation (23, 76-77).

1.4.6 *Vibrio cholerae* Cytolysin

Vibrio cholerae cytolysin (VCC) is a prominent member in the family of β-barrel pore-forming toxins (β-PFTs) (22). It is secreted by the bacterium as a water-soluble monomer (78), which upon binding to the host eukaryotic cell membranes converts into the heptameric transmembrane β-barrel channels (79). The VCC mode of action involves (Figure 1.9) (i) secretion of the water-soluble monomers in an inactive state (Pro-VCC), (ii) conversion of the Pro-VCC into mature VCC by proteolytic removal of the N-terminal Pro-domain, (iii) binding of the mature VCC to the host eukaryotic cell membranes, (iv) heptamerization to form intermediate assembly states known as Pre-pore oligomers, (v) conversion of the Pre-pore oligomers into the functional transmembrane β-barrel pores leading toward the killing of the host cells by colloid-osmotic lysis.

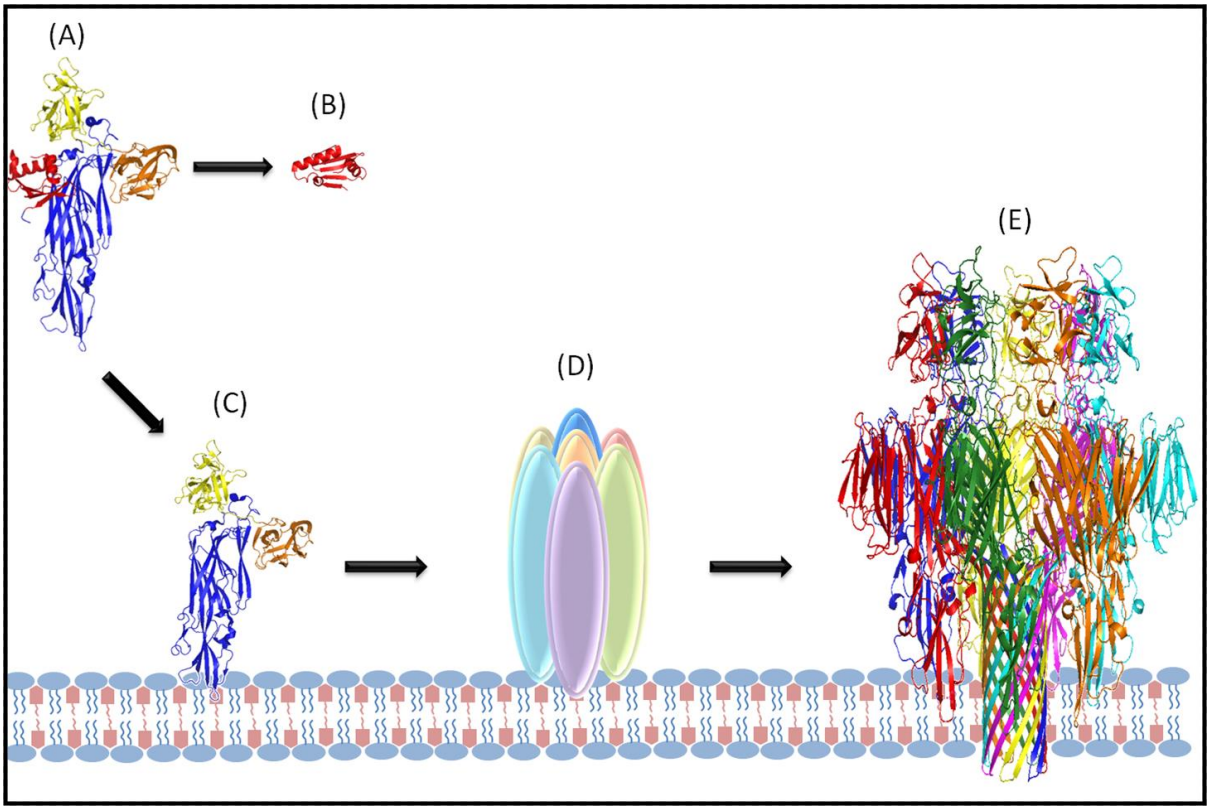

Figure 1.9: Mode of action of *Vibrio cholerae* cytolysin. (A) Secretion of the toxin as soluble monomer by *V. cholerae*, (B) proteolytic removal of the N-terminal Pro-domain, (C) binding of the mature form of the toxin onto the host cell membrane, (D) self-assembly of 6-7 monomers to form a non-functional pre-pore oligomer, (E) conversion of pre-pore oligomer into functional transmembrane β-barrel channel.

The present research thesis deals with the structure-function mechanism of VCC as a prototype in the β-PFT family. Therefore, a more detail literature review regarding VCC, in the context of the *V. cholerae* pathogenesis process is presented in the subsequent pages. Also, a detail overview of its mode of action is presented here.

VCC is secreted by most of the pathogenic strains of the Gram-negative bacterium *V. cholerae*, the causative agent of the severe diarrhoeal disease cholera (80). Cholera is characterised by the passage of stools of rice water leading to rapid dehydration. *V. cholerae* has been responsible for seven pandemics of cholera (81).

V. cholerae is a curved rod-shaped, Gram-negative bacteria. It is facultatively anaerobic, non-spore forming microorganism (81). *V. cholerae* belongs to the family *Vibrionaceae*. Of the 63 species in the genus Vibrio, many are pathogenic to humans, including *V. cholerae, V. vulnificus, V. parahaemolyticus, V. hollisae, V. fluvialis, V. mimicus, V. alginolyticus, V. damsela, V. furnissii, V. metschnikovii, and V. cincinnatiensis.*

V. cholerae is classified into three serogroups: O1, O139 and non-O1 based on the differences in heat-labile surface antigen "O". *V. cholerae* O1 serogroup is further subdivided into two biotypes, classical and El Tor. The current cholera pandemic is caused by *V. cholerae* O1 El Tor. Pathogenic strains of *V. cholerae* O1 are characterised by the presence of gene for Cholera Toxin (CT), the major virulence factor of the organism. The first step in the pathogenesis of cholera induced by *V. cholerae* is ingestion of the contaminated food or water. The organism after passing the acidic stomach, colonizes in the small intestine by means of several colonization factors. *V. cholerae* produces its characteristic toxin, CT that disrupts the ion transport by the intestinal epithelial cells, causing loss of water and electrolytes, leading to severe dehydration. However, strains of *V. cholerae* lacking the gene encoding for CT have been shown to cause mild to moderate form of diarrhea, suggesting the roles of accessory virulence factors in the cholera pathogenesis (81).

V. cholerae has been shown to produce many extracellular toxins with deleterious effects on human intestinal cells. The well-studied toxins include:

i. Cholera Toxin (CT) (82-84)
ii. Zonula Occludens Toxin (Zot) (85-86)
iii. Accessory Cholera Enterotoxin (Ace) (87-88)
iv. Shiga-like Toxins (SLTs) (89-90)
v. *V. cholerae* hemolysin/cytolysin (VCC) (91-92)

Hemolytic *V. cholerae* strains of the biotype El Tor were first isolated during the seventh cholera pandemic during 1973–1978. Subsequently, hemolytic activity was established as an epidemiological marker for characterising different *V. cholerae* strains (80). During the early 1980s, hemolytic *V. cholerae* O1 strains lacking the gene for CT were isolated from the patients with severe diarrhea (80). This suggested the presence of unknown virulence factor(s) responsible for the diarrhea-like symptoms.

Toward characterising the source of hemolytic activity in *V. cholerae*, the *V. cholerae* hemolysin protein was cloned, sequenced (93-94) and purified (94-95). *V. cholerae* hemolysin purified from the wild type bacteria or extracted from the recombinant expression systems was found to display potent lytic activity against a wide range of erythrocytes. Moreover, it was found to display critical cytotoxic activities against wide variety of nucleated eukaryotic cells, and thus was also named as *V. cholerae* cytolysin (VCC) (93, 95-96). Subsequently, it was shown that the purified form of VCC from the *V. cholerae* El Tor strains resulted in the accumulation of the bloody and mucoid fluids in the ligated rabbit ileal loops (91). It was also shown that VCC was an enterotoxic factor responsible for causing

diarrhea-like symptoms in patients infected with the *V. cholerae* strains lacking the gene for CT (80). Based on such observations, VCC has been considered as a potential virulence factor of *V. cholerae* capable of contributing toward the cholera pathogenesis process.

Figure 1.10: Primary amino acid sequence of VCC

V. cholerae hemolysin/cytolysin (henceforth abbreviated as VCC) is encoded by the structural gene *hlyA* in the form of pre-pro-VCC of M_r ~82 kDa. It contains an 18-amino acid long N-terminal signal sequence. The protein, after removal of the signal peptide, is secreted as an inactive ~79 kDa precursor known as Pro-VCC (93). The ~ 79 kDa proteins is processed into its active form, the mature VCC, by removal of ~15 kDa N-terminal peptide, known as the Pro-peptide. The soluble haemagglutinin protease (HA protease), a major protease secreted by *V. cholerae* has been implicated in the proteolytic removal of the Pro-peptide. However, other proteases such as trypsin, α-chymotrypsin, subtilisin and papain have also been shown to activate VCC in vitro by proteolytic removal of the N-terminal Pro-

peptide (95). Crystal structure of the monomeric Pro-VCC revealed a cross-shaped architecture of the molecule (Figure 1.10) with a central 325 amino acid long "cytolysin" domain, onto which three ~15 kDa accessory domains are attached (22). These additional domains are the N-terminal Pro-domain, C-terminal β-trefoil lectin-like domain, and a β-prism lectin-like domain. The central cytolysin domain contains the transmembrane β-hairpin structure known as the Pre-stem loop (Figure 1.10).

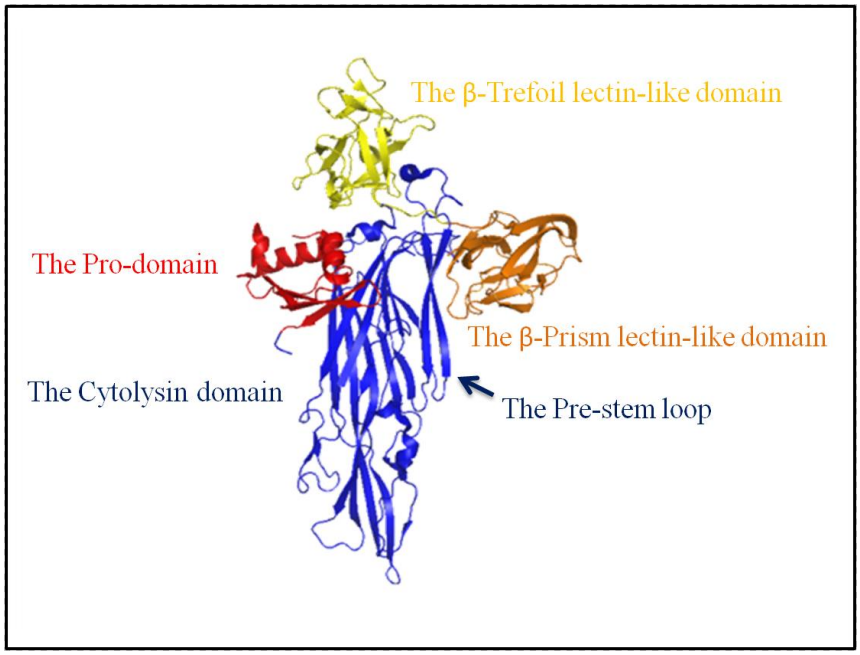

Figure 1.11: Crystal structure of Pro-VCC (PDB ID: 1XEZ)

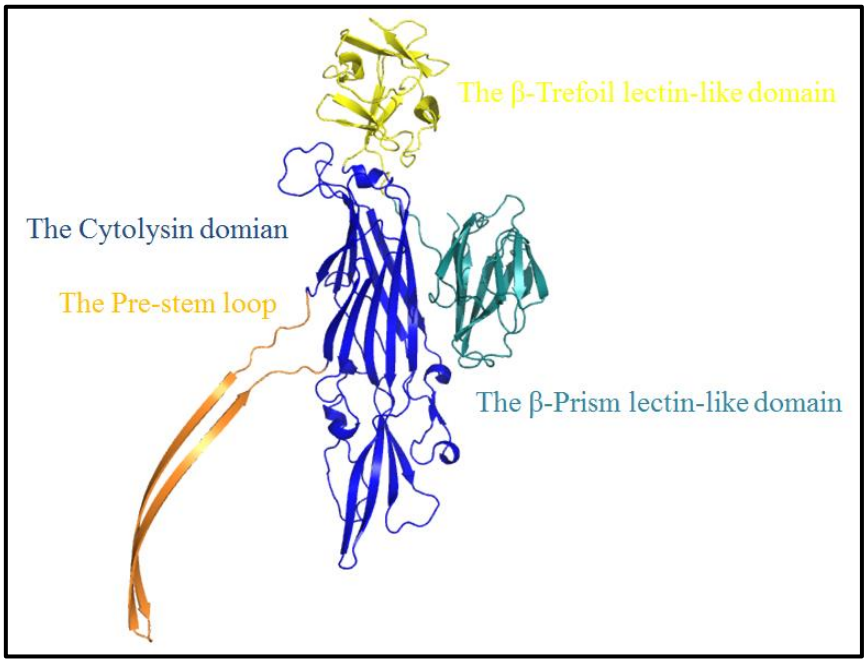

Figure 1.12: Structure of the mature-VCC protomer displaying the structutal changes during the process of oligomerisation

The Pro-domain

Pro-domain is an N-terminal domain of ~15 kDa. Presence of the Pro-domain maintains VCC molecules in a functionally inactive precursor form (95). Although the presence of the Pro-domain does not inhibit binding of VCC to target cell membranes, it possibly inhibits the monomer-monomer interaction required for oligomerization of the toxin. It is connected to the cytolysin domain by a flexible linker of approximately 15 amino acids that harbours the recognition sequences for various proteases (95). Pro-domain is composed of four β-strands and three α-helices (22). It has sequence homology to Hsp90 family of heat shock proteins. Deletion of the Pro-domain form the *hlyA* gene results in the degradation of the toxin in bacterial periplasm (97). Pro-domain is speculated to act as an intra-molecular chaperone, and that it might act to assist in proper folding of VCC into its native architecture (97).

The Cytolysin domain

Cytolysin domain forms the central core of VCC onto which all other domains are attached. Cytolysin domain is the structural and functional core of VCC (22). During pore-formation on target cell membrane, it forms the rim-domain of the oligomer which remains seated on the cell membrane and forms the entry of the pore (79). The folds in VCC cytolysin domain have been shown to be similar to folds in the cytolysin domain of *S. aureus* α-hemolysin (22). The cytolysin domain harbours the so called 'pre-stem' loop, which in the process of membrane pore formation contributes to the generation of the stem region of the β-barrel pore structure.

The β-trefoil lectin-like domain

The β-trefoil lectin-like domain is a C-terminal ~15 kDa domain composed mainly of β-sheet structure (22). Sequence alignments studies show that it has sequence similarity to Ricin, a toxic carbohydrate-binding protein produced by plant, *Ricinus communis* (98). The β-trefoil lectin-like domain also contains the conserved QXW carbohydrate-binding site.

The β-prism lectin-like domain

The ~15 kDa C-terminal β-prism lectin-like domain is connected to the β-trefoil domain by a long linker (22). It has sequence similarity to *Maclura pomifera* agglutinin (MPA) (99) and jacalin (100). (98). Super position of the C-terminal lectin-loke domain of VCC and MPA show a root mean square deviation of 1.8 Å in α-carbon for 96 out of 130

amino acids. Deletion of the β-prism domain abolishes VCC hemolytic activity (101). The β-prism domain binds to carbohydrate receptors on the target cell membrane, thereby increasing the local toxin concentration presumably aiding in monomer-monomer interaction leading to pore-formation (102-104).

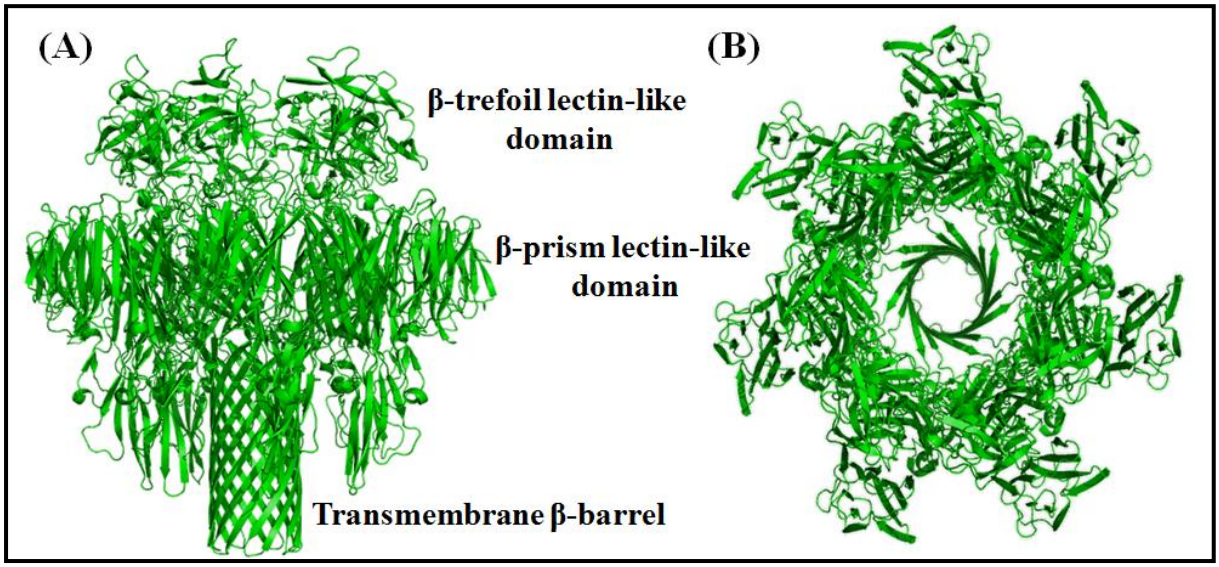

Figure 1.13: Structure of VCC heptamer (PDB ID: 3O44). (A) Shows the position of the β-trefoil lectin-like domain, β-prism lectin-like domain and the transmembrane β-barrel composed of the pre-stem motif. (B) Shows the central pore.

Mechanism of oligomeric membrane pore formation by VCC

High-resolution three-dimensional structures have been determined for the water-soluble monomeric state, as well as the transmembrane oligomeric pore state of VCC (22, 79). Analysis of the structural models reveals important insights regarding the mechanism of membrane pore formation process employed by VCC. The structural models show that in the event of pore-formation, each monomer contributes a pre-stem motif toward formation of the transmembrane β-barrel pore structure comprising 14 β-sheets. In this process VCC protomers undergo a major conformational rearrangement in the overall protein structure leading to the insertion of the pre-stem loop into the membrane lipid bilayer, a crucial step for the conversion of the pre-pore state into a functional transmembrane pore structure (79).

The most important step in VCC mode of action is the formation of a membrane bound pre-pore oligomer, followed by insertion of the pre-stem into membrane lipid bilayer leading to formation of a functional transmembrane β-barrel. In the water-soluble form of VCC, pre-stem loop is bracketed by an extended loop (residue 191-204) which maintains hydrophobic contact with pre-stem loop (22). It also interacts with numerous charged and

polar residues at the interface of the pre-stem- β-sandwich (22). The pre-stem loop is also bound on the edge to the adjacent β-prism lectin domain, creating a stearic effect for the loop. Hence, in order for the stem to penetrate membrane lipid bilayer, VCC undergoes a major conformational rearrangement. During the event of pore-formation, the β-prism lectin domain takes a 180˚ rotation around the core cytolysin domain followed by movement of the extended loop that might result in the destabilization of the interactions holding pre-stem in the water-soluble state and initiate partial unfolding of the pre-stem resulting in its insertion into the membrane lipid bilayer (79). In the transmembrane β-barrel, each of the seven pre-stem loops contributed by seven protomers transforms into a 19 residue long antiparallel β-sheet structure that forms 21 hydrogen bonds with each of its two neighbouring stem loops, thereby, stabilizing the pore structure leading to formation of a anion specific pore 1-2 nm in diameter (79).

1.5 Unsolved issues in the VCC mode of action

VCC has been shown to be a potential virulence factor of *V. cholerae*. Previous studies have established that VCC exerts its pathophysiological effects on the target host eukaryotic cells by acting as a membrane-damaging β-barrel pore-forming toxin. In its mode of action, the toxin is secreted as an inactive precursor (Pro-VCC), which upon removal of its N-terminal Pro-domain converts into the active mature form of the toxin. Pro-domain has been suggested to act as an intramolecular entity, facilitating proper folding and secretion of the toxin. It is however still not known how exactly the presence of the Pro-domain modulates the structure-function mechanism of VCC. In the same direction, functional implication of the other unique structural features present in the VCC molecule has not been addressed in mechanistic detail. Membrane pore-formation process employed by VCC also represents a mechanism that poses several intriguing aspects requiring in depth structure-function investigation. In particular, regulation of the structural rearrangement within the VCC molecule in the process membrane pore-formation has been explored only to a limited extent. Analysis of the structural models have suggested that conversion of the pre-stem motif into stem configuration acts as a key step leading toward the functional β-barrel pore-formation. Covalent locking of the pre-stem motif has been shown to trap the toxin in its membrane-bound pre-pore state. However, it has not been explored yet whether the physical presence/absence of the pre-stem motif is indeed required for the membrane binding and pre-pore formation by the VCC protomers. Another aspect of VCC mode of action also remains unsolved: the mechanistic basis of the cholesterol-dependency for its membrane binding and functional pore-formation. Presence of cholesterol in the target membrane has been shown to be critical for the functional membrane pore-formation by VCC. It has also been indicated that cholesterol modulates the efficacy of the VCC mode of action, not by altering the physicochemical properties of the target membranes, rather by physically interacting with as yet unknown structural motif present within the VCC molecular structure. However, structural basis of VCC-cholesterol interaction and its implication for the VCC mode of action remains to be validated.

1.6 Specific Objectives

Vibrio cholerae cytolysin (VCC) is a prominent member of the β-barrel family of pore-forming toxins (β-PFTs). It is produced by most of the pathogenic strains of the Gram-negative bacterium *V. cholerae*. VCC is secreted in the form of a water-soluble monomeric precursor of ~79 kDa, known as Pro-VCC. Pro-VCC becomes activated by proteolytic removal it's N-terminal ~15 kDa Pro-domain to generate the mature form of the VCC toxin. Mature VCC binds to the target eukaryotic cell membranes, and forms heptameric transmembrane β-barrel pores, leading to the colloid-osmotic lysis of the target host cells. A large number of studies have indicated VCC as a potential virulence factor of *V. cholerae* contributing toward the disease process caused by the bacterium. Previous studies have explored the molecular mechanisms associated with the membrane pore formation process employed by VCC. Structural studies done on the monomeric and the oligomeric pore state of VCC have also provided valuable insights regarding the structural mechanisms of its membrane pore formation process. However, a large number of issues regarding the structure-function mechanism of VCC remain only partly explored and/or addressed. For example, functional implications of the distinct structural domains/motifs/modules present in the VCC molecular structure have not been explored previously. Several studies have probed the mechanism of membrane pore-formation employed by VCC. However, the structural constraints that regulate the distinct steps of membrane pore-formation have not been elucidated in mechanistic detail. Also, membrane interaction mechanisms of VCC, and the roles of cholesterol in the process have been studied in a large number of studies. However, it has not been tested earlier whether VCC contains any specific structural signature/motif having implication for the cholesterol-dependent membrane interaction mechanism and subsequent steps of the membrane pore-formation process. Therefore, in this background, the present thesis work investigates the structure-function mechanisms of VCC with special emphasis on the following three objectives:

(i) To elucidate the role of the Pro-domain in the structure-function mechanism of VCC.

(ii) To explore the implication of the pre-stem motif in regulating the structure-function mechanism of VCC.

(iii) To explore the structural basis of cholesterol-dependent membrane interaction mechanism of VCC.

Successful exploration of these objectives would not only provide novel insights regarding the mode of action of VCC, but would also enrich our current understanding regarding the structure-function mechanisms of b-PFT family of bacterial protein toxins.

Chapter 2

Implications of the Pro-domain in the structure-function mechanism of VCC*

2.1 Abstract

Vibrio cholerae cytolysin (VCC) is a prominent member in the β-barrel pore-forming toxin (β-PFT) family. VCC is secreted by most of the pathogenic strains of *V. cholerae*. VCC causes colloid-osmotic lysis of the target eukaryotic cells by forming transmembrane oligomeric β-barrel pores. VCC is released by the bacteria as a ~79 kDa inactive precursor, known as Pro-VCC. Upon proteolytic processing of the N-terminal Pro-domain, this precursor form is converted into the active mature form of the toxin, Mature-VCC. Previous studies have suggested an intramolecular chaperone-like function of the Pro-domain, where it has been shown to assist in proper folding and efficient secretion of the toxin. However, exact implication of the Pro-domain in the structure-function mechanism of VCC remains unknown. In this direction, we compared the Pro-VCC and Mature-VCC in terms of structural changes during the event of protein unfolding under a wide range of conditions including low pH-induced unfolding, urea-induced denaturation and thermal denaturation. We found that the Pro-VCC molecule displayed a more profound tendency to undergo unfolding-related structural changes under given conditions, as compared to Mature-VCC. Exposure of isolated Pro-domain to similar denaturing conditions revealed that it is a much more stable entity as compared to both the variants of VCC. Hence, an increased propensity of Pro-VCC toward unfolding could not be attributed to an increased unfolding tendency of Pro-domain within the Pro-VCC structure. Altogether, it appears from our study that the presence of the Pro-domain allows Pro-VCC to adopt a natively folded architecture with sufficient structural/conformational plasticity, which might be critically required for proper folding, efficient secretion, and maturation of the toxin under the physiologically relevant conditions.

2.2 Introduction

Many proteins exist in a functionally inactive precursor form, which upon limited proteolysis undergo physiological and/or biochemical changes and become active. Most common examples of such proteins are the enzymes secreted by the pancreas such as trypsinogen (105), chymotrypsinogen (106) and pepsinogen (107), enzymes involved in the programmed cell death (procaspases) (108), proteolytic enzymes secreted by bacteria such as α-lytic protease by *Lysobacter enzymogenes* (109), subtilisin E (110) and carboxypeptidase Y

(111). Generally, the removal of inactivating peptide (also known as the "Pro" peptide) is accompanied by either some conformation change(s) or exposure of the active site(s) (35).

The pro-domain has been shown to help/aid in the folding of the protein molecules into their functionally active native forms. In some proteins, the pro-domain has been shown to guide protein folding without any physical linkage with the protein (109). Sibtilisin E, an alkaline serine protease, contains a 77-amino acid long pro-region. Deletion of the pro-sequence yields an inactive enzyme. Hence the pro-sequence must be present in order to guide the mature protein toward an active conformation. The pro-domain in isolation is able to activate the unfolded mature subtilisin, when exogenously added to mature subtilisin denatured in 6M guanidine hydrochloride, showing that the pro-domain can guide the refolding of its denatured mature counterpart in an intermolecular process in-vitro (110). α-lytic protease, an extracellular serine protease, contains a 166-amino acid long pro-sequence. When recombinantly expressed in *E. coli*, the protein is autocatalytically processed in periplasmic space, and the functional protease domain lacking the pro-region accumulates extracellularly. The protein lacking the 166-amino acid pro-sequence is inactive, and remains cell associated rather than being secreted by the bacterium. Hence, the pro-region, which is covalently associated with the protease domain, is necessary for correct folding of the protein. However, when the pro-domain and the protease-domain are independently expressed in-vivo, it results in the secretion of the protease domains in its active configuration, suggesting that the pro-domain does not require any covalent linkage for efficient folding, activation and secretion of the protease domain (109). Thus, it can be concluded that the pro-domain acts as a template that binds to and stabilizes the intermediate unfolded state of the protein for folding into functionally active configuration.

The β-barrel Pore forming toxins (β-PFTs) are a unique class membrane damaging cytolytic proteins that are secreted as accessory virulence factors by many pathogenic bacteria. The β-PFT mode of action involves, binding of the toxin onto the target eukaryotic cell membranes, and its subsequent oligomerization into transmembrane β-barrel channels. Although, the general scheme among the members of the β-PFT family is highly conserved, these toxins differ in the intricate details of their mechanisms of action (3).

Vibrio cholerae cytolysin (VCC) is a prominent member in the β-PFT family (22). It is secreted as a ~79 kDa inactive precursor form known as Pro-VCC. Subsequent proteolytic removal of it's N-terminal segment leads to conversion of the toxin into a ~65 kDa active form known as Mature-VCC (95). The proteolytic activation of VCC is the first step in the VCC mode of action. X-ray crystal structure of Pro-VCC shows the presence of a ~15 kDa

N-terminal Pro-domain (residue 1-118) (22). Presence of the Pro-domain keeps VCC in a functionally inactive form presumably via blocking the protomer-protomer interaction surfaces. Proteolytic removal of the Pro-domain leads to the generation of the Mature-VCC, which in contact with the target cell membranes, oligomerises into heptameric transmembrane β-barrel channels, thus exerting the cytotoxic action. It is not known whether the removal of the 'Pro-domain' results in any major structural and conformational change(s) in the VCC molecular structure. It has been suggested that the presence of the N-terminal 'Pro-domain' possibly allows the VCC molecule to adopt a suitable configuration that might be critical for efficient secretion and proper folding of the toxin (97). Moreover, it has also been shown that the presence of the 'Pro-domain' preserves the toxin molecule in an inactive precursor state, which is incapable of displaying the cytolytic activity towards its target cells.

Removal of the Pro-domain from VCC gene (*hlyA*) results in the degradation of VCC in the bacterial periplasmic space. Chemically denatured Pro-VCC recovers complete activity after denaturation, but Mature-VCC lacking the Pro-domain does not get activated upon renaturation from the unfolded states. The Pro-domain also bears sequence similarity with the Hsp90 family of chaperones (97). Since the location of the Pro-domain is within the VCC molecule, it has been proposed as an intramolecular chaperone, suggesting that the N-terminal Pro-domain might play some role in the folding of VCC molecule into its native architecture (97).

Aerolysin, a β-PFT secreted by the bacterium *A. hydrophila* also contains a C-terminal Pro-peptide (41). Proteolytic removal of the pro-peptide is essential for subsequent activation and oligomerization of the toxin. Proteolytic removal of the C-terminal pro-peptide from pro-aerolysin causes a little change in the tertiary and secondary structures as monitored by near- and far-UV circular dichroism spectroscopy respectively. However, intrinsic tryptophan fluorescence emission studies show that removal of pro-peptide results in a red shift in intrinsic tryptophan fluorescence emission spectra accompanied by an increase in the tryptophan emission of mature aerolysin (lacking the pro-peptide) suggesting a change in the tryptophan environment. The results from Rayleigh light scattering show that pro-aerolysin in monomeric form could not scatter light but light scattering increased with the addition of trypsin presumably due to formation of mature aerolysin and its subsequent oligomerization. Removal of the pro-peptide also results in an increase in the binding of hydrophobic probe 1-anilino-8-naphthalene sulfonic acid to mature aerolysin, indicating that the pro-peptide might mask a hydrophobic surface required for the necessary protomer-protomer interactions (35).

Information regarding exact role of Pro-domain in the structure-function mechanism of VCC is unknown. In the present study, we characterised the precursor and mature form of VCC namely, Pro-VCC and Mature-VCC, respectively, in terms of changes in the tertiary and the secondary structures during the events of protein unfolding. We studied the changes in the protein structure in its solution state in response to a wide range of conditions, namely, low pH-induced unfolding, urea-induced unfolding and thermal denaturation to induce unfolding of the protein.

2.3 Materials and Methods

Cloning and Expression of the Pro-VCC

The nucleotide sequence encoding Pro-VCC was amplified by the PCR-based method using the VCC chromosomal DNA as the template. Amplified PCR product was cloned into the expression vector pET14b (Novagen), between Nde1 and BamH1 restriction digestion sites. The pET14b vector allows addition of an amino terminal hexahisitidine tag into the recombinant protein. To remove the histidine tag from the protein, a TeV (Invitrogen) cleavage site was introduced between the sequence and hexahistidine tag using PCR-based method. Recombinant nucleotide sequence was verified by DNA sequencing. Recombiant pET14b vector harbouring the nucleotide sequence for Pro-VCC was transformed into *E .coli* Origami B cells

Expression and Purification of Soluble Pro-VCC

E. coli Origami B cells harbouring recombinant pET14b vector containing nucleotide sequence for Pro-VCC were grown in LB medium supplemented with 50 µg/ml of carbenicillin. A seed culture was inoculated with transformed Origami cells and grown overnight at 37 ˚C. The overnight culture was diluted 50-fold into 2 liters of LB broth, the culture were grown at 37 ˚C to an A_{600} of 0.6. Protein expression was induced with 1 mM IPTG (Isopropyl β-D-1-thiogalactopyranoside), and the cultures were grown for additional three hours with shaking at 30 ˚C. Cells were pelleted by spinning at 4000 rpm for 20 minutes in a hanging bucket centrifuge and cells were resuspended in 10 ml phosphate buffered saline (PBS), pH 7.0 containing bacterial protease inhibitor cocktail (Sigma). Cells were lysed using a Mesonix Ultra sonicator with six pulses of thirty seconds each at an amplitude of 20 followed by centrifugation at 12,000 rpm for 10 minutes at 4 ˚C. The supernatant was adjusted with 20 mM imidazole before passing through Ni-NTA chelating column (Qiagen) pre equilibrated with PBS (pH 7.0). The column was washed with 50 x volume of the same buffer adjusted with 20 mM imidazole. - Bound protein was eluted with 300 mM imidazole.

The peak fractions were diluted five times with a buffer containing 10 mM Tris-HCl and 1 mM EDTA (pH 8.0), and loaded onto a Q–sepharose column (GE healthcare) pre equilibrated with the same buffer. Bound protein was eluted in a linear gradient of 0 to 500 mM NaCl over 50 ml in an FPLC system (AKTA purifier, GE healthcare), at a 2 ml per minute flow rate. Eluted protein fractions were analysed for Pro-VCC by SDS-PAGE and Coomassie staining. The histidine tag was removed by incubating with 1 unit of TeV protease (Invitrogen) per 10 µg of protein for overnight at 25˚C followed by a second round of purification on a Q-sepharose column. Purified Pro-VCC was analysed by SDS-PAGE and Coomassie staining. Protein concentration was estimated by monitoring A_{280} using the theoretically calculated absorbance values as predicted from the protein's primary structure (1.43 for 1 mg/ml Pro-VCC).

Generation of Mature-VCC

Mature-VCC was generared by treating Pro-VCC with trypsin at a protein:protease ratio of 2000:1 for 10 minutes at room temperature. Reaction was terminated with 1 mM Phenyl Methyl Sulfonyl Fluoride (PMSF). The Mature-VCC was purified by passing through Q-sepharose column. Purified Mature-VCC was analysed by SDS-PAGE and Coomassie staining. Protein concentration was estimated by monitoring the A_{280} using the theoretically calculated absorbance value as predicted from the protein's primary structure (1.6 for 1 mg/ml Mature-VCC).

Purification of Pro-domain protein

Nucleotide sequence encoding the Pro-region of Pro-VCC was PCR-amplified and cloned into the pET14b expression vector between the Nde1 and BamH1 sites. Nucleotide sequence was verified by DNA sequencing. Recombinant vector harbouring the cloned gene was transformed into *E. coli* Origami B cells. Protein expression was induced with 1 mM IPTG. Protein was purified by Ni-affinity chromatography followed by anion-exchange chromatography on Q-sepharose. Homogeneity of the purified protein was analysed by SDS-PAGE and Coomassie staining. Protein concentration was estimated by monitoring A_{280} based on the theoretically predicted extinction coefficient based on the primary structure of the protein.

Fluorescence Measurements

Fluorescence spectra were measured using Perkin-Elmer LS55 spectrofluorimeter in a quartz cell of 10 mm pathlength. Protein concentration of 75 nM was used for Pro-VCC and Mature-VCC. For purified Pro-domain, a protein concentration of 1 µM was used.

For intrinsic tryptophan fluorescence spectra, the protein samples were excited at wavelength of 290 nm, and tryptophan fluorescence emission was measured between 310-400 nm. The slit widths were kept at 2.5 nm and 5 nm for excitation and emission, respectively. For measuring the steady-state tryptophan fluorescence intensity, data was collected in triplicates at 340 nm and 355 nm. Integration time of 20 seconds was used. All the spectra were corrected with respect to the buffer spectra.

1-anilinonaphthalene-8-sulfonic acid (ANS) (Sigma-Aldrich) binding to the protein was measured using a Perkin-Elmer LS55 spectrofluorimeter. Protein solutions containing a final ANS concentration of 2 μM were excited at 350 nm using an excitation and emission slit width of 2.5 nm and 5.0 nm, respectively. For steady state ANS fluorescence intensity measurements, data were collected in triplicates at an emission wavelength of 480 nm and 20 second integration time. For measuring the kinetics of ANS binding to protein samples, intensity values at 480 nm were collected with an interval of 10 seconds and integration time of 5 seconds. Data were collected with an initial delay of 10 seconds after mixing ANS into the protein samples. All spectra and intensity values were corrected with suitable buffer blanks containing ANS only.

Aggregation of protein was followed by monitoring the increase in light scattering using the Perkin-Elmer LS 55 spectrofluorimeter setup. For measurement of the aggregation kinetics, light scattering intensities were recorded at 550 nm upon excitation at the same wavelength, using excitation and emission slit widths of 2.5 and 2.5 nm, respectively. Data were recorded at an interval of 10 s with an integration time of 5 s.

Far-UV circular dichroism experiments

Far-UV circular dichroism (CD) measurements were taken on an Applied Photophysics Chirascan spectropolarimeter with a Peltier based temperature controlled sample chamber in a quartz cuvette of 5 mm pathlength. A final protein concentration in the range of 0.5-1 μM for Pro-VCC and Mat-VCC was used. For Pro-domain alone, a concentration range of 2-4 μM was used. All the CD spectra were corrected for the respective buffer blanks.

Structural Analysis

The coordinates for Pro-VCC crystal structure were obtained from the Protein Data Bank (PDB) (Entry 1XEZ). The coordinate for Mature-VCC lacking the N-terminal Pro-domain was generated using the PDBSET in CCP4 suite (112). Areaimol (113) in CCP4 was used to calculate the accessibility of tryptophan residues in both the structures. APBS tool in

PyMol was used to calculate the surface electrostatic potential of both the structures (114). For determining the surface hydrophobic patches on the proteins, HOTPATCH server (http://hotpatch.mbi.ucla.edu/) was used. The Pymol Molecular Graphics System found online (http://www.pymol.org) was used for visualizing the structures (115).

Data Analysis

The data obtained were analysed using OriginPro version 8.0. Steady state and kinetics data obtained from the fluorescence, light scattering and CD experiments were analysed using the Non-linear curve fittings function in OriginPro 8.0. R^2 values and residuals were analysed to check the quality of the curve fitting.

2.4 Results

Purification and structural analysis of Pro-VCC and Mature-VCC

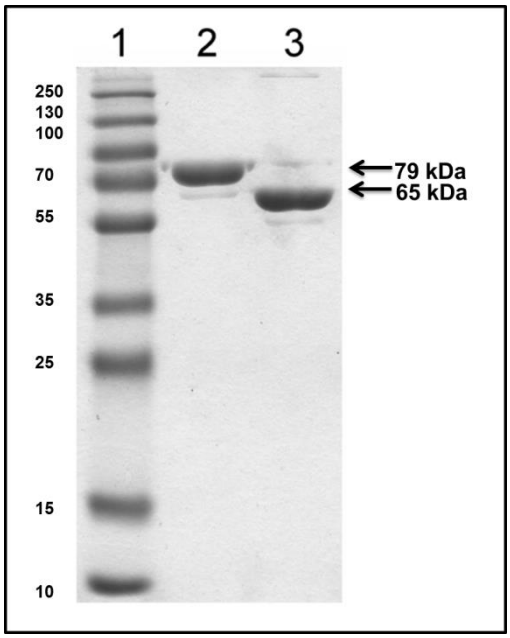

Figure 2.1: SDS-PAGE profile of Pro-VCC (Lane 2) and Mature-VCC (Lane 3) as visualized by Coomassie staining.

The gene for Pro-VCC lacking the signal peptide was cloned into the expression vector pET14b, and the protein was overexpressed in *E. coli* Origami B cells. The hemolytically inactive form (Pro-VCC) was purified to homogeneity (Figure 2.1). The functionally active form of the protein (Mature-VCC) was generated by proteolytic removal of the N-terminal Pro-domain (Figure-2.1). The primary amino acid sequence of Pro-VCC and the mature form of the toxin show the presence of 12 and 11 tryptophan residues,

respectively (1 tryptophan residue in Pro-VCC being contributed by the Pro-domain). Removal of the N-terminal Pro-domain does not result in any major change in the %content of the tryptophan residues in the Pro- and Mature-VCC (1.7% and 1.9%, respectively).

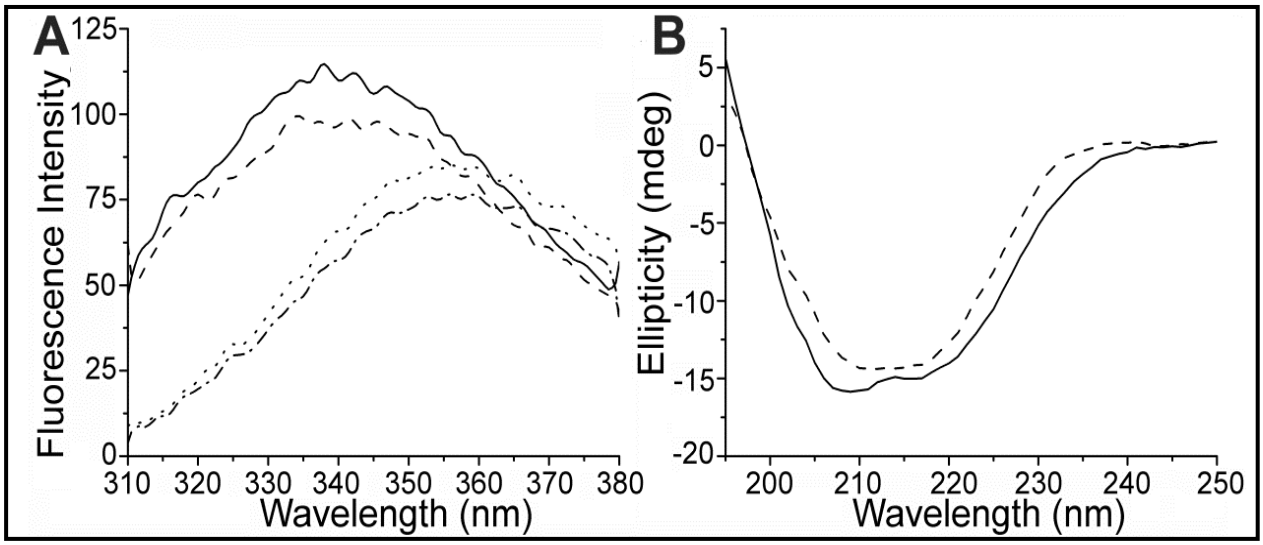

Figure 2.2: Characterization of the recombinant Pro-VCC and Mature-VCC proteins. (A) Intrinsic tryptophan fluorescence emission spectra of Pro-VCC and Mature-VCC under native and denatured conditions. Pro-VCC in 0 M urea; (– –), Mature-VCC in 0 M urea; (—), Pro-VCC in 8 M urea; (– · –), Mature-VCC in 8 M urea; (····). (B) Far-UV CD profile of Pro-VCC; (– –) and Mature-VCC; (—).

Consistent with this, the two proteins displayed similar intrinsic tryptophan fluorescence spectra upon excitation at 290 nm (Figure 2.2). Both the variants displayed intrinsic tryptophan fluorescence spectrum with maxima at around ~339 nm, upon excitation at 290 nm, when tested under the native condition. When tested under the denaturing condition in presence of 8 M urea, the two proteins exhibited nearly overlapping tryptophan fluorescence emission profile with emission maxima at around ~355 nm (Figure 2.2). Taken together, intrinsic tryptophan fluorescence spectra indicated overall similar environments for the tryptophan residues in the precursor and the mature form of the VCC molecule (Figure 2.2). This, in turn, indicated overall similar global tertiary structures for the Pro-VCC and the Mature-VCC molecules. The analysis of the surface distribution of the electrostatics/hydrophobic patches on the two protein variants also predicted a similar trend (Figure 2.3).

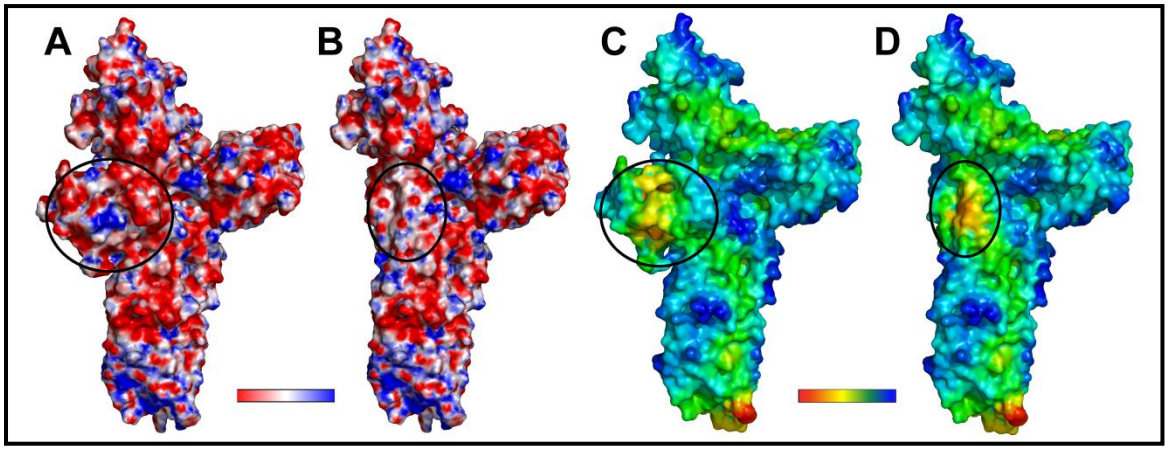

Figure 2.3: Analysis of surface distribution of the electrostatics/hydrophobic patches on Pro-VCC and Mature-VCC. Surface electrostatic potentials on the Pro-VCC **(A)** and Mature-VCC structures **(B)** were calculated and visualized using PyMol APBS tools, and are contoured from -10 (red) to +10 (blue). The probability of surface hydrophobic patches on the Pro-VCC **(C)** and Mature-VCC structures **(D)** were calculated using the HOTPATCH server (http://hotpatch.mbi.ucla.edu/), and were visualized using PyMOL (115) as colored from red (hydrophobic) to blue (hydrophilic) gradient.

Pro-VCC and Mature-VCC show similar changes in the global tertiary structure during low pH-induced unfolding as monitored by intrinsic tryptophan fluorescence

Since the two proteins displayed an overall similarity in terms of global tertiary structures under the native condition (as revealed by the intrinsic tryptophan fluorescence emission profile), we wanted to probe if Pro-VCC and Mature-VCC have similar physicochemical properties. To differentiate between the physicochemical properties of the two variants, we first studied the unfolding behaviour of the two forms of the toxin under low pH conditions using intrinsic tryptophan fluorescence emission spectroscopy. Changes in pH conditions are known to influence protein stability by altering the net charge on a protein molecule. This destabilisation causes the protein molecules to unfold resulting in an increase in the solvent exposure of buried tryptophan residues, which would be reflected in a red shift in the intrinsic tryptophan fluorescence emission maxima. To monitor low pH-induced unfolding propensity, the proteins (Pro-VCC and Mature-VCC) were incubated with buffers of varying pH in the range of 2.25-7.0. The intrinsic tryptophan fluorescence spectra of the two proteins were compared as a function of different low pH conditions to monitor the unfolding behaviour of the precursor and mature form of the toxin (Figure 2.4).

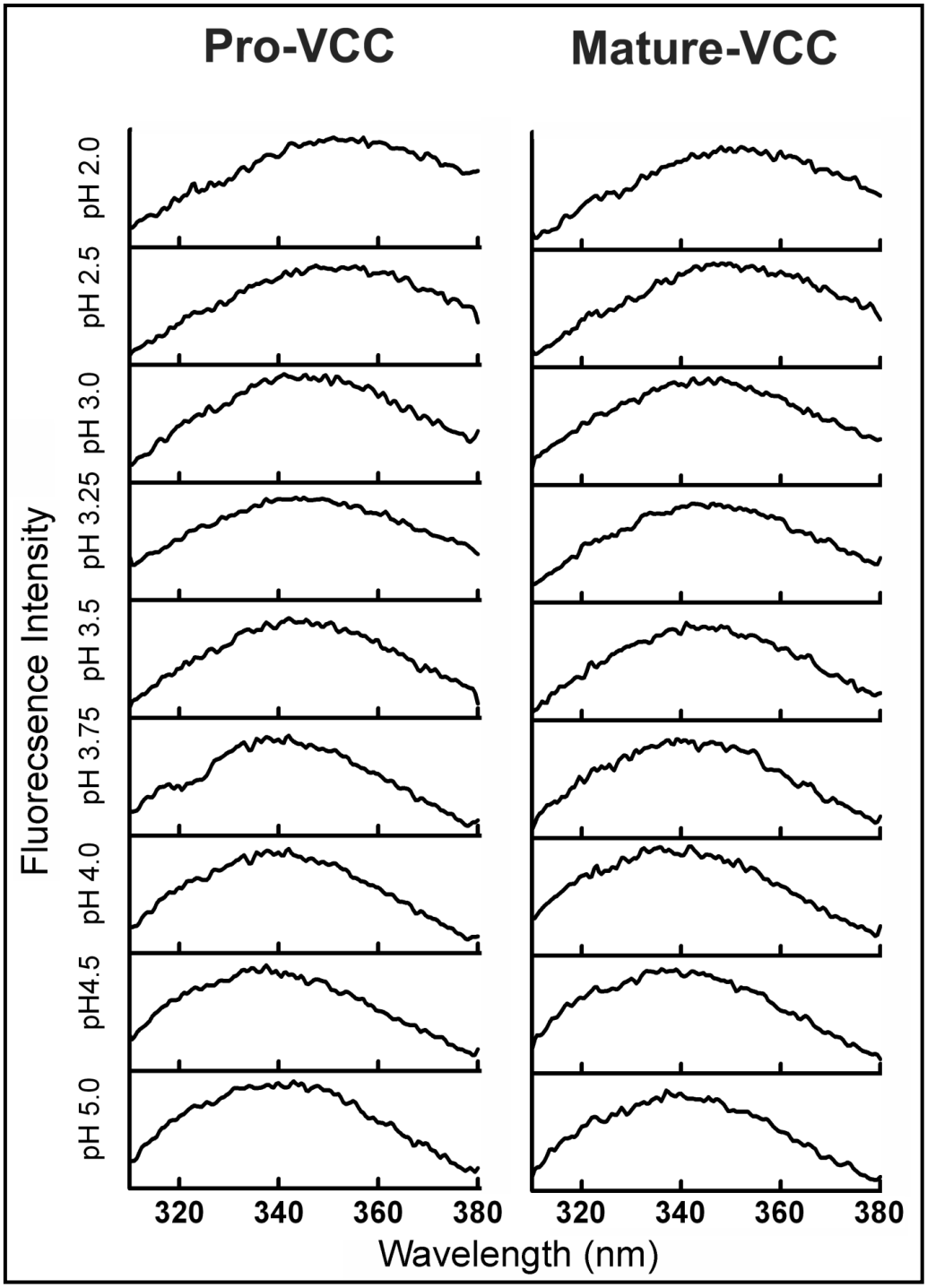

Figure 2.4: Low pH-induced conformational changes in Pro-VCC and Mature-VCC as monitored by intrinsic tryptophan fluorescence emission spectroscopy.

To gain a quantitative insight into the low pH-induced unfolding behaviour of the proteins, we compared the changes in the ratio of fluorescence emission pattern i.e. I_{340}/I_{355} (fluorescence emission intensities at 340 nm and 355 nm), upon excitation at 290 nm (Figure 2.5). A drop in the I_{340}/I_{355} ratio indicated a red shift in the tryptophan fluorescence emission maxima, resulting from the increased solvent exposure of tryptophan residues. Both the

proteins showed a two-step transition in response to low pH-induced unfolding: the first transition in the I_{340}/I_{355} value came in the pH range of 3.0-4.0, followed by the second transition in the pH range of 2.0-3.0 (Figure 2.5). Our data suggested that Pro-VCC and Mature-VCC follow a similar pattern during low pH-induced unfolding in terms of changes in the global tertiary structures.

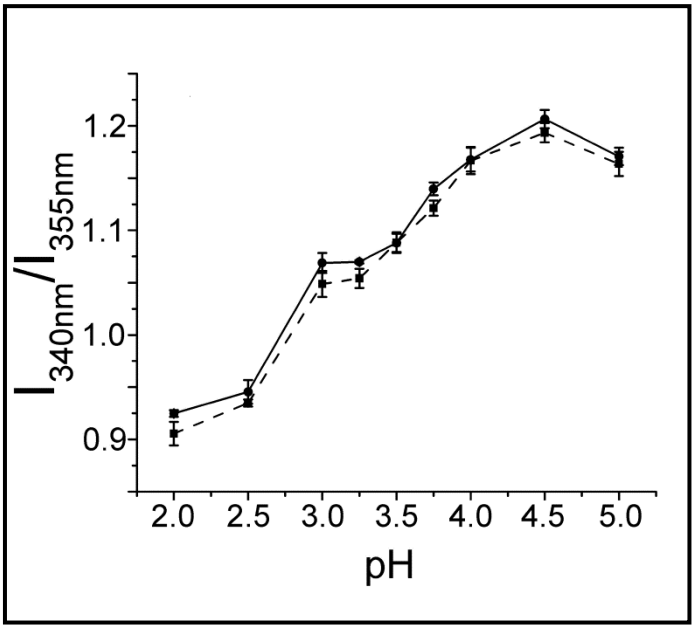

Figure 2.5: Changes in the ratio of fluorescence emission pattern i.e. I_{340}/I_{355} (fluorescence emission intensities at 340 nm and 355 nm) under low pH conditions. I_{340}/I_{355} values were plotted as function of pH. Error bars indicate the standard deviations determined from at least three measurements.

Low pH-induced unfolding induces different extents of local conformational changes in Pro-VCC and Mature-VCC as revealed by ANS binding

Pro-VCC and Mature-VCC showed no difference in terms of changes in the global tertiary structures in response to low pH-induced unfolding. Next, we wanted to probe if the two proteins show a similar trend with respect to local conformational changes in terms of opening up of surface-exposed hydrophobic patches. Initial events during acid-induced unfolding of proteins lead to local conformational changes (primarily, surface exposure of hydrophobic patches). 1-Anilino-8- naphthalene sulfonic acid (ANS) is a dye that binds to pre-existing hydrophobic (nonpolar) patches on protein surfaces (through its nonpolar anilino-naphthalene group) that are mostly absent in the native and completely denatured forms of the protein. This binding results in an increase in ANS fluorescence emission intensity and a blue shift in the fluorescence emission maxima (from 520 nm in water to 480 nm in nonpolar environment). Hence, the increase in ANS fluorescence intensity can be directly correlated with the extent of opening of hydrophobic patches on the protein surface.

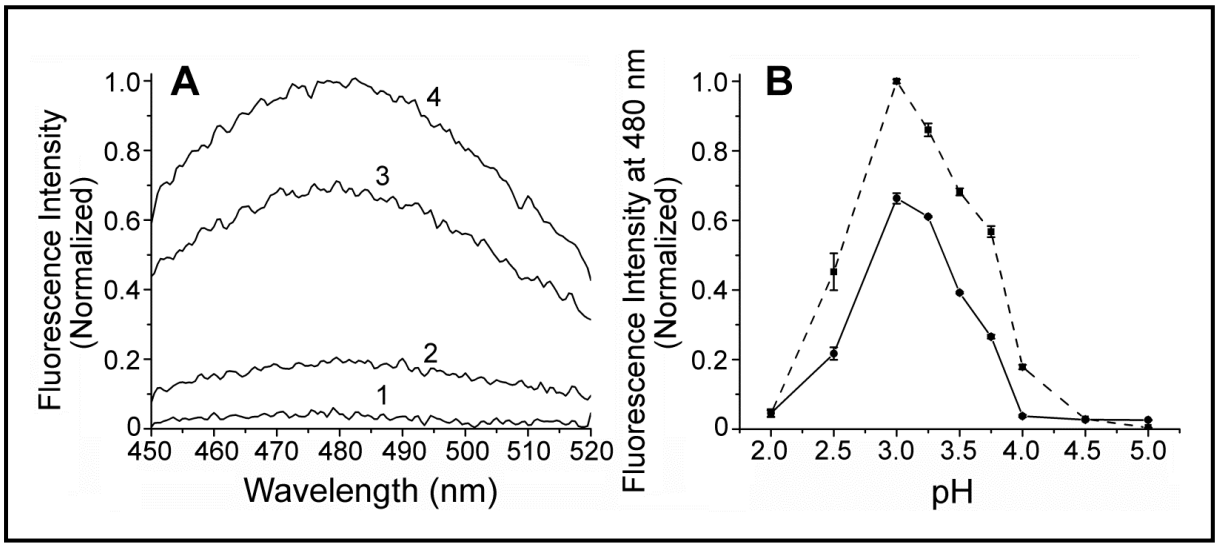

Figure 2.6: Local conformational changes in Pro-VCC and Mature-VCC due to low pH-induced unfolding as monitored by ANS binding. (A), ANS fluorescence emission spectra of Pro-VCC (curve 2, at pH 4.0; curve 4, at pH 3.0) and Mature-VCC (curve 1, at pH 4.0; curve 3, at pH 3.0). (B) Comparison of ANS fluorescence emission intensities of Pro-VCC (– –) and Mature-VCC (—) at different low pH conditions.

Exposure of the proteins in the pH range of 3.0-4.0 resulted in a drastic change in ANS fluorescence emission intensity (Figure 2.6). Interestingly, both the proteins displayed maximum ANS binding (as revealed from the fluorescence intensity measurements at 480 nm) at pH 3.0 with the Pro-VCC showing considerably higher ANS binding in comparison to Mature-VCC. Also, the precursor form of the protein displayed ANS binding even at pH 4.0, which is a condition where no change in the global tertiary structure of the protein was observed (Figure 2.6). This observation suggested that the precursor protein is much more amenable to low pH-induced local conformational changes in terms of exposure of surface hydrophobic patches as compared to the mature form. Further unfolding at pH<3.0 resulted in a loss of ANS binding by both the proteins. This could be a result of the loss of the surface hydrophobic patches that existed in the conformational states in the pH range of 3.0-4.0. This is also consistent with our data from the intrinsic tryptophan fluorescence study, where the exposure of the proteins below pH 3.0 resulted in a drastic change in the I_{340}/I_{355} value, presumably resulting in the loss of protein structures supporting the surface hydrophobic patches.

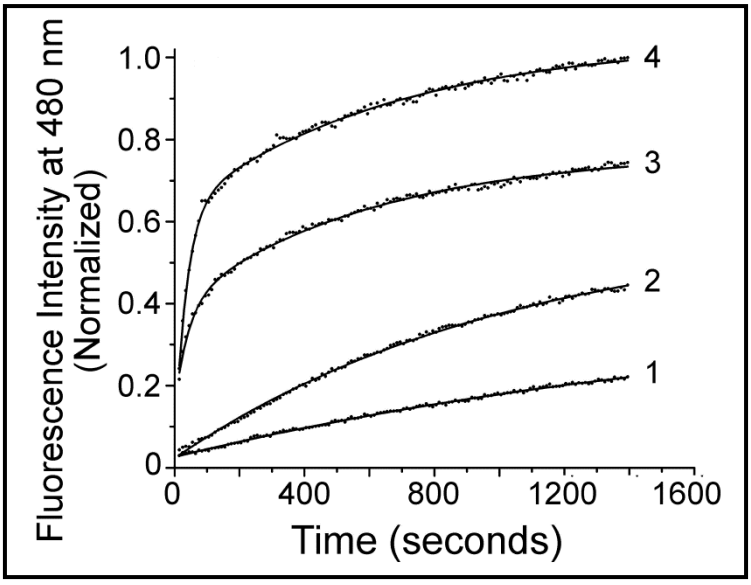

Figure 2.7: Kinetics of ANS binding to Pro-VCC and Mature-VCC. Kinetics of ANS binding was monitored for Pro-VCC (curve 2, at pH 4.0; curve 4, at pH 3.0) and Mature-VCC (curve 1, at pH 4.0; curve 3, at pH 3.0).

Since, the two proteins displayed a significant difference in steady state binding to ANS, we decided to compare the kinetics of ANS binding to the two proteins at pH 3.75 (pH condition at which both the proteins started to exhibit ANS binding) and pH 3.0 (pH condition at which both the proteins show maximum ANS binding) (Figure 2.7). The fitting of kinetics data at pH 3.75 to single exponential function revealed the time constants (t) of 9.6 x 10^{-4} s^{-1} and 5.26 x 10^{-4} s^{-1} for Pro-VCC and Mature-VCC, respectively. Similarly, the kinetics of binding to ANS at pH 3.0 fitted to bi-exponential function revealed the following time constants: t_{fast} = 0.0285 s^{-1} and t_{slow} = 0.0015 s^{-1} for Pro-VCC, and t_{fast} = 0.0245 s^{-1} and t_{slow} = 0.00166 s^{-1} for Mature-VCC. The above fittings showed that, at both the pH conditions Pro-VCC binds to ANS at a much faster rate as compared to Mature-VCC. Since, the increase in ANS binding can be directly correlated with the increase in surface exposed hydrophobic patches, the data suggested that the Pro-VCC molecule responds to low-pH conditions by undergoing local conformational changes in terms of surface exposed hydrophobic patches at a significantly higher rate as compared to Mature-VCC.

Pro-VCC differentiates from Mature-VCC in terms of changes in the secondary structure elements during low pH-induced unfolding

We wanted to probe whether the removal of the Pro-domain results in any changes in secondary structure composition of Mature-VCC using far-UV circular dichroism (CD). Studies with model proteins have shown that α-helical and β-sheet containing proteins display characteristic far-UV CD spectra: α-helical proteins displaying two negative minima, one at 222 nm and the other at 208 nm; β-sheet containing proteins showing negative ellipticity minima at around 216 nm. Pro-VCC at neutral pH displayed broad negative minima between 218-209 nm, characteristic of proteins composed primarily of β-sheet structures. Interestingly, removal of the Pro-domain resulted in a notable change in the secondary structure composition of VCC. Mature-VCC displayed prominent negative minima at 209 nm with a shoulder at 218 nm. Far-UV CD spectra of the two proteins suggested that Pro-VCC and Mature-VCC have distinct secondary structure composition (Figure 2.8).

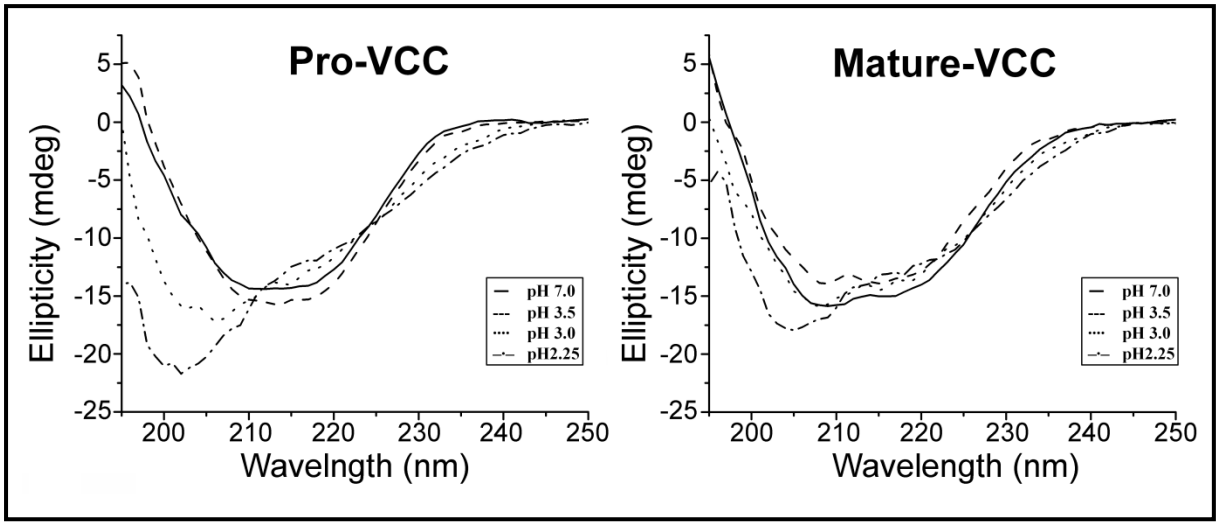

Figure 2.8: Changes in the secondary structure composition of Pro-VCC and Mature-VCC under low pH conditions as monitored by far-UV CD spectroscopy. Pro-VCC and Mature-VCC proteins were incubated with buffers in the pH range of pH 7.0 to pH 2.25; changes in the secondary structure composition were probed by far-UV CD spectroscopy**.**

We wanted to explore whether the Pro-VCC and Mature-VCC show similar pattern in terms of changes in the secondary structure composition when subjected to low pH-induced unfolding. Mature-VCC displayed a rather stable secondary structure in response to low pH range 3.0-7.0, as there was no major effect on the far-UV CD spectra of the protein. At pH 2.25, Mature-VCC displayed a drastic change in the far-UV CD spectrum with negative minima at 205 nm, suggesting a major transition toward random coil secondary structure

(Figure 2.8). Interestingly, Pro-VCC displayed more profound changes in the secondary structure composition due to low pH induced unfolding. At pH 3.0, the negative minima shifted to 205 nm; more acidic condition at pH 2.25 resulted in a severe change in the Pro-VCC secondary structure with a shift of negative minima to 202 nm (Figure 2.8). Overall, the results clearly indicated that the two proteins, Pro-VCC and Mature-VCC have distinct secondary structure composition, and they respond differently to low pH-induced unfolding, with Pro-VCC being much more amenable to changes in the secondary structure composition as compared to Mature-VCC.

Pro-VCC and Mature-VCC exhibit different extents of aggregation during low pH-induced unfolding

Our ANS binding clearly indicated that low pH-induced unfolding of Pro-VCC and Mature-VCC in the pH range 2.5-4.0 led to exposure of hydrophobic patches on surface of both the proteins. During the event of protein unfolding, changes in the secondary and tertiary structure of the proteins lead to exposure of hydrophobic regions that remain buried in the native protein conformation. The hydrophobic regions in a partially unfolded protein tend to aggregate to minimize exposed surface area. Therefore, we wanted to explore the possibility of surface hydrophobicity-triggered aggregation of Pro-VCC and Mature-VCC. Aggregation of both the proteins was monitored by using light scattering (Figure 2.9). The intensity of light scattering is proportional to mass of the macromolecule. Thus, any increase in light scattering would directly relate to an increase in protein aggregation.

Exposure to low pH conditions in the range 3.0-4.0 triggered aggregation in both proteins, with Pro-VCC displaying a significantly increased propensity toward formation of soluble aggregates. Starting at pH 4.0, both proteins showed formation of aggregates with a peak at pH 3.5 (Figure 2.9). At pH 3.0, it nearly approached basal level, contradicting our ANS binding data where both proteins displayed maximum ANS binding at pH 3.0 (pH range triggering maximum exposure of surface hydrophobic patches). It should be noted that proteins become highly positively charged at low pH conditions due to excessive protonation of glutamate and aspartate residue. This causes repulsion in the protein molecule, which hinders any intra- or intermolecular interactions. Hence, maximum aggregation of Pro-VCC and Mature-VCC at pH 3.5 could be a result of an optimal compromise between the exposure surface hydrophobic patches and repulsion caused by an overall net positive charge on the protein. The kinetics of aggregation at pH 3.5 and 3.75 could be fit to sigmoidal function for both the proteins. The fitting showed presence of a transient lag phase followed by an

exponential phase. Presence of a transient lag phase clearly indicates that aggregation of both proteins is triggered by low-pH induced exposure of surface hydrophobic patches. ANS binding data showed an increased tendency of Pro-VCC toward exposure of surface hydrophobic patches under low pH conditions. Consistent with ANS binding data, Pro-VCC also demonstrated an increased tendency to form aggregates triggered by low pH-induced exposure of surface hydrophobic patches as compared to Mature-VCC. Interestingly, Pro-VCC displayed increased aggregation as the result of exposure of surface hydrophobic patches even in the absence of any major changes in the global tertiary or secondary structure of the protein, as observed form the combined intrinsic tryptophan fluorescence, ANS binding, far-UV CD and light scattering data.

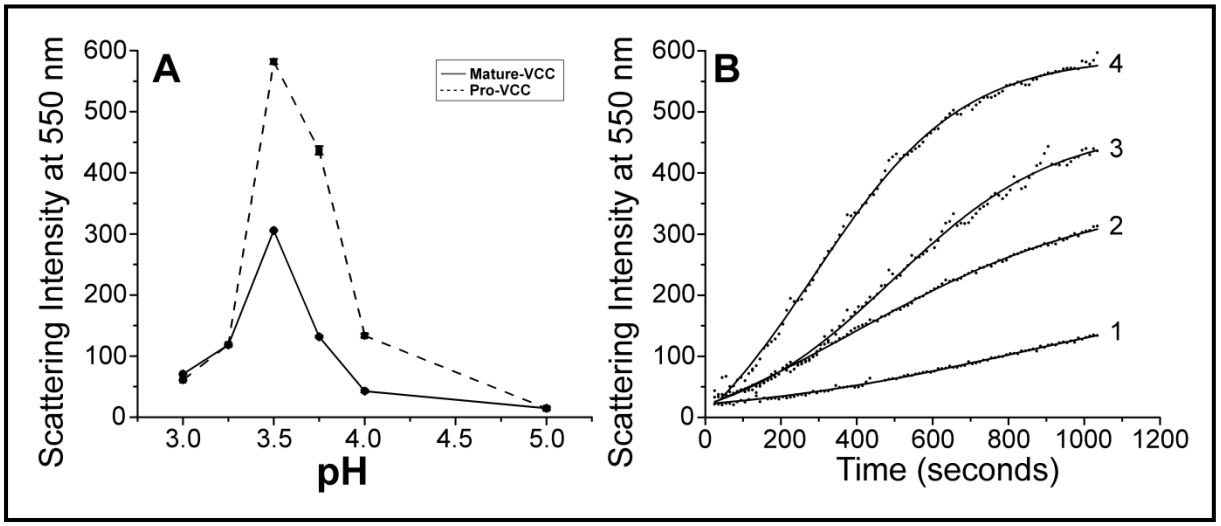

Figure 2.9: Comparison of aggregation propensity of Pro-VCC and Mature-VCC under low pH conditions. (A) Pro-VCC and Mature-VCC were incubated with buffers in the pH range pH 5.0 to pH 2.0, aggregation propensity of the two proteins was estimated by measuring the extent of light scattering. Error bars indicate standard deviation determined from three measurements. (B) Time courses of protein aggregation followed at two particular low-pH conditions for Pro-VCC (curve 3, at pH 3.75; curve 4, at pH 3.5) and Mature-VCC (curve 1, at pH 3.75; curve 2, at pH 3.5). Data could be best fit to a sigmoidal function as shown by solid lines.

Pro-VCC displays an increased propensity toward urea-induced denaturation at physiological pH as compared to Mature-VCC

The data so far clearly indicated that Pro-VCC was much more susceptible low pH-induced changes in global tertiary and secondary structure in terms of exposure of surface hydrophobic patches, changes in the secondary structures, and propensity toward aggregation, as compared to Mature-VCC. To further distinguish the physicochemical

properties of the two proteins at physiological pH, we studied the response of Pro-VCC and Mature-VCC toward urea-induced denaturation by monitoring changes in the intrinsic tryptophan fluorescence (in terms of I_{340}/I_{355}) of the two proteins as a function of different concentrations of the denaturant (Figure 2.10). Chemical denaturants like urea destabilize protein structure by disrupting non-covalent interactions that hold the protein in its folded state. The data obtained from the urea-induced denaturation of Pro-VCC and Mature-VCC were fit to a two state sigmoidal function, and mid-point of transition from native to unfolded state were estimated. For Pro-VCC the mid-point of unfolding transition occurred in urea concentration range of ~2.25, whereas for its mature counterpart, the mid-point occurred in the urea concentration range of ~3.25 (Figure 2.10). Consistent with the previous observations, Pro-VCC displayed an increased propensity to undergo changes in global tertiary structure as compared to Mature-VCC in terms of urea-induced unfolding even at physiological pH of 7.0.

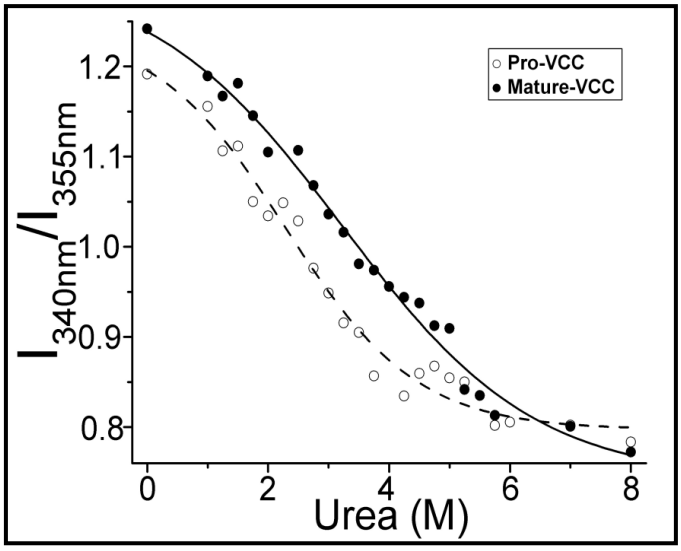

Figure 2.10: Comparison of unfolding of Pro-VCC and Mature-VCC under different urea concentrations. Unfolding behaviour of Pro-VCC and Mature-VCC was monitored by measuring intrinsic tryptophan fluorescence emission in terms of changes in the ratio of I_{340}/I_{355} as a function of urea concentration. Data were globally fit to a sigmoidal function to determine the apparent denaturant concentration at the midpoint of the curve.

Pro-VCC and Mature-VCC show distinct conformational changes in response to the thermal denaturation

To further explore the differences in the structural stability of Pro-VCC and Mature-VCC, we studied thermal denaturation of the two proteins in the temperature range 25 ˚-80 ˚C

using far-UV circular dichroism (CD) (Figure 2.11). Thermal denaturation involves increasing the temperature of a protein solution, which weakens non-covalent interactions that hold the protein in its native folded state. Far-UV CD spectra of Pro-VCC (Figure 2.11A) and Mature-VCC (Figure 2.11B) under different temperature conditions showed a striking difference in the thermal stability profile of the two proteins. To gain a quantitative insight into the secondary structural changes in Pro-VCC and Mature-VCC as a function of temperature, the ratio of ellipticity values in the wavelength range of 208-210 to those in 217-219 ($mdeg_{208-210}/mdeg_{217-219}$) were plotted (Figure 2.11C). The combined analysis of far-UV CD spectra, and $mdeg_{208-210}/mdeg_{217-219}$ plot, revealed two-step conformational change for both the proteins, during the event of thermal denaturation.

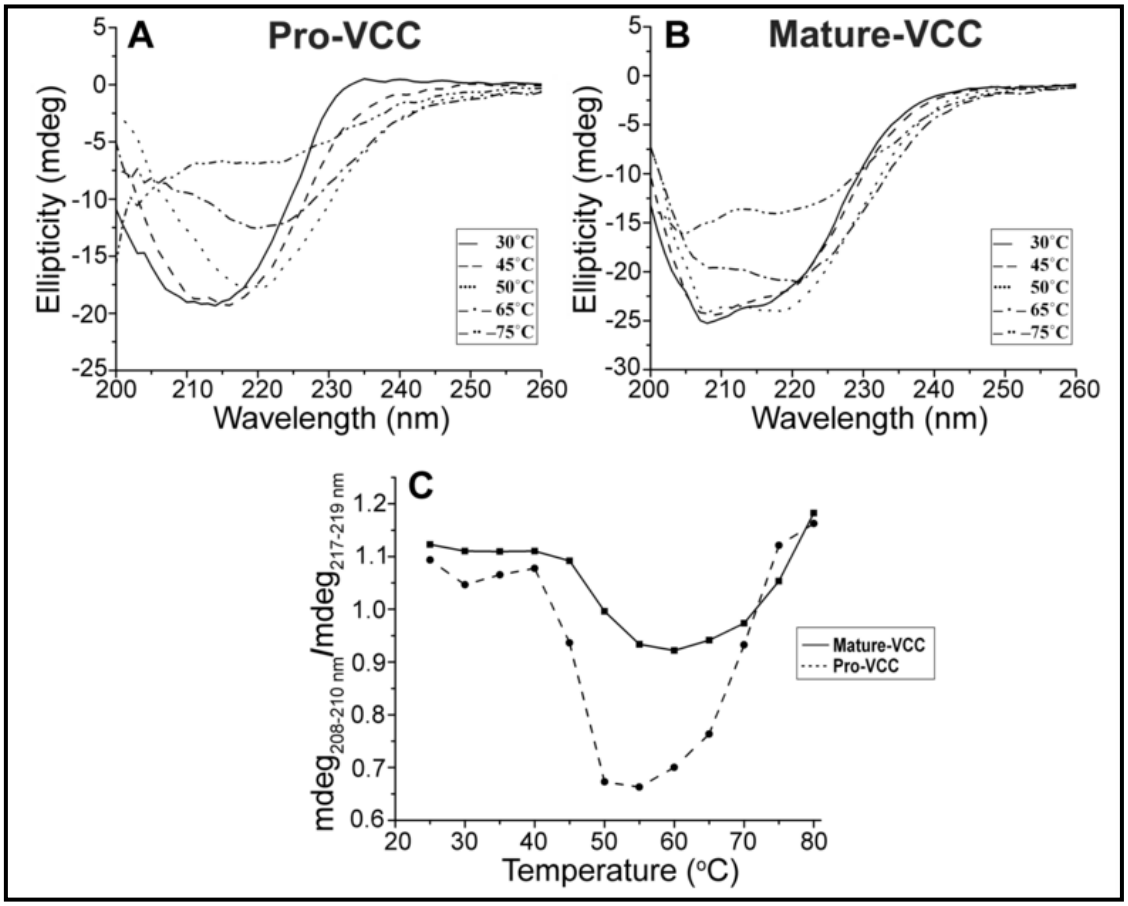

Figure 2.11: Thermal unfolding of Pro-VCC and Mature-VCC monitored by far-UV CD spectroscopy. (A-B) Pro-VCC and Mature-VCC proteins were incubated under different temperature conditions in the range of 25˚C - 80˚C, changes in the secondary structure composition were probed by far-UV CD spectroscopy. (C) Plot of ratio of $mdeg_{208-210nm}/mdeg_{217-219nm}$ for Pro-VCC and Mature-VCC as a function of different temperature.

Starting at a temperature range of 50 ˚-55 ˚C Mature-VCC showed the first transition in the form of unfolding intermediates with slightly altered secondary structure. At higher

temperatures (>55˚C), the negative ellipticity minima shifted to ~219 nm. Mature-VCC approached random coil structure at temperatures higher than 65 ˚C (Figure 2.11B). Pro-VCC exhibited more profound changes in the secondary structure in response to high temperature-induced denaturation, with the first transition at a temperature range of 45 ˚-50 ˚C; the far-UV CD spectra experienced a red-shift in negative ellipticity minima at ~218 nm due of formation of unfolding intermediates. At temperatures above 60 ˚C, Pro-VCC approached a random coil structure (Figure 2.11A). Thus, consistent with previous observations, Pro-VCC was more susceptible to changes in the secondary structure as compared to Mature-VCC.

Unfolding behaviour of the Pro-domain in isolation

So far, our studies, probing the structural and conformational changes in Pro-VCC and Mature-VCC in response to a wide array of denaturing conditions, clearly suggested that Pro-VCC had an enhanced propensity to undergo unfolding compared to the Mature-VCC. Pro-VCC is a ~79 kDa molecule with an additional ~15 kDa Pro-domain. So, we wanted to explore the possibility whether the strengthened unfolding propensity displayed by Pro-VCC was due to the increased unfolding of Pro-domain alone in the Pro-VCC structure. In this direction we probed the structural and conformational stability of Pro-domain in response to several denaturing conditions (Figure 2.12). The X-ray crystal structure of Pro-VCC showed that Pro-domain contains a single slightly exposed tryptophan residue. Consistent with this, intrinsic tryptophan fluorescence emission spectra of Pro-domain showed emission maxima at 339 nm (Figure 2.12A). The far-UV CD spectra of Pro-domain revealed two negative ellipticity minima, one at 222 nm and the other at 208 nm, consistent with the typical α-helical proteins (Figure 2.12A).

Pro-domain displayed a strong resistance toward low pH-induced unfolding in term of global tertiary structural changes. There was no major change in the intrinsic tryptophan fluorescence emission and ANS fluorescence profile upon low pH treatment (data not shown). Similarly, Pro-domain showed no significant change in the secondary structural organization during low pH-induced unfolding as monitored by far-UV CD spectroscopy (Figure 2.12B). Up to pH 3.0, a slight decrease in ellipticity value was noted without any change in the positions of the negative ellipticity minima. Only at a more acidic pH of 2.0, an increase in the non-native α-helical structures was observed (Figure 2.12B). Consistent with this the Pro-domain exhibited resistance toward thermal denaturation (Figure 2.12D). The data revealed a two-state unfolding from the native α-helical to random coil structure, with transition mid-point at temperature range of 65 ˚-70 ˚C. Pro-domain protein also displayed

similar resistance toward urea-induced unfolding with transition mid-point of 4.75 M (Figure 2.12C), as compared to 2.25 M and 3.25 M for Pro-VCC and Mature-VCC, respectively. Altogether, the Pro-domain displayed increased resistance toward unfolding upon exposure to a wide array of denaturing conditions, and thus represented a stable and robust component of the Pro-VCC structure. This clearly suggested that the strengthened unfolding propensity exhibited by Pro-VCC was not the result of the increased unfolding propensity of the Pro-domain itself within the Pro-VCC architecture.

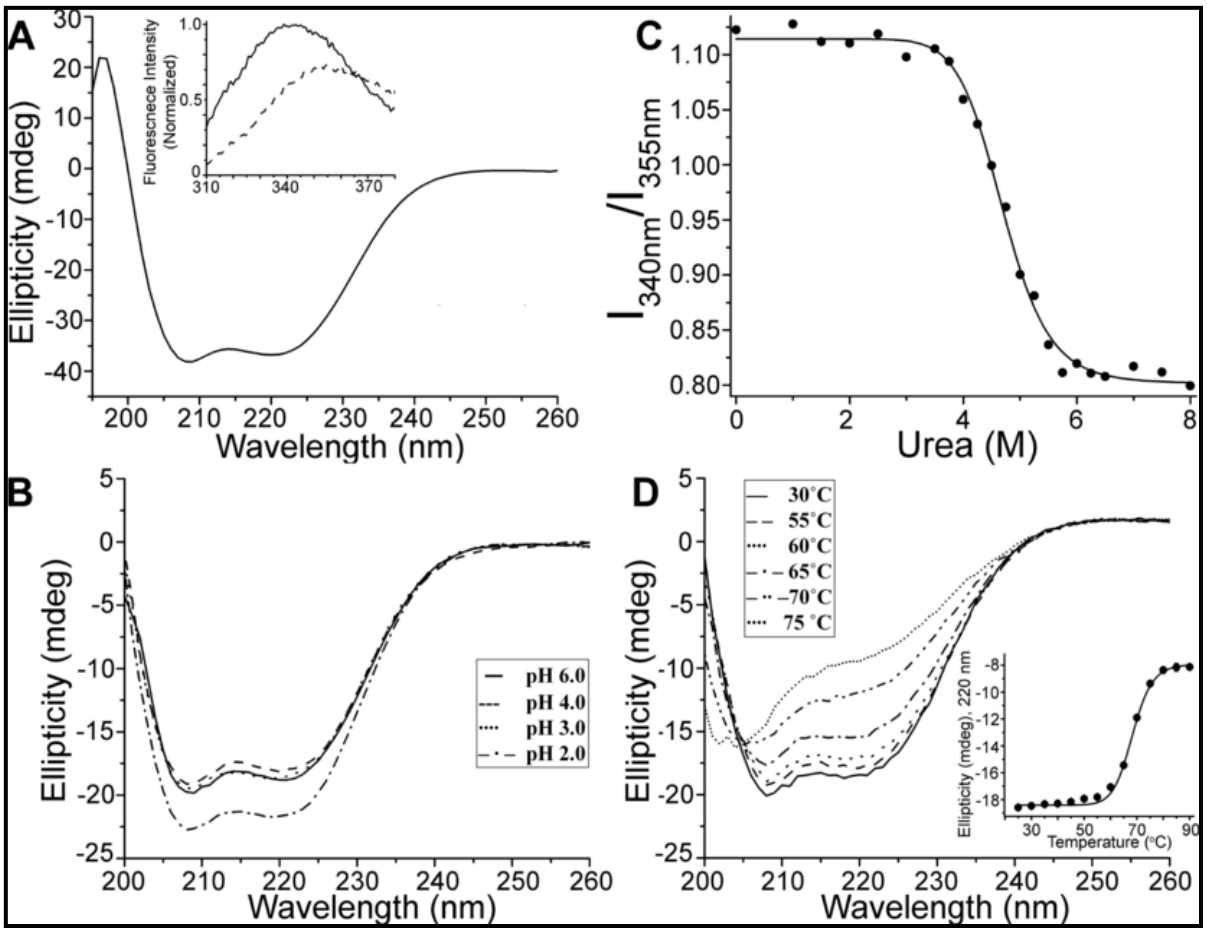

Figure 2.12: Physico-chemical characterization of the VCC Pro-domain (A) Far-UV CD spectra of Pro-domain. (Inset) Intrinsic tryptophan fluorescence emission spectra of pro-domain under native conditions (—), under denaturing conditions (8M urea) (--) (B) Far-UV CD spectra of Pro-domain at different pH. (C) Urea-induced unfolding of 'Pro-domain' protein as monitored by intrinsic tryptophan emission fluorescence. (D) Thermal unfolding of 'Pro-domain' monitored by far-UV CD spectroscopy.

2.5 Discussion

The primary characteristic of the structural architecture of the β-PFTs is the presence of a central cytolysin domain. The cytolysin domain alone is responsible for membrane

binding and subsequent oligomerization of the toxin on the target cell membranes. VCC is a prominent member in the β-PFT family. VCC is one of the few members of this family to have an atypical domain architecture, i.e. presence of accessory domains. X-ray crystal structure of Pro-VCC shows presence of three additional domains, namely, the N-terminal Pro-domain, C-terminal β-trefoil lectin-like domain, and a β-prism lectin-like domain (22). Although the exact functions of these domains remained unknown, the C-terminal lectin-like domains are proposed to play role(s) in the recognition and binding of specific cell surface glycan receptors on the target cells (104). The N-terminal Pro-domain is not a part of the functional Mature-VCC, as it is proteolytically removed during activation of the toxin. Earlier studies have shown that the absence of the Pro-domain results in the degradation of VCC in the bacterial periplasmic space. Chemically denatured Pro-VCC recovers complete activity upon refolding, but Mature-VCC lacking the Pro-domain does not refold into its native architecture (97). These studies suggest that Pro-domain might aid in the efficient folding of VCC molecule into its native architecture. The Pro-domain also bears sequence similarity with the Hsp90 family of chaperones (95). Since the location of the Pro-domain is within the VCC molecule, it has been suggested as an intramolecular chaperone-like entity. Apart from this, the exact role of the Pro-domain in the structure-function mechanism of VCC remains largely unclear. The other examples of β-PFTs that contain Pro-domains in the toxin precursor forms include aerolysin from *A. Hydrophila* (41) and α-toxin from *Clostridium septicum* (17). In order to explore the role of the Pro-domain in the VCC mode of action, we probed the role of the VCC N-terminal Pro-domain in the context of the structural and conformational properties of the toxin.

In order to probe the implication of the Pro-domain in VCC structure-function mechanism, we compared the physicochemical properties of Pro-VCC and Mature-VCC. Under native conditions, both the variants exhibited similar tryptophan environments as revealed by the intrinsic tryptophan fluorescence emission profile. This suggested that both the variants of VCC share a similar global tertiary structure. However, the variants displayed notable differences in terms of secondary structural composition when probed by far-UV CD spectroscopy. It must be noted that differences in the secondary structure of Pro-VCC and Mature-VCC could be explained by the contributions from the Pro-domain alone. We explored the possibility whether the two variants of VCC differ in terms of their physicochemical properties that might be relevant in terms of the overall VCC mode of action. To explore this hypothesis, we have conducted a detailed comparison of unfolding behaviour of the two forms of the VCC toxin, the precursor Pro-VCC and its proteolytically

processed active variant, Mature-VCC. We have monitored unfolding of the VCC variants induced by an array of denaturing conditions such as exposure to low pH, chemical denaturants such as urea, and high temperatures, using intrinsic tryptophan fluorescence emission, far-UV CD and light scattering. Both the proteins displayed similar changes in their global tertiary structures during low pH-induced unfolding, but the Pro-VCC displayed a higher tendency toward local changes in the structure owing to increased exposure of surface hydrophobic patches. Similarly, Pro-VCC displayed a strengthened unfolding propensity toward chemical and high temperature-induced unfolding. Overall, the precursor Pro-VCC appears to be more susceptible to structural and conformational changes and unfolding than Mature-VCC. It would be a valid argument that the increased unfolding changes observed in Pro-VCC could be due to an increased unfolding tendency of the Pro-domain. To test this, we exposed the Pro-domain in isolation to similar denaturing conditions. Surprisingly, the Pro-domain displayed a much decreased tendency to unfold as compared to both Pro-VCC and Mature-VCC. These data suggest that the increased unfolding propensity of Pro-VCC is not contributed by the unfolding tendency of Pro-domain itself. Rather, it appears that the presence of the Pro-domain modulates the physicochemical properties of the entire Pro-VCC molecule, presumably via a, not yet characterized, long-range regulatory mechanism.

Our data suggest that the molecular structure of Pro-VCC can be perturbed more readily than that of the mature form of VCC. It appears that the presence of the Pro-domain imparts some level of structural and conformational plasticity into the Pro-VCC molecular structure. Such a structural plasticity of the precursor Pro-VCC molecule possibly makes it suitable for efficient transport of the VCC toxin from the bacterial periplasmic space into the extracellular environment. Secretion of VCC through the bacterial inner cell membrane is facilitated by the presence of an N-terminal ~25-residue long signal sequence. During passage through the bacterial plasma membrane, this signal sequence is cleaved off, thus resulting in the generation of the Pro-VCC molecule. Now, for extracellular secretion of Pro-VCC, it has to be transported across the bacterial outer membrane. A detail description of the specific transport machinery used by Pro-VCC is not known. A general consensus is that a number of periplasmic chaperones, and protein complexes form tunnel-like structures/secretion apparatus across the bacterial outer membrane, that are involved in such transport processes for the extracellular secretion of the bacterial exotoxins. It is possible to propose that during transport through bacterial outer membrane, Pro-VCC, although natively folded, would be able to adjust its structure/conformation so as to allow interactions with the chaperones and transport apparatus. Our study shows that the Pro-VCC structure is more

favoured toward structural and conformational alteration depending on its physicochemical environment. The Pro-VCC structure is, therefore, possibly better designed than its mature form to satisfy the criteria for its efficient extracellular secretion. To validate such hypothesis, however, future studies would be required toward testing the interactions of the Pro-VCC molecule with the components of the bacterial outer membrane transport machinery.

In summary, we have studied the role of Pro-domain in the structure-function mechanisms of VCC. We found that the presence of the Pro-domain in the precursor form of VCC, Pro-VCC, increases its propensity toward unfolding upon exposure to a range of denaturing conditions. Earlier studies suggest that Pro-domain might act as an intra-molecular chaperone in the native VCC architecture aiding in efficient secretion and folding of the VCC molecule in the bacterial periplasm. In the absence of the Pro-domain, the VCC molecule tends to refold to an oligomeric species that lacks the cytolytic activity (116). In this background, our present results indicate that the presence of the Pro-domain, which in itself is a much stable entity, provides a sufficient level of structural and conformational plasticity to the Pro-VCC molecule. This makes Pro-VCC much more amenable to undergo folding/unfolding processes, presumably aiding in its secretion, folding, and subsequent proteolytic maturation into the functionally active mature form.

Note:

* This part of the study has been published in the journal Biochemistry.

Paul, K**.** and Chattopadhyay, K. (2011) Unfolding distinguishes the *Vibrio cholerae* cytolysin precursor from the mature form of the toxin. Biochemistry, 50 (19), 3936-3945.

This part of the thesis has been adapted with permission from "Paul, K**.** and Chattopadhyay, K. (2011) Unfolding distinguishes the *Vibrio cholerae* cytolysin precursor from the mature form of the toxin. Biochemistry, 50 (19), 3936-3945" (American Chemical Society).

Chapter 3

Membrane pore-formation mechanism of VCC: truncation of the pre-stem region traps the toxin in its membrane-bound pre-pore oligomeric state*

3.1 Abstract

Vibrio cholerae cytolysin (VCC) is a β-barrel pore-forming toxin (β-PFT) that causes colloid-osmotic lysis of the target eukaryotic cells by forming transmembrane oligomeric β-barrel channels. Mode of action of β-PFTs, in general, involves binding of the toxin monomers onto the target cell membranes, and formation of a transient non-functional pre-pore oligomeric complex, followed by insertion of the β-strands from each of the toxin protomers into the membrane, forming functional transmembrane β-barrel channels. Consistent with this, X-ray crystal structure of the monomeric Pro-VCC shows the presence of a two-strand β-structural motif known as the pre-stem loop within the core cytolysin domain of VCC. In the transmembrane oligomeric pore state, pre-stem region from each of the toxin protomers converts into the, so called, stem structure, which becomes the part of the transmembrane β-barrel. Previous studies have shown that the covalent locking of the pre-stem loop blocks the transition of the pre-pore complex into the functional transmembrane pore. This clearly indicates that the pre-stem-to-stem conversion plays a crucial role in the transition of the non-functional pre-pore complex into the transmembrane β-barrel pore structure of VCC. In our present study, we wanted to explore whether the physical presence or absence of the pre-stem motif plays any role in the early steps of the VCC mode of action, namely, membrane binding and pre-pore complex formation. We constructed a recombinant variant of VCC lacking the pre-stem loop. Our results demonstrated that the absence of the pre-stem loop completely abrogates hemolytic activity of the toxin, and traps VCC in a pre-pore state, without showing any significant effect on the initial membrane binding and subsequent pre-pore complex formation by this VCC variant. Hence, the pre-stem loop in VCC appears to be involved only in the process of conversion of the pre-pore complex toward the functional β-barrel pore structure.

3.2 Introduction

Bacterial β-barrel pore-forming toxins (β-PFTs) constitute a unique class of protein toxins, which damage the target eukaryotic cell membranes by forming transmembrane oligomeric β-barrel channels (117). These toxins have been implicated in the virulence mechanisms of many pathogenic bacteria (118). β–PFTs are secreted by the bacteria as water-

soluble monomers, which upon binding to the respective target cell membranes transform into transmembrane oligomeric channels, thereby causing colloid-osmotic lysis of the target host cells (117).

Vibrio cholerae cytolysin (VCC) is a prominent member in the β-PFT family (22). VCC is secreted by most of the pathogenic strains of *V. cholerae (80)*, the causative agent of severe diarrhoeal disease, cholera (81). The mechanism of action of VCC involves secretion of the toxin as a ~79 kDa water-soluble monomeric precursor form, subsequent proteolytic activation into 65 kDa mature form, followed by binding to the host cell membranes and formation of heptameric transmembrane β-barrel channels. Comparison of the X-ray crystal structures of the water-soluble monomeric precursor form Pro-VCC (22) and the transmembrane oligomeric pore state of the toxin (79) suggest gross organizational change(s) in the toxin molecule. The structures also highlight the notion that the process of oligomerization and membrane pore-formation requires a series of structural/organizational/conformational changes in the protein (Figure 3.1).

The most important step in the β-PFT mode of action is the formation of a membrane bound pre-pore oligomeric intermediate, followed by insertion of the pre-stem motif into the membrane lipid bilayer leading to the formation of a functional transmembrane β-barrel pore. The structural analysis of the water-soluble monomeric form of VCC shows presence of a two strand β-structure, known as the pre-stem loop (spanning the residue 281-322). In the water-soluble form of VCC, pre-stem loop is bracketed by an extended loop (residue 191-204), which maintains the hydrophobic contact with the pre-stem loop. It also interacts with numerous charged and polar residues at the interface of the pre-stem β-sandwich. The pre-stem loop is also bound on the edge to the adjacent β-prism lectin-like domain, creating a steric effect for the loop (22). Hence, in order for the pre-stem region to penetrate the membrane lipid bilayer, VCC has to undergo a major conformational rearrangement. During the event of pore-formation, the β-prism lectin domain takes 180 ˚ rotation around the core cytolysin domain, followed by movement of the extended loop that might result in the destabilization of the interactions holding the pre-stem in the water-soluble state, and thus initiating partial unfolding of the pre-stem resulting in its insertion into the membrane lipid bilayer. In the transmembrane β-barrel pore state, each of the seven pre-stem loops contributed by seven protomers transforms into a 19 residue long antiparallel β-strand structure (so called stem-region) that forms 21 hydrogen bonds with each of its two neighbouring stem loops, thereby, stabilizing the stem region of the transmembrane β-barrel pore structure (79). Studies have shown that the covalent locking of the VCC pre-stem via

engineered disulfide bonds arrests the toxin in an abortive non-functional pre-pore state. In the non-reduced form, mutants were able to bind rabbit erythrocytes and form non-functional SDS-labile oligomers. This abortive state can be rescued by release of the pre-stem under reducing conditions to form a functional transmembrane β-barrel pore (119).

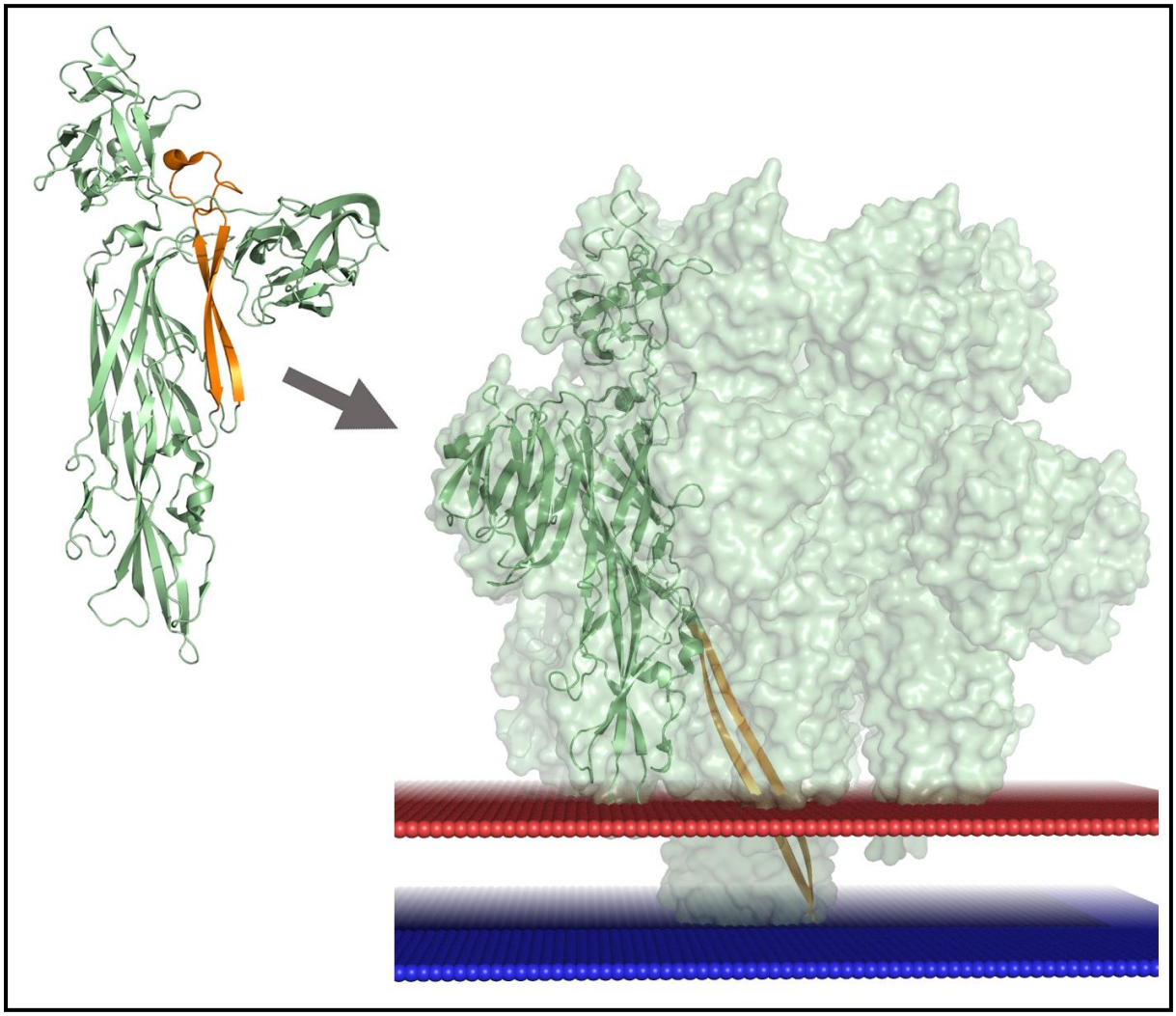

Figure 3.1: Mode of action of VCC. In the water-soluble monomeric state, the pre-stem loop (highlighted in orange) (residues 281-322) remains in a locked position within the cytolysin domain. During formation of a transmembrane β-barrel, the pre-stem from each protomer inserts into the membrane lipid bilayer contributing toward the formation of a functional β-barrel.

Data from previous studies show that the conformational rearrangement in the overall protein structure leading to the insertion of pre-stem loop into the membrane lipid bilayer is crucial for the conversion of the pre-pore state into a functional transmembrane pore structure (78). Extensive hydrogen-bond formation by the stem loop imparts a remarkable structural stability to the pore structure (e.g. SDS-stability). Although the pre-stem loop plays a central

role in the formation of a functional channel and its subsequent stabilisation, the role of the pre-stem in membrane binding and formation of a pre-pore oligomer remains unknown. To explore the involvement of the pre-stem loop in the early steps of membrane binding and pre-pore oligomer formation, we characterized a variant of VCC lacking the pre-stem loop region. Using this VCC variant we explored the role of the pre-stem motif (i) in maintaining the structural integrity of VCC, (ii) binding to target lipid membranes, (iii) formation of a pre-pore complex, and finally (iv) in the conversion of VCC into a functional transmembrane pore state.

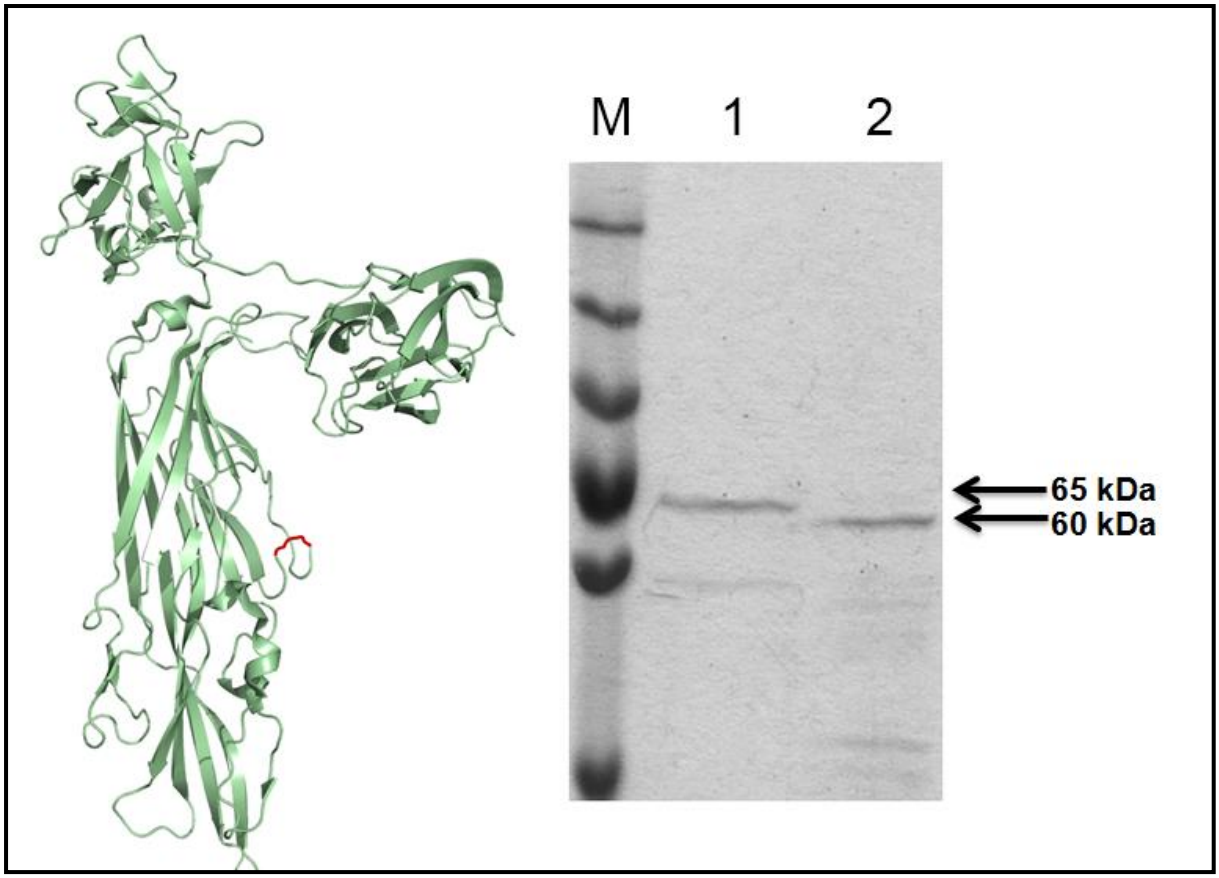

Figure 3.2: Ribbon model of VCC variant representing the deletion of the pre-stem loop and its replacement with a Gly-Gly-Ser linker. SDS-PAGE/Coomassie staining profile, Lane 1, molecular weight marker, Lane 2, WT-VCC and Lane 3, ΔPS-VCC

3.3 Materials and Methods

Protein expression and purification

Cytolytically active mature form of VCC was purified as described in the earlier section (please see the Materials and Methods of Chapter 2). The nucleotide sequence encoding Pro-VCC mutant lacking the pre-stem region (residues spanning 281-322 of Pro-

VCC) was constructed using a PCR-based approach, and was cloned into the pET14b bacterial expression vector. The pre-stem loop in the Pro-VCC was replaced with a flexible linker of Gly-Gly-Ser. The recombinant protein was overexpressed in *E. coli* Origami B cells, and was purified to homogeneity as described for the wild type Pro-VCC protein. Proteolytic removal of the Pro-domain was carried out as described before (please see the Materials and Methods of Chapter 2). The purified form of the truncated VCC lacking the pre-stem loop (ΔPS-VCC) was analysed by SDS-PAGE and Coomassie staining. Protein concentration was determined by monitoring absorbance at 280 nm, based on the theoretical extinction coefficient as predicted from the amino acid sequence of the protein.

Intrinsic tryptophan fluorescence emission measurements

Intrinsic tryptophan fluorescence emission spectra for the wild type VCC and ΔPS-VCC were recorded using a Fluoromax-4 spectrofluorometer (Horiba scientific, Edison, NJ) equipped with a peltier-based temperature controller. Excitation wavelength of 290 nm and slit widths of 2.5 nm and 5.0 nm for excitation and emission, respectively were used. Protein concentrations used were ~250 nM. All spectra were corrected with respect to the buffer spectra.

Far-UV circular dichroism measurements

Far-UV circular dichroism (CD) measurements were taken on an Applied Photophysics Chirascan spectropolarimeter with a Peltier-based temperature controlled sample chamber in a quartz cuvette of 5 mm pathlength. A final protein concentration in the range of 0.5-1 µM for was used. All spectra were corrected with respect to buffer.

Assay of hemolytic activity

Hemolytic activity of the VCC variants was monitored against human erythrocytes. Briefly, human erythrocytes were adjusted to an optical density (OD) of 0.8 – 0.9, corresponding to wavelength at 650 nm in phosphate buffered saline, pH 7.4 (PBS). Erythrocytes were incubated with a protein concentration of 100 nM in a reaction volume of 1 ml. The lysis of erythrocytes was monitored as decrease in the OD value at 650 nm upon incubation with the protein at 25 ˚C.

Assay of binding to human erythrocytes by flow cytometry

Human erythrocytes (1 X 10^6 cells) were treated with various concentrations of wild type VCC and ΔPS-VCC at 4 ˚C for 30 min in a reaction volume of 100 µl. The cells were centrifuged at 500 x g, washed twice with ice-cold PBS, resuspended in 50 µl PBS containing rabbit anti-VCC serum (1:100 v/v dilution and 0.1% w/v BSA; Sigma-Aldrich), and incubated at 4 ˚C for 30 min. After washing twice, the pellet was resuspended in 50 µl PBS

containing fluorescein-isothiocynate (FITC)-conjugated goat anti-rabbit IgG (1:100 v/v dilution and 0.1% w/v BSA; Sigma-Aldrich), and incubated at 4 ˚C for 30 min, washed twice and resuspended in 500 µl PBS. FITC fluorescence was monitored using an excitation wavelength of 488 nm and emission wavelength of 530 nm in the FL-1 channel using FACSCalibur (BD Biosciences, San Jose, CA, USA) flow cytometer.

Assay with liposomes

Asolectin, cholesterol and calcein were procured from Sigma-Aldrich. Equal amounts (5 mg) of Asolectin and cholesterol were dissolved in 2 ml chloroform in a round-bottom flask. The solvent was evaporated at room temperature under constant shaking in order to form a lipid film. The lipid film was dried under vacuum for 2 hours, followed by resuspension in PBS at 37 ˚C for 2 hours. For preparing uniform large unilamellar vesicles (LUVs), liposomes were repeatedly extruded through a 0.1 µm polycarbonate membrane using a Mini-Extruder apparatus (Avanti Polar Lipids, Inc., Alabaster, AL, USA). Briefly, the liposome samples were loaded into a gas-tight syringe and placed into one end of the Mini-Extruder. Another empty gas-tight syringe was placed into the other end of the Mini-Extruder. The fully assembled extruder apparatus was placed into the extruder stand. Plunger of the filled syringe was gently pushed until lipid solution was transferred into the empty syringe through the 0.1 µm polycarbonate membrane. The solution was transferred back to the previous syringe 0.1 µm polycarbonate membrane. This process was repeated 10 times to obtain a homogenous population of large unilamellar vesicles.

For analyzing the binding and oligomerization of VCC variants in Asolectin-cholesterol liposomes, a pull-down assay was used. Briefly, 1 µM protein was incubated with 50 µg liposome in 1 ml PBS for 1 hour at 25 ˚C. The protein-liposome complex was pelleted by ultracentrifugation at 105,000 g for 20 minutes. The pellet was washed in PBS. Binding and oligomerization was analyzed by SDS-PAGE/Coomassie staining.

For analyzing SDS-labile pre-pore oligomer formed by the VCC mutant, BS^3 (bis[sulfosuccinimidyl] suberate; Thermo Pierce) cross-linking was performed. The protein-liposome complex was pelleted by ultracentrifugation at 105,000 g for 20 minutes, washed twice with PBS to remove unbound protein and finally resuspended in PBS containing 5 mM BS^3 for 1 hour at 25 ˚C. The samples were analyzed by SDS-PAGE/Coomassie staining.

For preparing, calcein-trapped liposomes, the lipid film was resuspended in HBS (20 mM HEPES, 150 mM NaCl, pH 8.0) containing 50 mM calcein for 2 hours at 37˚C. Unbound calcein was removed by ultracentrifugation. The calcein entrapped liposomes were pelleted at 105,000 g for 20 minutes. The supernatant containing untrapped calcein was discarded and

calcein containing liposome pellet was washed 5-6 times with HBS. To obtain a homogenous mixture of large unilamellar vesicles, the calcein trapped liposomes were repeatedly extruded through a 0.1 µm polycarbonate membrane using a Mini-Extruder apparatus. After extrusion, free calcein molecules were removed by passing the liposome suspension through Sephadex G-50 (GE Healthcare Life Sciences) size-exclusion chromatography column equilibrated with HBS. Calcein-release assay was performed on a Perkin-Elmer LS 55 spectrofluorimeter. Protein (1 µM) was incubated in presence of 100 µg calecein-trapped Asolectin-cholesterol liposome in a 2 ml reaction volume. Calcein fluorescence was measured at 520 nm upon excitation at 488 nm, using 1 cm cuvette, excitation and emission slit widths of 2.5 nm and 2.5 nm, respectively. The 100% calcein release was induced by treating liposome with 6 mM sodium deoxycholate.

For preparing 1,6-Diphenyl-1,3,5-hexatriene (DPH)-labelled Asolectin-cholesterol liposomes, DPH stock of 1 mg/ml was prepared in 1,2-Dioxane. Liposomes resuspended in PBS were incubated with DPH (1:200, w/w) for 1 hour at 25 ˚C.

Fluorescence resonance energy transfer (FRET) form the tryptophan residue at position 318 (in Pro-VCC) to DPH incorporated in the Asolectin-cholesterol liposome was monitored using Perkin Elmer LS-55 spectrofluorometer in a quartz cell with 10 mm pathlength. The FRET from tryptophan to DPH was monitored by measuring the change in fluorescence intensity at 470 nm upon excitation at 290 nm with slit widths of 2.5 nm and 5 nm for excitation and emission, respectively. 1 µM protein was incubated with 100 µg DPH-labelled liposome in 2 ml PBS. All the spectra were corrected for respective buffer blanks containing untreated DPH-labelled liposomes.

Structural models

Structural coordinates for monomeric and oligomeric form of VCC were obtained from protein data bank (PDB) (PDB ID for monomeric VCC – 1XEZ, PDB ID for oligomeric VCC – 3O44). Structural model of VCC depicting the alignment of VCC in membrane lipid bilayer was generated using the online OPM server (http://opm.phar.umich.edu/server.php) (120). Different protein structural models were represented using PyMol [DeLano WL, The PyMOL Molecular Graphics System (2002) found online (http://pymol.org)](115, 120).

3.4 Results

Truncation of the pre-stem region from VCC does not affect the structural integrity of the protein

The transmembrane hairpin loop, known as the pre-stem region in VCC plays a major role in the formation of a functional transmembrane β-barrel pore structure (Figure 3.1). To further explore its role in the structure-function mechanism of VCC, we constructed a truncated variant of the protein lacking the pre-stem loop (ΔPS-VCC) within the core cytolysin domain of VCC (Figure 3.2). The pre-stem loop in VCC is composed of two β-strands comprising 281 – 322 amino acids. So, to test the effect of truncation of the pre-stem region on the structural integrity of the VCC protein, we probed the intrinsic tryptophan fluorescence emission and far-UV circular dichroism profile of the ΔPS-VCC in comparison to the wild type mature VCC protein. The intrinsic tryptophan fluorescence spectra of ΔPS-VCC revealed a red shift in the tryptophan fluorescence emission maximum (Figure 3.3). Since wild type VCC molecule contains 11 tryptophan residues, the intrinsic tryptophan fluorescence observed for VCC is a cumulative effect of the different environments of 11 tryptophan residues located at distinct positions in the VCC protein structure. So, the red shift observed in the tryptophan spectra could be explained by the fact that ΔPS-VCC contains one less tryptophan residue (10 tryptophan residues) located at 318 position in the pre-stem loop of the wild type VCC. Therefore, removal of the pre-stem region from the wild type VCC molecule does not cause s drastic effect on the overall global tertiary structure of the toxin. The far-UV CD profile of the ΔPS-VCC showed a decreased signal at 217 nm region (corresponding to the β-sheet structures) (Figure 3.3). This could be explained due to the absence of two β-strands in the pre-stem loop region of the wild type VCC. Overall, the intrinsic tryptophan fluorescence spectra and far-UV CD profile of ΔPS-VCC revealed that the removal of pre-stem loop region of the VCC molecule does not cause any drastic effect on the structural integrity of the toxin.

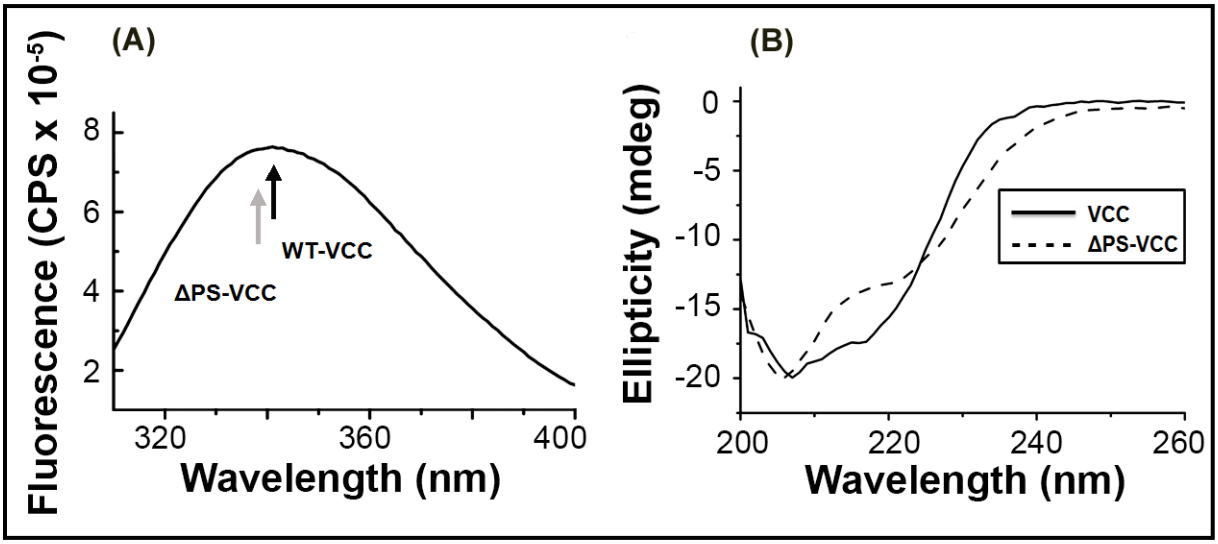

Figure 3.3: Intrinsic tryptophan fluorescence emission (A) and far-UV CD profile (B) of WT-VCC and ΔPS-VCC under native conditions.

Removal of the pre-stem region from VCC abolishes the membrane permeabilization activity but does not affect binding of the toxin to the target membranes

In the β-PFT mode of action, one of the most important steps toward formation of the functional β-barrel pores is the insertion of the transmembrane region composed of two β-strands into the cell membranes. According to the heptameric pore assembly structure of VCC (79), the pre-stem loop plays the most important role toward formation of a functional β-barrel. Each monomer contributes a pre-stem loop (two β-strands) that inserts into the membrane lipid bilayer, and leads to the formation of the functional transmembrane pore-structure. Hence, from the data available it seems that the deletion of the pre-stem loop would abolish the formation of a transmembrane β-barrel structure hence rendering the toxin as non-functional. However, it has not been explored yet whether the absence of the pre-stem would have any effect on the VCC-membrane interactions, and also on the efficacy of the formation of the pre-pore oligomers. We found that the deletion of the pre-stem loop severely compromised the membrane pore-forming activity of VCC against human erythrocytes. As reported earlier, wild type VCC, at a concentration of 100 nM (6.5 µg/ml), induced 100% lysis of human erythrocytes, when incubated for 1 hour at 25˚C (Figure 3.4A). The ΔPS-VCC did not show any activity upon incubation with human erythrocytes under similar experimental conditions.

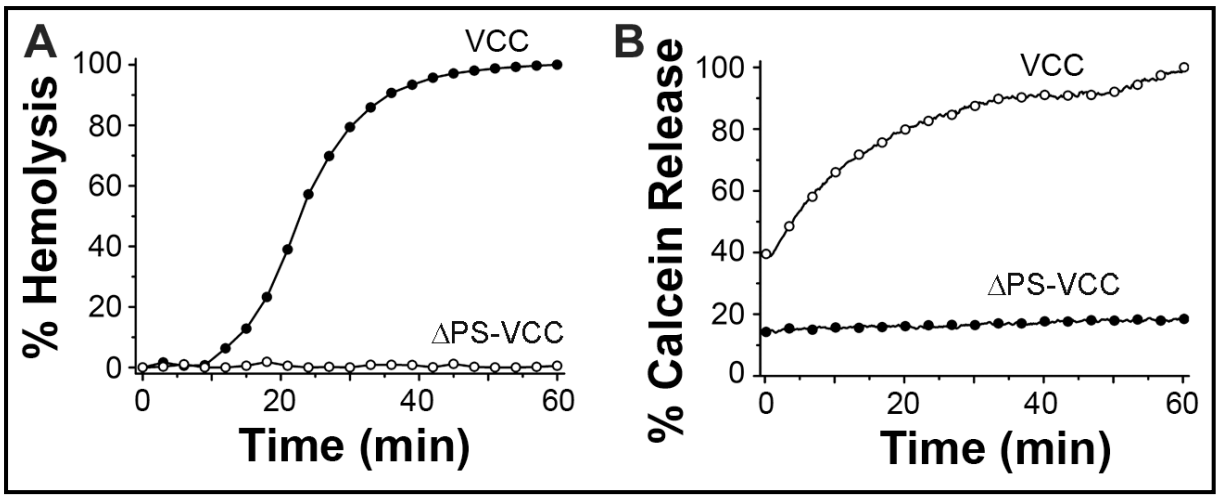

Figure 3.4: Comparison of hemolytic activity and membrane permeabilization by WT-VCC and ΔPS-VCC. (A) Kinetics of hemolytic activity by WT-VCC and ΔPS-VCC against human erythrocytes. Human erythrocytes were treated with WT-VCC and ΔPS-VCC, kinetics of hemolytic activity was determined by monitoring the decrease in optical density at 650 nm using UV-Vis spectrometer (B) Membrane permeabilization effect of WT-VCC and ΔPS-VCC against calcein containing asolectin-cholesterol liposome monitored by measuring the release of calcein form the artificial lipid vesicles.

We also tested the membrane-damaging activity of ΔPS-VCC by using Asolectin-cholesterol liposome system containing trapped fluorescent dye calcein. Membrane damage due to action of VCC leads to the leakage of calcein dye from the liposomes resulting in an increase in calcein fluorescence. Increase in calcein fluorescence with time can be directly correlated with the membrane damaging effect of VCC. Wild type VCC at a concentration range of 1 μM displayed prominent release of calcein, presumably due to the membrane damaging effect of functional pore-formation (Figure 3.4B). The ΔPS-VCC could not trigger the release of calcein to any significant extent. Incubation with ΔPS-VCC leads to a calcein release of only ~18%

To check whether removal of the pre-stem loop has any effect on the membrane binding activity of VCC, we employed a flow cytometry-based binding assay. Human erythrocytes were treated with VCC at 4 ˚C. The membrane-bound VCC were probed with anti-VCC followed by treatment with FITC-conjugated secondary antibody. The increase in FITC fluorescence would reveal the increased binding of VCC to human erythrocytes. The results showed that both the wild type VCC and ΔPS-VCC displayed an overall similar binding to the human erythrocytes (Figure 3.5).

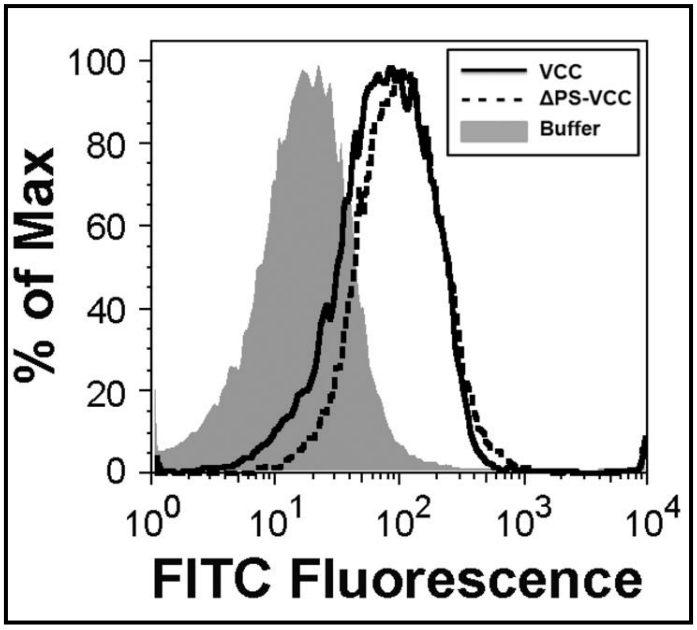

Figure 3.5: Comparison of membrane binding of WT-VCC and ΔPS-VCC using flow cytometry based binding assay. WT-VCC and ΔPS-VCC were incubated with human erythrocytes and binding was estimated using flow cytometry-based experiment.

We also probed the binding of the wild type and pre-stem truncated VCC to Asolectin-cholesterol liposome by using a pull down-based assay (Figure 3.6). Proteins were incubated in presence of the liposome vesicles, protein-liposome complexes were pelleted, dissolved in SDS-PAGE sample buffer with or without boiling. Sample without boiling would allow detection of any SDS-stable oligomers, as observed in case of the wild type VCC protein. Boiling of the sample in SDS-PAGE sample buffer would dissociate the oligomeric complex into monomeric bands, and would reflect the membrane-bound fractions of the VCC variants under the experimental conditions tested. Wild type VCC showed efficient association with the membrane lipid bilayer of the Asolectin-cholesterol liposomes (Figure 3.6). Moreover, membrane-bound fractions of VCC showed formation of SDS-stable oligomers.

ΔPS-VCC variant showed efficient association with the Asolectin-cholesterol membrane lipid bilayer (Figure 3.6). However, it could not form any SDS-stable oligomeric species. Overall, the data indicated that the truncation of the pre-stem loop completely abolished the membrane damaging pore-forming activity of the toxin, but did not affect the binding to the target membranes.

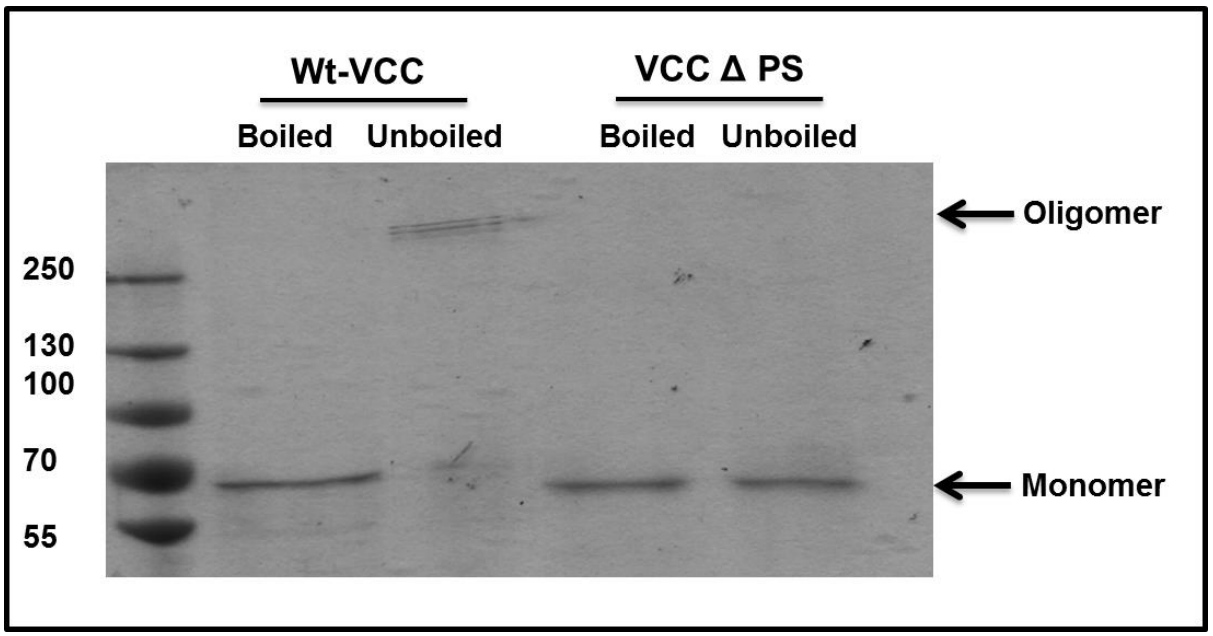

Figure 3.6: Binding and oligomerization by WT-VCC and ΔPS-VCC with Asolectin-cholesterol liposomes. SDS-PAGE/Coomassie staining profile of bound fractions of WT-VCC and ΔPS-VCC. Arrow represents formation of a SDS-stable oligomer**.**

Truncation of pre-stem loop does not block pre-pore oligomer formation

So far, our data clearly suggested that the truncation of the pre-stem loop abolished SDS-stable oligomer formation by VCC in the membrane lipid bilayer of the Asolectin-cholesterol liposome membranes, a prominent signature of the archetypical β-PFTs (Figure 3.6). We wanted to check whether ΔPS-VCC had the ability to form any SDS-labile oligomeric species representing the pre-pore intermediate state of the membrane-bound toxin. We tested this by using a crosslinking agent, BS^3. BS^3 contains an amine-reactive N-hydroxysulfosuccinimide (NHS) ester at each end of an 8-carbon arm; NHS esters react with primary amines at pH range of 7-9 to form stable amide bonds, along with release of the N-hydroxysulfosuccinimide leaving group. Proteins generally contain several primary amines in the side chain of lysine residues, and at the N-terminus of each polypeptide chain. So, BS^3 would covalently trap any oligomeric species formed by ΔPS-VCC in its membrane-bound state in the Asolectin-cholesterol liposomes. Indeed, ΔPS-VCC mutant formed oligomeric assembly upon incubation with Asolectin-cholesterol liposomes, which could be covalently trapped by BS^3 cross-linker.

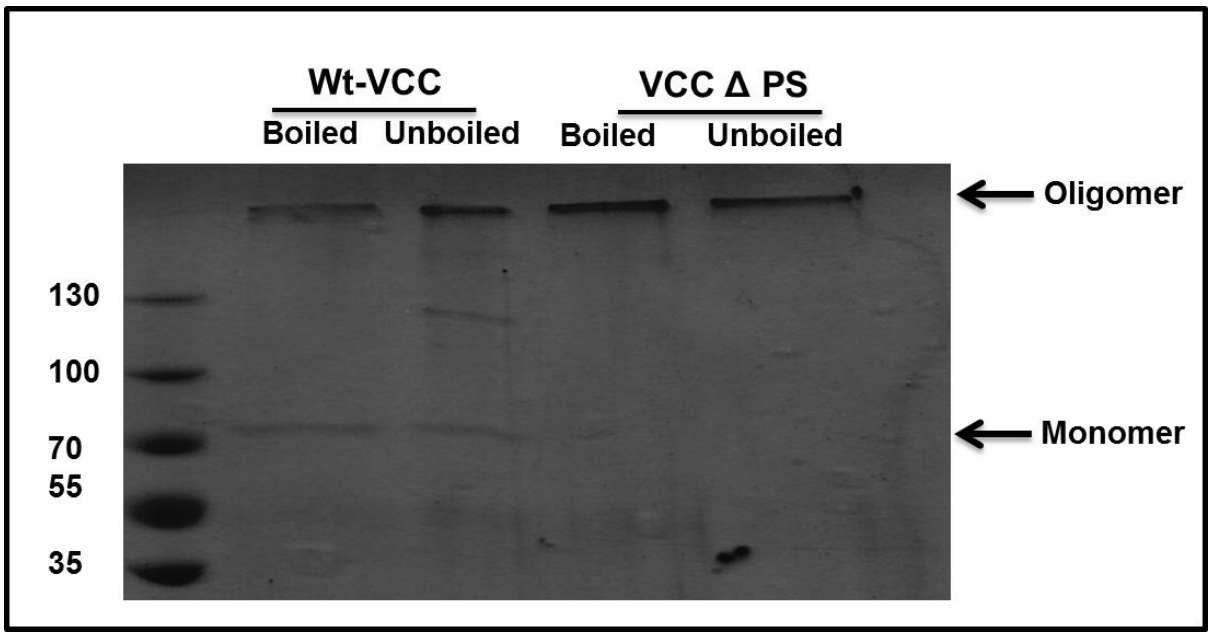

Figure 3.7: Formation of SDS-labile oligomers by ΔPS-VCC as detected by BS^3 crosslinking. SDS-PAGE/Coomassie staining profile of membrane-bound fractions of WT-VCC and ΔPS-VCC crosslinked by using BS^3 to detect formation of SDS-labile oligomers. Arrow indicates the formation of SDS-labile oligomers.

Figure 3.7 shows the presence of SDS-labile oligomeric species in the lane corresponding to ΔPS-VCC under both boiled and unboiled conditions. This suggested that, although pre-stem loop truncation abolished the formation of SDS-stable oligomers for ΔPS-VCC, the mutant variant still retained the ability to form SDS-labile pre-pore oligomeric assembly in the presence of artificial liposome membranes. This suggested that the presence of the pre-stem loop was not critical for the membrane oligomerization step employed by the VCC toxin.

Pre-stem deletion leads to abrogation of the membrane insertion step

We wanted to confirm the inability of the ΔPS-VCC variant to exert the membrane insertion step in absence of the pre-stem segment. For this, we employed a qualitative FRET (fluorescence resonance energy transfer)-based assay to monitor the membrane insertion step of the VCC variants. Wild type VCC contains a tryptophan residue at position 318 (W318) within the pre-stem motif. During membrane insertion of the pre-stem region of wild type-VCC W318 would be placed in the proximity of the membrane lipid bilayer. Therefore, presence of a membrane-embedded fluorophore (e.g. DPH), having an overlapping fluorescence excitation wavelength with that of the tryptophan fluorescence emission regime, would allow detection of the membrane insertion step by monitoring the tryptophan-to-DPH

FRET signal (Figure 3.8).1,6-diphenyl-1,3,5-hexatriene (DPH) is a fluorescent molecule (Figure 3.8).

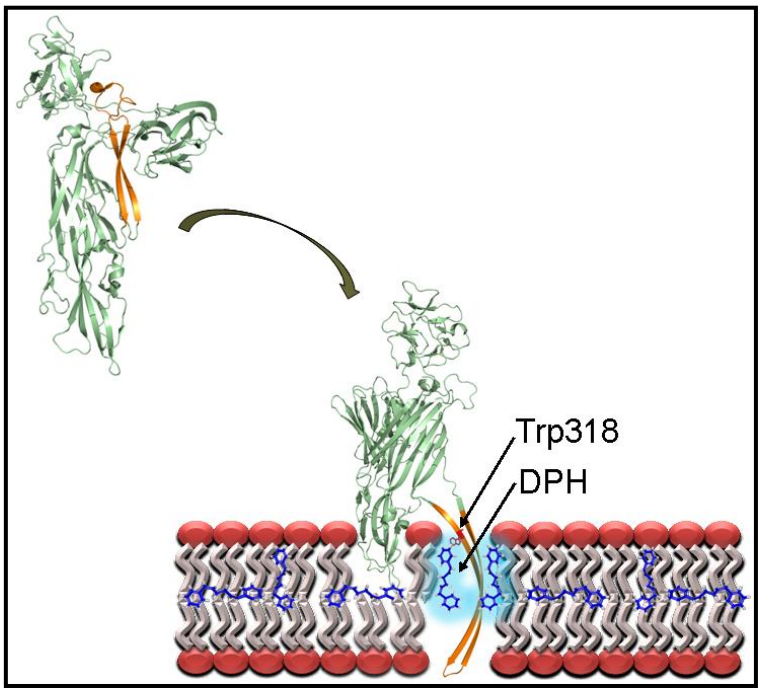

Figure 3.8: Model showing the mechanism of tryptophan-to-DPH FRET. During membrane insertion of the pre-stem loop, the tryptophan at 318 position in the loop comes in proximity with the DPH molecule intercalated in the lipid bilayer to allow a successful transfer of energy between the donor (tryptophan) and acceptor (DPH)

DPH has been shown to insert specifically in the nonpolar interior of the membrane lipid bilayer. It is non-fluorescent in water but shows strong fluorescence property when intercalated into the lipid membranes. Since tryptophan has a fluorescence emission in the range of 340-355 nm and DPH has an fluorescence excitation wavelength in the range of 370 nm, tryptophan and DPH serve as an excellent FRET donor-acceptor pair. We monitored increase in the DPH fluorescence (incorporated in the core of membrane lipid bilayer) upon exciting tryptophan at 290 nm. If the W318 and DPH are in close proximity, it would result in increased FRET signal resulting in enhanced DPH fluorescence. Consistent with such notion, wild type VCC when incubated with DPH-labelled Asolectin-cholesterol liposomes showed a prominent increase in the tryptophan-to-DPH FRET (Figure 3.9). The ΔPS-VCC on the other hand did not show any increase in the DPH emission presumably due to the absence of the W318 present within the pre-stem loop (Figure 3.9). These data, therefore confirmed an abortive membrane insertion step for the truncated VCC variant lacking the pre-stem loop structure.

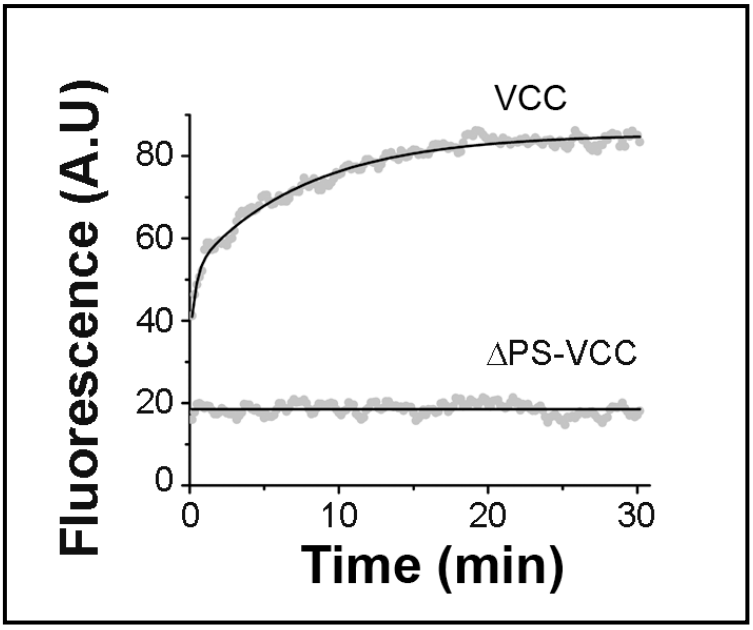

Figure 3.9: Membrane insertion of WT-VCC and ΔPS-VCC probed by tryptophan-to-DPH FRET. Membrane insertion of WT-VCC leads to an increase in the fluorescence of DPH intercalated in the membrane lipid bilayer due to tryptophan-to-DPH FRET whereas ΔPS-VCC could not trigger any FRET.

3.5 Discussion

VCC is a member of the family of β-barrel pore-forming toxins. The mechanism of membrane pore assembly and membrane insertion step of VCC has been only poorly characterized. Of particular interest is the mechanism of assembly of cell-bound VCC into the non-lytic oligomeric pre-pore intermediates as described previously for the oligomeric β-PFTs like *S. aureus* α-toxin (121). The process of oligomerization and pore formation requires a series of organizational/conformational changes involving protein-protein interactions occurring in concert. To dissect the intermediate processes, the toxin needs to be trapped at the intermediate stages of the membrane pore formation. Earlier studies have made attempt to arrest the pre-pore oligomeric intermediate step of VCC, where the pre-stem loop was trapped by engineered disulfide bonds with the adjacent lectin-like domains. The mutants with covalently trapped pre-stem loop displayed no detectable hemolytic activity against rabbit erythrocytes, but hemolytic activity was regained under the reducing conditions in presence of DTT. The inability of the toxin mutants to lyse erythrocytes in the absence of DTT indicated that the disulfide bond-trapping of the pre-stem loop prevented assembly into a lytic pore. Surprisingly the disulfide mutants when incubated with rabbit erythrocytes in the presence of the wild type VCC displayed reduced hemolytic activity as compared to the wild type-only treatment. Osmotic protection assay-based experiment was performed to examine

the pore-forming activity of the hybrid oligomers composed of the disulphide-trapped insertion-deficient mutant VCC and the wild type molecule (119). Such assay revealed that the wild type toxin and the insertion-deficient mutant formed hetero-oligomeric with reduced functional pore diameters. Previous studies have also indicated that in the case of the mixed oligomers, the pore-forming stem regions were derived from the active wild type-VCC protomers, whereas the pre-stem sequences from the disulfide-trapped mutant were locked onto the extra-membrane domain of the toxin.

Although the role of the pre-stem segment in the formation of a functional β-barrel pore has been studied, no speculation could be made earlier about the role of the pre-stem sequence in the membrane-binding, and in the formation of the pre-pore oligomeric intermediate. To explore this, we constructed a variant of VCC lacking the pre-stem loop, ΔPS-VCC. The ΔPS-VCC displayed no detectable hemolytic activity against human erythrocytes. This could result from either formation of a non-functional oligomer or due to the decreased binding to the erythrocyte membranes. The flow cytometry-based binding assay and liposome pull down assay revealed that the binding of ΔPS-VCC to human erythrocytes and Asolectin-cholesterol liposomes was similar to those of the wild type VCC, indicating that the pre-stem loop, which is a part of the core cytolysin domain, does not contribute toward binding of VCC to the membrane lipid bilayer. We found that the truncation of the pre-stem loop in the ΔPS-VCC variant resulted in the formation of SDS-labile oligomers in the Asolectin-cholesterol liposome membranes. Crosslinking experiment revealed that the ΔPS-VCC mutant formed SDS-labile pre-pore oligomeric assembly upon incubation with the Asolectin-cholesterol liposomes, which could be covalently trapped by BS^3 crosslinker. This suggested that although the pre-stem loop truncation abolished the formation of the SDS-stable, functional oligomeric pore formation by VCC, ΔPS-VCC variant still retained the ability to bind to the membranes, and to form the SDS-labile pre-pore oligomeric assembly in the presence of the membrane lipid bilayer of the liposome systems. We also confirmed whether the inability of the ΔPS-VCC variant to form the SDS-stable oligomeric assembly was due to the absence of the membrane insertion of the β-barrel-forming pre-stem loop region. For this we employed a tryptophan-to-DPH FRET-based assay. Wild type VCC, when incubated with DPH-labelled Asolectin-cholesterol liposomes resulted in a prominent increase in the tryptophan-to-DPH FRET, thus validating the membrane insertion of the pre-stem loop. The ΔPS-VCC variant, on the other hand, did not show any increase in the DPH fluorescence emission presumably due to the absence of the Trp318 (contributing toward the FRET to the membrane-embedded DPH) within the pre-

stem loop, thus clearly explaining that the inability of the ΔPS-VCC to execute the membrane insertion of the pre-stem loop region.

In summary, this part of the study extends our existing insights regarding the implications of the pre-stem loop in the VCC structure-function mechanism. Our study establishes that the pore-forming pre-stem loop plays a critical role in the formation of the functional transmembrane β-barrel pore by the VCC toxin. Based on our study, however, presence of the pre-stem loop does not appear to be critical for the membrane binding and pre-pore assembly of the toxin. Such observation, not only provides critical insights regarding the mode of action of VCC, but also extends our understanding regarding the mechanism of actions of the β-PFT family of bacterial protein toxins.

Note:

* This part of the study has been published in the journal Biochem. Biophys. Res. Comm.

Paul, K. and Chattopadhyay, K. (2014) Pre-pore oligomer formation by *Vibrio cholerae* cytolysin: insights from a truncated variant lacking the pore-forming pre-stem loop. Biochem. Biophys. Res. Com., 443 (1), 189-193.

This part of the thesis has been adapted with permission from "Paul, K. and Chattopadhyay, K. (2014) Pre-pore oligomer formation by *Vibrio cholerae* cytolysin: insights from a truncated variant lacking the pore-forming pre-stem loop. Biochem. Biophys. Res. Com., 443 (1), 189-193" (Elsevier).

Chapter 4

Cholesterol-dependent membrane interaction mechanism of VCC: implication of a single point mutation in the toxin*

4.1 Abstract

Vibrio cholerae cytolysin (VCC) belongs to the β-PFT family of pore-forming toxins. One of the initial steps in the β-PFT mode of action is the binding to target cell membranes. Although high-resolution crystal structures are available for both the water-soluble monomeric state and the membrane-embedded oligomeric pore state of the protein, very little is understood about the interaction of VCC with the target cell membranes. In the present study we have characterised a mutant variant of VCC harbouring a single point mutation (Ala425Val) in the putative membrane-binding loop of VCC. The mutant displayed severely compromised hemolytic activity along with the drastically reduced membrane binding efficacy. Membrane-bound fraction of this mutant was found to form non-functional abortive oligomers. Further analysis revealed that the Ala425Val mutation in VCC critically impaired the cholesterol-dependent membrane interaction mechanism of VCC, along with the loss of its ability to form functional transmembrane oligomeric pores in the target membrane lipid bilayer.

4.2 Introduction

Bacterial β-barrel pore-forming toxins (β-PFTs) constitute a unique class of membrane-damaging cytolytic proteins, and they are implicated in the virulence mechanisms of a wide spectrum of pathogenic bacteria (5). Elucidating the mechanistic details of the bacterial β-PFT mode of actions is critically important in understanding their association with the bacterial virulence mechanisms. These toxins are secreted by the bacteria in a water-soluble monomeric form, which bind to their eukaryotic host cell membranes and convert into transmembrane oligomeric β-barrel channels, triggering colloid-osmotic lysis of the target cells. In the overall mode of action of bacterial β-PFTs, formation of a transient 'pre-pore' oligomeric state has been speculated and/or detected on the membrane surface. The formation of a pre-pore oligomer is followed by considerable conformational change(s) in the molecule, leading to membrane-insertion of β-strand(s) donated by each monomeric subunit to form the transmembrane β-barrel structure of the pores (32). In spite of such overall general scheme, β-PFTs deviate significantly from each other in the intricate mechanistic details of the membrane pore-formation process: (i) the mechanistic basis of the β-PFT

interactions with the target cell membranes, (ii) the mechanism of conversion of the membrane-bound monomer into the oligomeric structure, and (iii) the mechanism of generation of the transmembrane oligomeric β-barrel pores. In particular, targeting of the water-soluble toxin molecules onto the target cell membranes highlights a mechanism of enormous diversity. Also, in most of the cases, the exact role of the membrane components (lipid and/or non-lipid) in triggering the organizational and/or conformational changes required for the subsequent membrane insertion event remains elusive. Current structural information of many β-PFTs evoke the notion that the conversion of the water-soluble monomer into membrane-inserted oligomeric β-barrel channel involves complex cross-talk between the β-PFT protein and the membrane components, the exact mechanism of which are only partially understood.

Vibrio cholerae cytolysin (VCC) is a prominent member in the β-PFT family (22). VCC is expressed by most of the *V. Cholerae* strains with high pathogenic potential (80). VCC is secreted as a ~79 kDa inactive precursor (Pro-VCC), which after proteolytic removal of the 15 kDa N-terminal Pro-domain forms the active mature form of the VCC toxin with the potential to form oligomeric pores on the host cell membranes (95). The process of membrane pore formation by VCC involves two separate steps. The water-soluble monomers first bind to the target membranes. Subsequently, seven membrane-associated monomers assemble into oligomeric intermediates that insert into the membrane to surround a water-filled pore of ~1-2 nm diameter (79). The first step toward membrane pore-formation is the efficient membrane binding of the monomeric toxin molecules. The membrane permeabilization process also involves assembly of the membrane-bound monomers into oligomers of defined stoichiometry (i.e. heptamers) that assume a bilayer-inserted conformation. The process of membrane permeabilization has been observed even in the membrane lipid bilayers of the model membranes (i.e. synthetic lipid vesicles/liposomes), provided phospholipid membrane bilayers are supplemented with cholesterol (122). The X-ray crystal structure of the Pro-VCC molecule has been determined (22). More recently, X-ray crystal structure has been determined for the transmembrane heptameric β-barrel pore state of VCC (79). Comparison of the structural models of the water-soluble monomeric state and the transmembrane oligomeric pore state highlights significant extent of organizational/conformational changes in the VCC molecule during the process of the membrane pore formation of the toxin. However, the exact mechanism(s) that trigger such alterations in the VCC structure still remains elusive. It is commonly speculated that the

interactions of the VCC protein with the specific membrane components play critical role(s) in the process. In particular, presence of cholesterol in the membrane lipid bilayer has been suggested to be instrumental in regulating the multiple steps of the membrane pore-formation event: (i) membrane binding, (ii) oligomerization, (iii) membrane insertion, and (iv) functional pore-formation. It has also been indicated that the cholesterol molecule modulates VCC mode of action by physically interacting with an, as yet unidentified, structural motif present in the toxin, and not just by altering the physicochemical properties of the membrane lipid bilayer (122-124). It is important to note here that similar critical involvements of the membrane cholesterol have been reported in the mode of actions of the cholesterol-dependent pore-forming cytolysins: perfringolysin O (125), streptolysin O (126), and intermedilysin (74). Presence of a conserved motif has been implicated in the process of recognition and binding of the membrane cholesterol by these cholesterol-dependent cytolysins (76). In case of VCC, however, the detail structural mechanism of the toxin-cholesterol cross-talk remains unclear. Particularly, the exact location of the cholesterol-binding motif in the VCC structure needs to be mapped in molecular detail. Also, the specific role(s) of the membrane cholesterol in regulating the distinct steps of transmembrane pore-formation by the VCC toxin remains to be delineated.

Cholesterol-dependent cytolysins (CDCs) represent the largest class among β-PFTs. CDCs bind to the target host cell membrane by using cholesterol as a receptor. CDCs harbour a conserved structural motif (ECTGLAWEWWR) toward the C-terminus of the toxin implicated in the interaction of the toxin with membrane cholesterol. This motif is termed as the un-decapeptide or tryptophan rich motif. This structural motif contains three tryptophan residues and a single cysteine residue (76). CDC binding to membrane cholesterol is dependent on the presence of certain structural features in cholesterol, namely, an intact 3-β-hydroxyl group, an aliphatic side chain of appropriate length at carbon 17 of the D ring, a methyl group at carbon 20 and an intact B ring. Any modifications in these structural features results in loss of cholesterol recognition by CDCs (23). Mode of action of CDCs involve (i) cholesterol-dependent binding of monomeric proteins to the cell membranes, (ii) formation of a non-functional pre-pore oligomer, and (iii) insertion of the transmembrane hairpin loop leading to the formation of a functional transmembrane pore (24). The structure of CDCs contains four distinct domains. The binding of the monomer to membrane cholesterol is mediated by domain 4 that contains the un-decapeptide or tryptophan rich motif. Binding to cholesterol initiates a series of conformational changes in the membrane-bound monomers, which involves rotation of the loop comprised of β5 and α1 away from β4 of the domain 3

core β-sheets, leading to intermolecular interactions between adjacent membrane-bound monomers. The monomers continue to extend the oligomeric structure until a ring-shaped structure is formed. This structure has been termed as the pre-pore complex and is defined as the completed oligomeric complex without the formation of its characteristic β-barrel pore. Each monomer in the pre-pore complex contributes two transmembrane β-hairpins (TMH) toward the formation of a functional β-barrel pore structure of the CDCs.

VCC mode of action shows prominent requirement for the presence of cholesterol in the target cell membranes (102, 123-124). However, it is not clear how exactly membrane cholesterol regulates the functionality of VCC. In the present study, we have characterised a mutant variant of VCC lacking the functional membrane pore-forming activity. This VCC variant harbours a mutation in the membrane-proximal rim region of the toxin. The mutant shows a compromised cholesterol-dependent membrane interaction mechanism suggesting the presence of a distinct potential cholesterol-binding motif in the VCC toxin. Our study for the first time indicates a structural basis of the involvement of cholesterol in the process of functional membrane pore formation employed by VCC.

4.3 Materials and Methods

Wild type and the mutant construct of VCC

Nucleotide sequence encoding the Pro-VCC protein (precursor form of the VCC toxin, omitting the N-terminal signal sequence) was PCR-amplified with the gene specific primers, and the amplified PCR-product was cloned into the pET14b bacterial expression vector (Novagen). Recombinant construct was verified by DNA sequencing. The recombinant plasmid harbouring the cloned construct for Pro-VCC was introduced into the *Escherichia coli* Origami B cells (Novagen) for protein expression. Soluble Pro-VCC protein expressed in the Origami B cells was purified, and was proteolytically processed to generate the mature form of the wild type VCC molecule, following the method described earlier (please see the Materials and Methods of Chapter 2). In the process of cloning the recombinant Pro-VCC construct, we also obtained a construct that led to the generation of a VCC variant with drastically reduced hemolytic activity. DNA sequence analysis revealed that this construct of the VCC molecule harboured a single point mutation (from Ala-to-Val at the position 425 of the Pro-VCC sequence). The point mutation resulted from a change in the nucleotide sequence that was presumably introduced during the PCR-amplification

process. In the present study, we have designated this mutated form of VCC as Ala425Val-VCC, while the wild type form of the recombinant VCC has been referred as the WT-VCC.

Purification of WT-VCC and Ala425Val-VCC

WT-VCC was purified using the method as described earlier (please see the Materials and Methods of Chapter 2). Ala425Val-VCC was purified using the similar method. Briefly, Soluble Pro-VCC was expressed in *E. coli* Origami B cells. Bacterial growth medium was supplemented with 50 µg/ml of carbenicillin. A starter culture was inoculated with the transformed Origami B cells, and grown overnight at 37 ˚C. The overnight culture was diluted 50-fold into LB broth, and was grown to an A_{600} of 0.6. Protein expression was induced with 1 mM IPTG, and the culture was grown for additional three hours with shaking at 30 ˚C. Cells were pelleted by centrifugation at 4000 rpm for 20 minutes in a hanging bucket centrifuge, and the cells were resuspended in phosphate buffered saline (pH 7.0)(PBS), supplemented with bacterial protease inhibitor cocktail (Sigma). Cells were lysed by sonication, followed by centrifugation at 12,000 rpm for 10 minutes at 4 ˚C. The supernatant was adjusted with 20 mM imidazole before passing through Ni-NTA agarose column (Qiagen), pre-equilibrated with PBS. The column was washed with 50-volume of the same buffer adjusted with 20 mM imidazole, and the bound protein was eluted with 300 mM imidazole in PBS. The peak fractions were diluted five times with a buffer containing 10 mM Tris-HCl and 1 mM EDTA (pH 8.0), and loaded onto a Q-Sepharose anion exchange chromatography column (GE healthcare) pre-equilibrated with the same buffer. Bound protein was eluted using a linear gradient of 0-500 mM NaCl in 10 mM Tris-HCl buffer (pH 8.0) over 50 ml in an FPLC system (AKTA purifier, GE healthcare), at a 2 ml/minute flow rate. The N-terminal Pro-domain was removed by treating the precursor form of the VCC variants with trypsin at a protein:protease ratio of 2000:1 for 10 minutes at room temperature. Reaction was terminated with 1 mM Phenyl Methyl Sulfonyl Fluoride (PMSF). The mature form of the VCC variant was purified by passing through the Q-Sepharose column. Purified proteins were analysed by SDS-PAGE and Coomassie staining.

Assay of hemolytic activity

Hemolytic activity of WT-VCC and Ala425Val-VCC was assayed against human erythrocytes by monitoring the release of hemoglobin spectrophotometrically at 415 nm.

Rabbit anti-VCC serum

Polyclonal anti-VCC antiserum was generated in rabbit using the Custom made Polyclonal Antibody Service of GeNei/Merck, Bangalore, India

Western blot detection of VCC: binding to human erythrocytes

Human erythrocytes were resuspended in PBS to a final concentrations of OD_{650} = 0.8. The erythrocytes were incubated with various concentrations of the VCC variants at 25 ˚C for 1 hour in a reaction volume of 200 µl. The reaction mixture was subjected to ultracentrifugation at 105000 x g for 20 min, and was washed twice in PBS. The pellet was resuspended in SDS-PAGE loading buffer (50 mM Tris/HCl, pH 6.8, containing 2% w/v SDS, 2 mM beta-mercaptoethanol, 4% v/v glycerol, 0.01% w/v bromophenol blue), and separated on an SDS-PAGE. Following separation, the proteins were transferred onto a PVDF membrane (BioRad) using a complete wet transfer assembly (BioRad, Hercules, CA, USA) at 90 V for 90 minutes. The membrane was blocked with 3% non-fat milk powder (Santa Cruz Biotechnology, Santa Cruz, CA, USA) in PBS containing 0.05% Tween-20 (Himedia) (TPBS) at 4 ˚C overnight. After washing three times in TPBS, the blot was incubated with rabbit anti-VCC antiserum (1:5000 v/v) for 1 hour at room temperature. After washing three times in TPBS, it was incubated with horseradish peroxidise (HRP)-conjugated goat anti-rabbit IgG (Sigma-Aldrich) (1:10000 v/v) for 1 hour at room temperature and washed thrice with TPBS. The blot was developed using the ECL western blotting detection kit (GE Healthcare Life Sciences, Piscataway, NJ, USA), and exposed to X-ray film (Biomax, Kodak, Sigma-Aldrich, St. Louis, MO, USA) to detect the bands of monomers and oligomers of the VCC variants. Band intensities were quantitated by the ImageJ software (127).

Flow cytometry

Human erythrocytes (1 X 10^6 cells) were treated with various concentrations of wild type and mutant VCC at 4 ˚C for 30 min in a reaction volume of 100 µl. The cells were centrifuged at 500 x g, washed twice with ice-cold PBS and resuspended in 50 µl PBS containing rabbit anti-VCC antiserum (1:100 v/v dilution) and 0.1% w/v BSA (Sigma-Aldrich), and incubated at 4 °C for 30 min. After washing twice, the pellet was resuspend in 50 µl PBS containing fluorescein-isothiocynate (FITC)-conjugated goat anti-rabbit IgG (1:100 v/v dilution and 0.1% w/v BSA; Sigma-Aldrich), incubated at 4 °C for 30 min, washed twice, and resuspended in 500 µl PBS. Cells were analyzed using FACSCalibur (BD Biosciences, San Jose, CA, USA) flow cytometer. FITC fluorescence was monitored using an excitation wavelength of 488 nm and emission wavelength of 530 nm in the FL1 channel.

Geometric mean fluorescence (GMF) values were calculated using FLOWJO software (www.flowjo.com). The binding data were calculated using the equation:

$$\%\text{Binding} = [(GMF_{test}-GMF_{control})/(GMF_{maximum}- GMF_{control})] \text{ X } 100$$

Where, $GMF_{control}$ = GMF for the cells that were not treated with VCC variants, but incubated in presence of anti-VCC and anti-rabbit-FITC; $GMF_{maximum}$ = GMF for the cells treated with the highest concentration of WT-VCC used in the assay (4.875 µg ml^{-1}), followed by incubation with anti-VCC and anti-rabbit-FITC.

Preparation of liposomes

Asolectin, cholesterol, dansyl-Phosphatidylethanolamine (dansyl-PE) and calcein were procured from Sigma-Aldrich. Equal amount of Asolectin and cholesterol were dissolved in chloroform in a round-bottom flask. The solvent was evaporated at room temperature under constant shaking in order to form a lipid film. The lipid film was dried under vacuum for 2 hours, followed by resuspension in PBS at 37 ˚C for 2 hours. For preparing uniform large unilamellar vesicles (LUVs), liposomes were repeatedly extruded through a 0.1 µm polycarbonate membrane using a Mini-Extruder apparatus (Avanti Polar Lipids, Inc., Alabaster, AL, USA).

For preparing dansyl-PE-containing liposomes, 1% dansyl-PE (w/w) was added to the initial lipid mixture.

For preparing calcein-trapped liposomes, the lipid film was resuspended in HBS (20 mM HEPES, 150 mM NaCl, pH 8.0) containing 50 mM calcein for 2 hours at 37˚C. After extrusion, free calcein molecules were removed by passing the liposome suspension through Sephadex G-50 (GE Healthcare Life Sciences) size-exclusion chromatography column equilibrated with HBS.

Enzyme linked immunosorbent assay (ELISA)

An ELISA-based method was used to detect the binding of the WT-VCC and Ala425Val-VCC with Asolectin-cholesterol and Asolectin liposomes. Briefly, the wells of a 96-well microtiter plate (Nunc, Rochester, NY, USA) were coated in triplicate with 1 µg of liposome suspension in PBS by incubating overnight at 4 °C. The plates were washed thrice with TPBS (PBS containing 1% Triton X-100), followed by blocking with addition of 0.2 ml of 3% non-fat dry milk powder in PBS for 1 h. Wild type and mutant VCC proteins were incubated for 2 h at 25 °C to allow binding to the plate-bound liposomes, and then washed three times with TPBS. The bound VCC variants were probed by incubation with rabbit anti-VCC antiserum (1: 5000, v/v) for 90 min, followed by addition of horseradish peroxidase (HRP)-conjugated goat anti-rabbit IgG (1:10 000, v/v) for 1 h at 25 °C. VCC variants bound to liposomes were detected by color development upon addition of o-phenylenediamine (10 mg/ml) in 0.1 M sodium citrate buffer (pH 4.5) containing hydrogen peroxide (H_2O_2) (Merck) (2 µl/ml of 30% v/v H_2O_2). The reactions were stopped by the addition of 1 M

H_2SO_4, and absorbance was measured at 490 nm using a multi-well spectrophotometer (iMark; BioRad, USA).

Far-UV circular dichroism (CD)

Far-UV CD measurements were taken on an Applied Photophysics Chirascan spectropolarimeter with a Peltier-based temperature controlled sample chamber in a quartz cuvette of 5 mm pathlength. Protein concentrations in the range of 0.5-1 μM were used. All the CD spectra were corrected for the respective buffer blanks.

Fluorescence measurements

Intrinsic tryptophan fluorescence spectra for proteins were recorded using a Fluoromax-4 spectrofluorometer (Horiba scientific, Edison, NJ) equipped with a peltier-based temperature controller. Excitation wavelength of 290 nm was used. Slit width of 2.5 nm and 5.0 nm for excitation and emission, respectively, were used.

Calcein fluorescence measurements were taken as described earlier (please refer Chapter 3, Materials and Methods).

FRET from tryptophan residues in the VCC variants to dansyl-PE incorporated in Asolectin–cholesterol liposome was monitored with a Perkin-Elmer LS 55 spectrofluorimeter using a 1 cm cuvette at 25 °C. The fluorescence emission of dansyl was measured at 512 nm upon excitation of tryptophan residues at 280 nm, using excitation and emission slit widths of 5 nm, respectively. All spectra were corrected with control spectra of dansyl-PE-containing Asolectin–cholesterol liposomes resuspended in the same buffer.

Transmission electron microscopy

WT-VCC and Ala45Val-VCC (at a concentration of 65 μg/ml) were incubated with human erythrocyte stroma (with an estimated protein content of 130 μg/ml) (Stroma were prepared by lysis of the human erythrocytes under hypotonic conditions with 5 mM sodium phosphate buffer, pH 7.4) at room temperature for 1 hour. Following incubation, the samples were washed thrice with the same buffer, added onto the carbon-coated grid and negatively stained with 1% phosphotungstic acid. The negatively stained samples were analysed on a Hitachi H7500 Transmission Electron Microscope at the Sophisticated Analytical Instrumentation Facility of Panjab University, Chandigarh, India.

Protein structural models

Protein structural coordinates were obtained from the Protein Data Bank (PDB; 1XEZ for the precursor form of VCC and 3O44 for the oligomeric pore state of VCC). Protein structural model of the mature form of monomeric VCC was generated from the PDB file 1XEZ using PDBSET in the CCP4 suit (112). A homology-based structural model of the

Ala425Val-VCC was constructed with the SWISS-MODEL server (http://swissmodel.expasy.org/) (128-129) using the PDB coordinates 1XEZ as the template. Modelled structure was subjected to energy minimization using the CHIRON server (http://troll.med.unc.edu/chiron/index.php) (130). Protein surface hydrophobic patches were calculated using the HOTPATCH server (http://hotpatch.mbi.ucla.edu/). Protein structural models were rendered with PYMOL (115).

4.4 Results

Ala425Val-VCC is a recombinant variant of VCC

We obtained a mutant variant of VCC during the process of cloning the wild type VCC (WT-VCC). Sequencing data confirmed that the variant harboured a single point mutation of Alanine-to-Valine at position 425 in the Pro-VCC primary amino acid sequence. Analysis of the structural models showed that the mutation could be mapped onto the putative membrane interacting loop of VCC. The mutant displayed an overall similar profile in terms of protein expression and solubility as compared to wild type VCC. Comparison of the intrinsic tryptophan fluorescence emission spectra for changes in the global tertiary structures, and far-UV CD spectra for the changes in the secondary structures showed an almost overlapping profile suggesting that the mutation of Ala425Val did not cause any major change in the global tertiary or secondary structure of the protein (Figure 4.1).

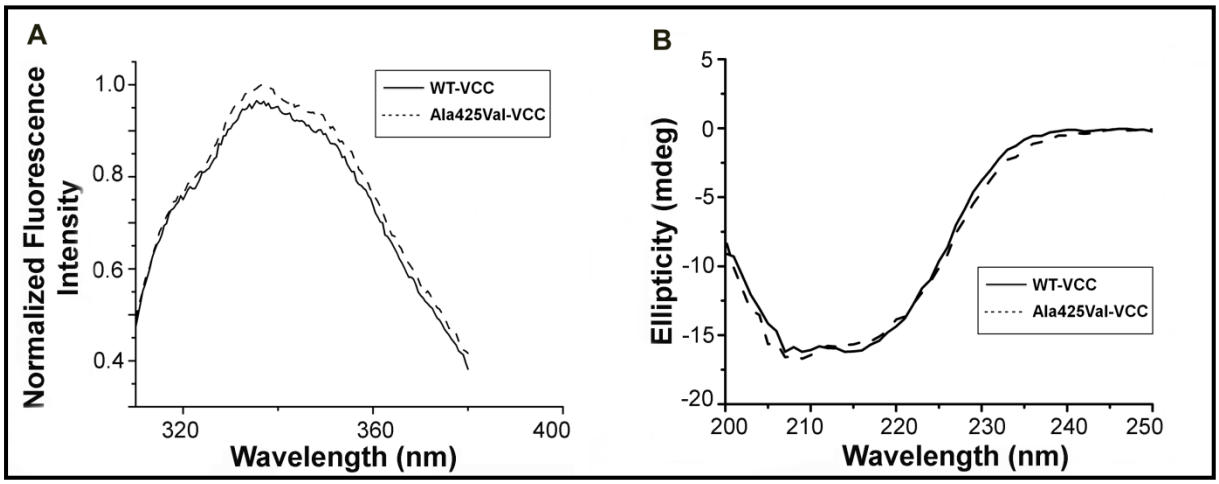

Figure 4.1: (A) Intrinsic tryptophan fluorescence emission spectra of WT-VCC and Ala425Val-VCC. (B) Far-UV CD spectra of WT-VCC and Ala425Val-VCC.

Our data, thus far, suggested that the Ala425Val mutation in VCC did not cause any major structural change in the molecule. To further explore the effect of Ala425Val mutation

on the VCC molecular structure, we constructed a homology-based structural model for Ala425Val-VCC, using the experimentally determined structure of Pro-VCC as the template. The wild type VCC structure showed the presence of a distinct hydrophobic patch on the VCC structure in the region corresponding to the location if the mutation. The homology-based structural model for Ala425Val-VCC showed increased hydrophobicity in the corresponding region, consistent with an increased hydrophobicity of the Valine residue as compared to Alanine (Figure 4.2). Overall, it appears that the Ala425Val mutation did not cause any major change in VCC structure but altered the local microenvironment on the protein surface at the corresponding region.

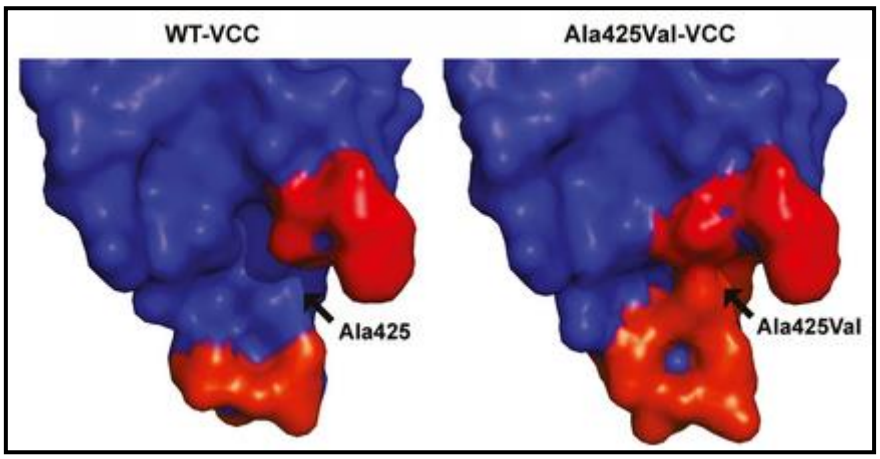

Figure 4.2: Comparison between structural model of WT-VCC (PDB ID: 1XEZ) and structure-based homology model of Ala425Val-VCC. The structural analysis of WT-VCC showed the presence of a hydrophobic patch encompassing the potential membrane-interacting loop harbouring the Ala425CVal-VCC. The analysis of the structure-based homology model of Ala425Val-VCC showed that the incorporation of replacement of alanine with valine increased the local hydrophobicity of this loop.
The surface-exposed hydrophobic patches are colored from red (hydrophobic) to blue (hydrophilic) gradient.

The single point mutation of Ala425Val in the VCC molecule critically impairs the hemolytic activity of the toxin

Recombinantly generated wild type form of the VCC molecule (WT-VCC) analysed in the present study, displayed strong hemolytic activity against human erythrocytes. WT-VCC induced 100% lysis of the human erythrocytes in the concentration range of ~6.5 µg/ml. Strikingly, the single point mutation of Ala425Val in the VCC molecule (Ala425Val-VCC) critically impaired the hemolytic activity of the toxin; no detectable hemolytic activity was observed for the Ala425Val-VCC mutant even at 5-fold higher concentration range (Figure 4.3). The present data clearly indicated that the Ala425Val mutation in the VCC molecule

critically impaired the functional pore formation ability of the toxin in the human erythrocyte cell membranes.

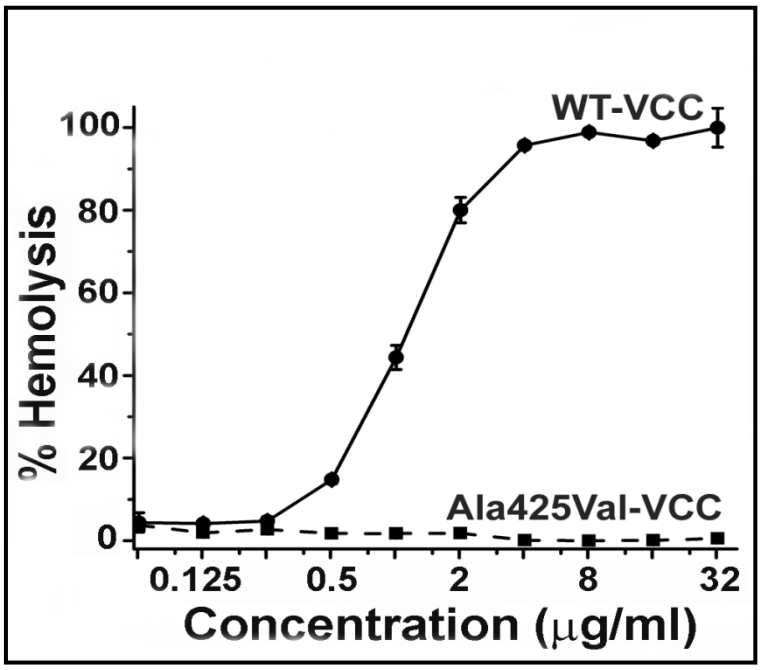

Figure 4.3: Hemolytic activity of WT-VCC and Ala425Val-VCC against human erythrocytes. Human erythrocytes were treated with WT-VCC and Ala425Val-VCC and hemolytic activity was determined by monitoring the release of hemoglobin at 415 nm using UV-Vis spectrometer

Binding and oligomerization propensities of the Ala425Val-VCC variant in the erythrocyte membranes

In order to explore the mechanism by which the Ala425Val mutation impaired the hemolytic activity of the VCC toxin, the binding of WT-VCC and the mutant variant to human erythrocytes membranes was compared. The targeted binding of the wild type and the Ala425Val variant of VCC to cell membranes of human erythrocytes was monitored by immunoblotting using custom-made anti-VCC IgG antibody (Figure 4.4). Quantitative analysis of the immunoblotting data showed that the single point mutant variant of VCC possessed ~0.5-fold of the wild type interaction propensity with the human erythrocyte cell membranes (Table-1). These data revealed that the incorporation of the Ala425Val single point mutation reduced the interaction of the VCC toxin molecule with the human erythrocyte cell membranes, at least to some notable extent.

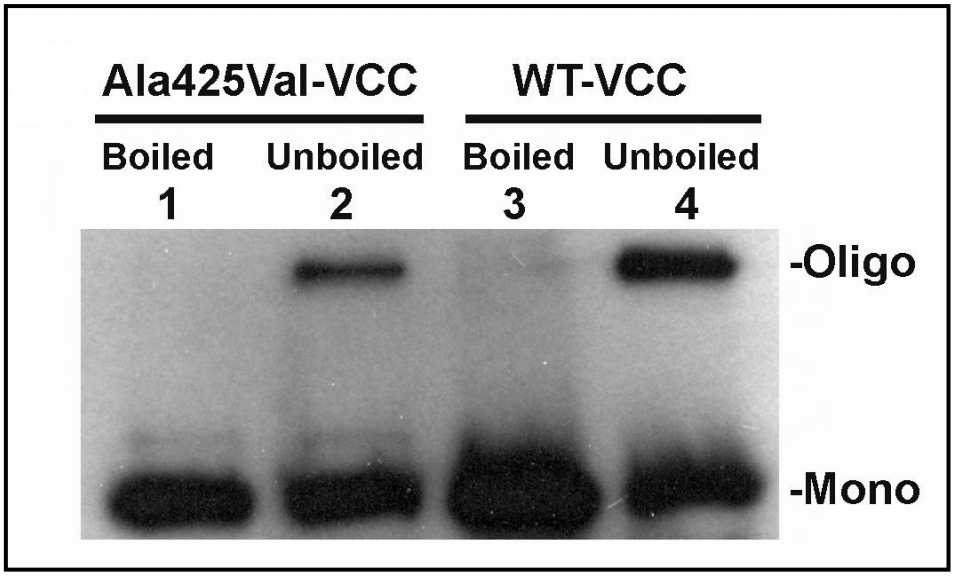

Figure 4.4: Binding and oligomerization of WT-VCC and Ala425Val-VCC with human erythrocytes. WT-VCC and Ala425Val-VCC were incubated with human erythrocytes and the bound fractions were probed for binding and oligomerization by western blotting using anti-VCC serum.

	Lane 1 (Ala425Val)	**Lane 3 (WT)**
Bound Protein	0.475-fold	1-fold

	Lane 2 (Ala425Val)	**Lane 4 (WT)**
Membrane-bound Oligomer	0.49-fold	1-fold

Table 4.1: Comparison of the band intensities of the membrane bound monomeric and oligomeric fractions in Figure 4.4

When probed for the efficiency to form the SDS-stable oligomeric assembly on the erythrocyte cell membranes (Figure 4.4), membrane-bound fraction of the Ala425Val-VCC mutant showed nearly equivalent oligomerization propensity as compared to the wild type protein (comparing the ratio of the total membrane-bound fractions versus the ratio of the oligomer fractions) (Table 4.1). This data clearly indicated that the incorporation of single point mutation (Ala425Val) did not affect the ability of VCC toxin molecule to form oligomers in human erythrocyte cell membrane to any significant extent. Also, it must be noted that, as observed with the WT-VCC protein, the mutant variant of VCC also formed the typical ring-like oligomeric structure on the stroma of human erythrocyte cell membranes (Figure 4.5).

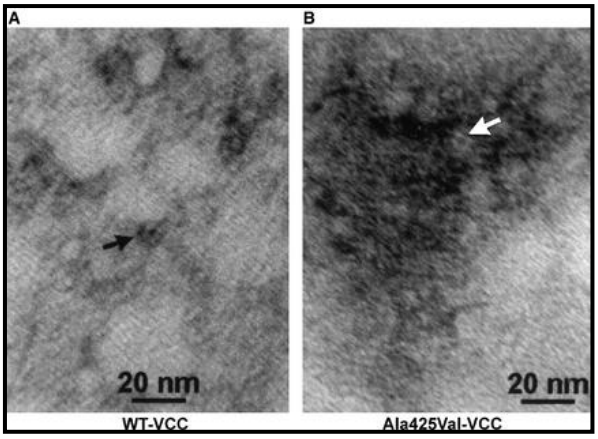

Figure 4.5: Formation of ring-like oligomeric structures by WT-VCC and Ala425Val-VCC on human erythrocytes. Transmission electron micrograph showing the formation of typical ring-like oligomeric structures by both the variants of VCC.

To get a more quantitative insight into the erythrocyte binding ability of the VCC variants, we employed a flow cytometry-based binding technique wherein the primary anti-VCC IgG was detected using a secondary anti-rabbit FITC conjugated antibody. The increase in FITC fluorescence would directly correlate with an increased binding by the VCC variants. The results clearly suggested that incorporation of single point mutation Ala425Val critically impaired the binding of VCC to human erythrocyte membrane (Figure 4.6).

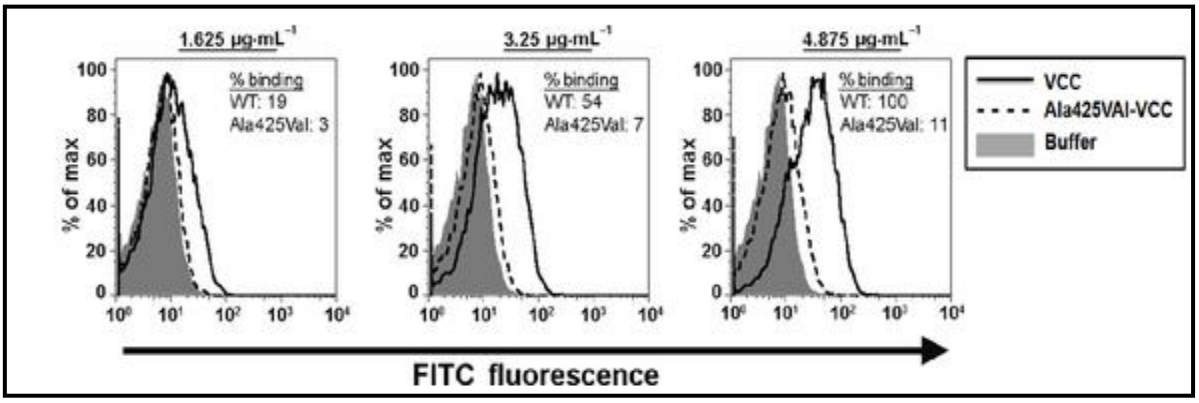

Figure 4.6: Comparison of membrane binding of WT-VCC and Ala425Val-VCC with human erythrocytes using flow cytometry-based binding assay. WT-VCC and Ala425Val-VCC were incubated with human erythrocytes and binding was estimated using flow cytometry based experiment.

Ala425Val mutation traps the VCC toxin into an abortive oligomeric state in the erythrocyte membranes

The analysis of the VCC mutant protein, in comparison to the wild type VCC toxin molecule thus far indicated that the Ala425Val-VCC variant was defective, at least to some notable extent, in terms of its ability to interact with the human erythrocyte membrane. However, it must be emphasized that the Ala425Val-VCC protein exhibited significant binding along which formation of considerable amount of SDS-stable oligomeric species in the human erythrocyte cell membrane, particularly in the concentration range of 65 µg/ml, although, the Ala425Val-VCC protein could not induce any considerable hemolytic activity in the same concentration range against human erythrocyte cells. One likely reasoning could be that the amount of the membrane-bound oligomers generated by Ala425Val might not be sufficient (due to the decreased membrane binding) to induce efficient lysis of the target cells. Alternative reasoning could be that the SDS-stable oligomeric species generated by the membrane-bound Ala425Val-VCC mutant may not represent the functional transmembrane oligomeric assembly of the toxin.

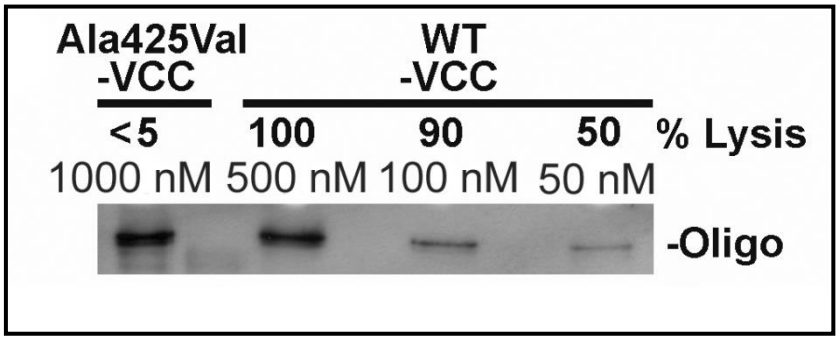

Figure 4.7: Comparison of oligomer load and hemolytic activity against human erythrocytes by WT-VCC and Ala425Val-VCC. Human erythrocytes were treated with different concentrations of WT-VCC and Ala425Val-VCC. The percent lysis (%lysis) of human erythrocytes was measured along with the oligomer load in the membrane-bound fractions, as probed by western blotting using anti-VCC antiserum.

	Lane 1 (Ala425Val) 65 µg/ml	**Lane 2 (WT) 32.5 µg/ml**	**Lane 3 (WT) 6.5 µg/ml**	**Lane 4 (WT) 3.25 µg/ml**
Membrane-bound Oligomer	1-fold	0.96-fold	0.25-fold	0.07-fold

Table 4.2: Comparison of the band intensities of the membrane-bound oligomeric fractions in Figure 4.7.

To investigate these possibilities, we compared the membrane-bound oligomer load for both the wild type and mutant variant of the toxin at two extreme concentrations: 65

μg/ml for Ala425Val-VCC, the concentration range, at which the mutant could not trigger any lysis of human erythrocytes, and 6.5 μg/ml for WT-VCC, the concentration range, at which the wild type VCC protein induced ~100 % hemolysis. In this experimental set up, the membrane-bound oligomer load of Ala425Val-VCC at a concentration of 65 μg/ml, was found to be almost equivalent to the WT-VCC at a concentration of 6.5 μg/ml (Figure 4.7) (Table 4.2). Even then, such load of the SDS-stable oligomers of the mutant in the erythrocyte membranes did not induce any considerable hemolysis. These data, therefore, clearly suggested that the SDS-stable oligomeric form of the Ala425Val-VCC protein generated in the human erythrocyte cell membranes did not represent the functional pore assembly of the toxin; rather such oligomeric assembly could be considered as being remained trapped in an abortive non-functional oligomeric state.

Ala425Val mutation affected the cholesterol-dependent interaction of the VCC toxin with the membrane lipid bilayer

Earlier, it has been speculated that cholesterol regulates the VCC mode of action by physically interacting with the toxin, and not by modulating the properties of the membrane lipid bilayer environment (131). However, the exact mechanism of cholesterol-dependency for the VCC mode of action still remains elusive. In particular, the description of the VCC structural motif recognizing the membrane-anchored cholesterol remains unknown. Since Ala425Val-VCC displayed critical deficit in its functional pore-forming activity in the erythrocyte membranes, we explored the possibility whether the Ala425Val mutation affected the cholesterol-dependent mechanism(s) of the VCC membrane channel formation process. For this, we investigated the interaction of the wild type and the mutant variant of VCC with the simple liposome systems, containing or lacking cholesterol molecules.

We first compared the membrane damaging effects of the Ala425Val-VCC and WT-VCC proteins against the Asolectin-cholesterol liposomes. We monitored the release of calcein from the liposome upon treatment with the wild type and the mutant VCC proteins (Figure 4.8). As reported earlier, wild type protein induced significant extent of calcein release from the Asolectin-cholesterol liposomes. On the other hand, the mutant protein, at similar concentration ranges, displayed significantly reduced potential to trigger the release of calcein from Asolectin-cholesterol liposomes. A nominal ~20% release of calcein was induced by Ala425Val-VCC at the highest protein concentration tested (65 μg/ml). The result, therefore, suggested that the Ala425Val mutation critically abrogated the membrane permeabilization effect of the VCC toxin against the simple liposome systems.

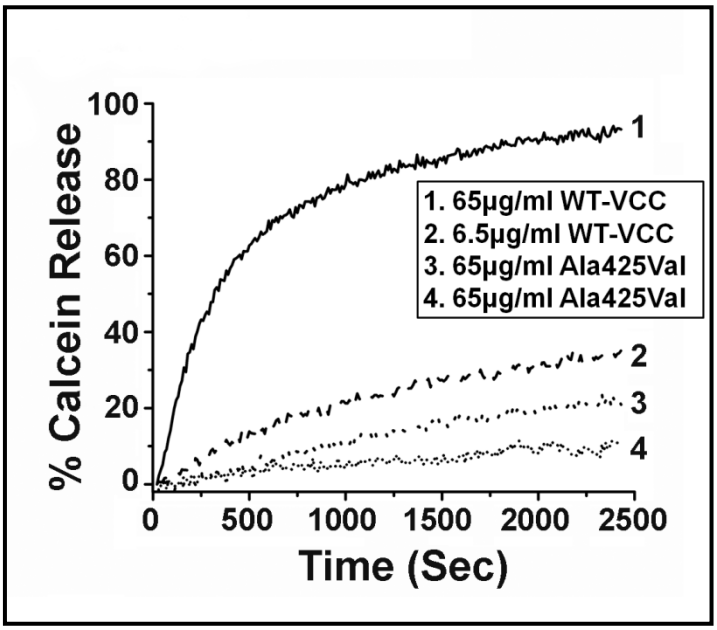

Figure 4.8: Membrane permeabilization of Asolectin-cholesterol liposomes by WT-VCC and Ala425Val-VCC. Membrane permeabilization effect of WT-VCC and Ala425ValVCC against Asolectin-cholesterol liposome was monitored by measuring the release of calcein from the artificial lipid vesicles.

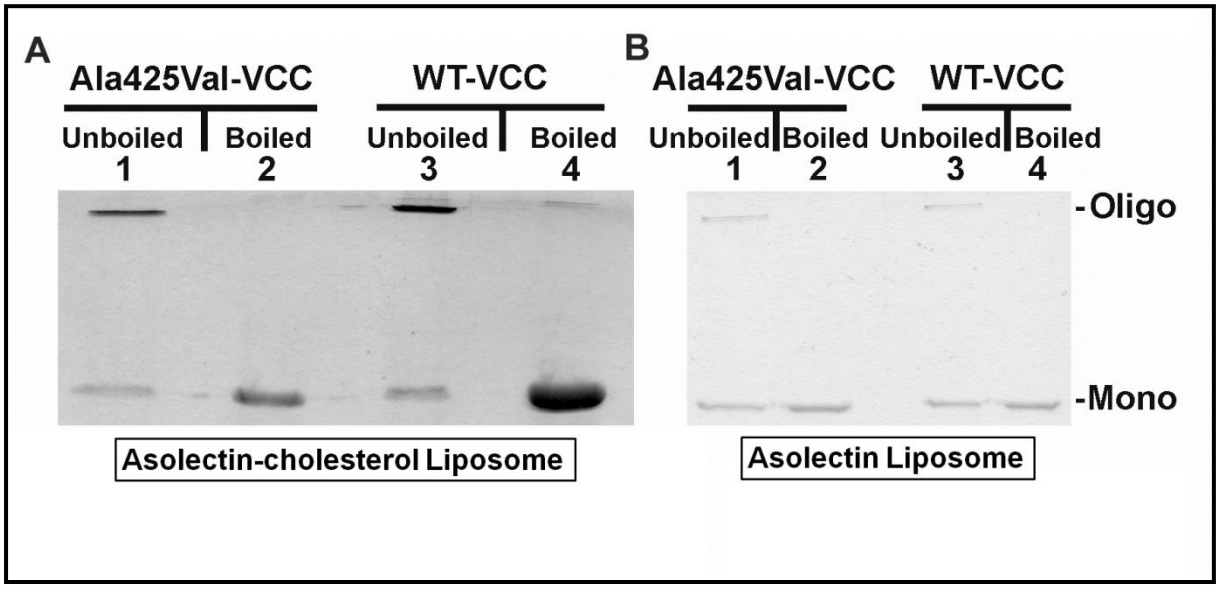

Figure 4.9: Binding and oligomerization efficacy of the bound fraction of WT-VCC and Ala425Val-VCC with asolectin-cholesterol liposome and asolectin liposomes. WT-VCC and Ala425Val-VCC were incubated with Asolectin-cholesterol liposome and asolectin liposomes, bound fraction of the protein was analyzed for binding and oligomerization by SDS-PAGE/Coomassie staining.

Next, we compared the interactions of the WT-VCC and Ala425Val-VCC variant with the cholesterol-containing Asolectin liposome membranes. We observed that a significantly reduced fraction of the Ala425Val-VCC mutant was converted into the SDS-

stable oligomeric form as compared to the WT-VCC toxin, when incubated in presence of the Asolectin-cholesterol liposomes (Figure 4.9A). Furthermore, we found that the Ala425Val-VCC protein showed considerably decreased binding propensity toward the Asolectin-cholesterol liposomes as compared to the WT-VCC toxin (Figure 4.10). However, the liposome-bound fractions of both the two proteins showed nearly equivalent propensities to convert into the oligomeric form. Therefore, the Ala425Val mutation caused significant defect in the VCC toxin in terms of its binding, and not in terms its oligomerization propensity, in the Asolectin-cholesterol liposome membrane. In this context, it is also important to note that the interactions to the Asolectin liposomes lacking cholesterol were drastically less for both the WT-VCC and Ala425Val-VCC molecules (Figure 4.9B). Moreover, binding to the Asolectin liposomes was comparable for both the wild type and the mutant variant (Figure 4.9B and 4.10). Such a lower extent of basal level interaction of the VCC variants with the Asolectin alone liposomes was presumably the result of amphiphilicity-driven non-specific association of the proteins with the membrane lipid bilayer. These data, therefore, confirmed the notion that the presence of cholesterol in the membrane lipid bilayer was crucial for the efficient membrane interaction of the VCC toxin. The data also suggested that the Ala425Val mutation critically abrogated the cholesterol-dependent interaction of the VCC protein with the membrane lipid bilayer, but not the oligomerization propensity of the membrane-bound toxin.

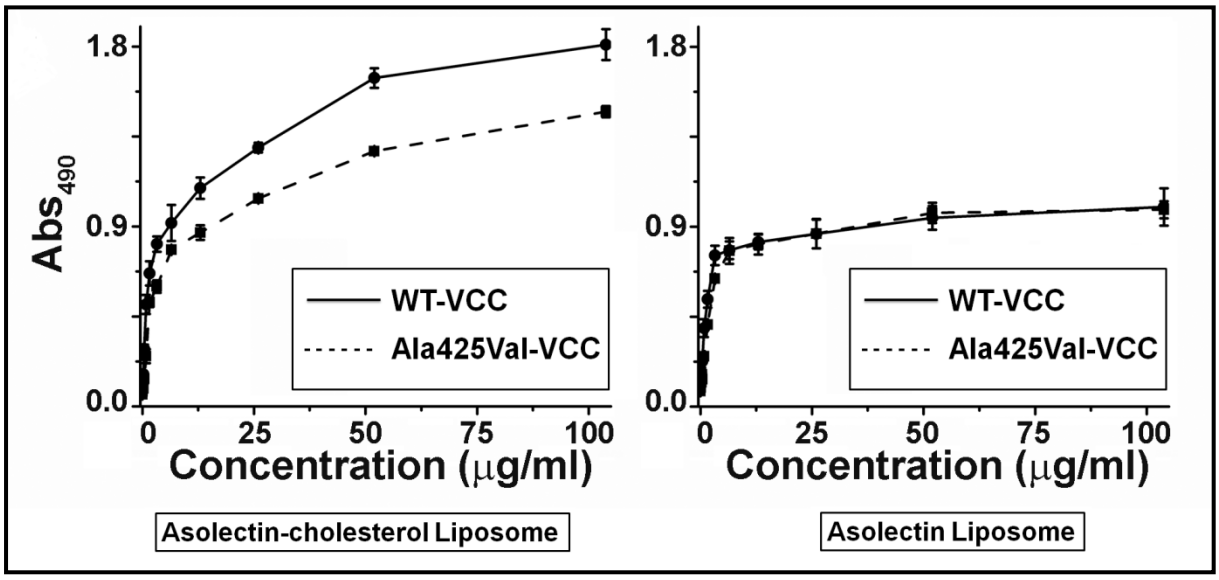

Figure 4.10: Binding to Asolectin-cholesterol and Asolectin liposomes by WT-VCC and Ala425Val-VCC measured by ELISA based binding assay. The binding of WT-VCC and Ala425Val-VCC proteins with Asolectin-cholesterol liposomes and Asolectin liposomes was measured by ELISA based binding assay. Error bars represent the standard deviation calculated from three measurements.

To further probe the mechanistic details of the differential modes of interaction of the WT-VCC and the Ala425Val-VCC variants with the cholesterol-containing Asolectin liposomes, FRET from the tryptophan residue(s) in the VCC proteins to the dansyl-PE incorporated in the Asolectin-cholesterol liposomes was monitored. The efficiency of energy transfer from tryptophan (donor) to dansyl (acceptor) depends, among many other factors, on the proximity both the donor and acceptor groups. Thus, an increase in the FRET signal (from tryptophan-to-dansyl-PE) could be directly correlated in terms of intimacy of binding of the VCC variants and the membrane lipid bilayer. In the present experimental set up, the wild type molecule displayed a steady increase in the FRET signal (from tryptophan in VCC to dansyl in lipid bilayer) upon incubation with the dansyl-PE-containing Asolectin-cholesterol liposomes. In contrast, the mutant protein Ala425Val-VCC did not induce any detectable increase in the FRET signal (Figure 4.11). This result suggested that the Ala425Val-VCC mutant, although capable of binding and forming SDS-stable oligomeric assembly on the Asolectin-cholesterol liposome membranes to some detectable extent, failed to make a more intimate interaction with the membrane lipid bilayer. Altogether, these data confirmed our notion that a critical cholesterol-dependent interaction of the VCC molecule with the membrane lipid bilayer was abrogated due to the Ala425Val mutation; such cholesterol-dependent interaction was necessary to generate more intimate association of the toxin molecule with the membrane lipid bilayer.

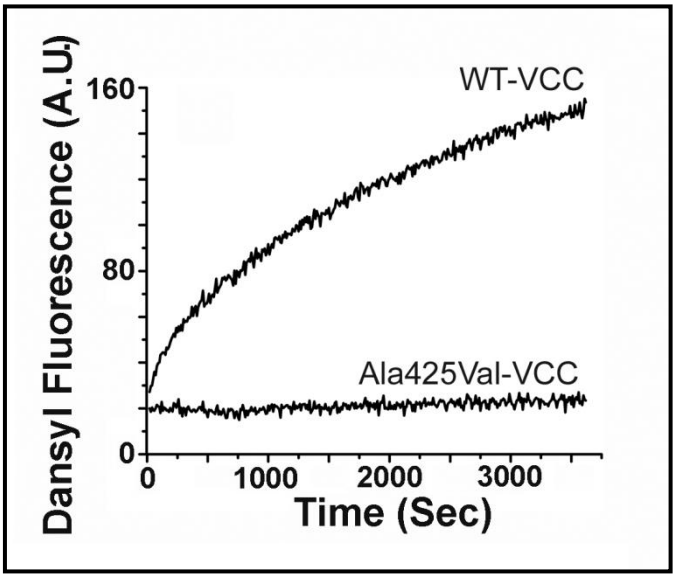

Figure 4.11: Interaction of WT-VCC and Ala425Val-VCC with Asolectin-cholesterol liposomes probed by tryptophan-to-dansyl FRET. Asolectin-cholesterol liposomes containing dansyl-PE were treated with WT-VCC and Ala425Val-VCC. Intimacy of binding of the two proteins with the liposome bilayer was estimated by measuring the tryptophan-to-dansyl FRET.

4.5 Discussion

In our present study, we found that the single point mutation of Ala425Val in the VCC protein critically affected its functional pore-forming ability in the erythrocyte membranes. The mutation affected binding of the toxin to the erythrocyte membranes to some notable extent, but did not detectably alter the oligomerization propensity of the membrane-bound fraction of the protein. Our data suggested that the Ala425Val mutation trapped the VCC molecule on the erythrocyte cell membranes in an abortive oligomeric assembly state. When we probed further the mechanistic basis of the functional defects caused by the Ala425Val mutation, we found that the mutation critically affected the cholesterol-dependent interactions of the VCC toxin with the membrane lipid bilayer.

Since the Ala425Val mutation in the VCC molecule critically abrogated its cholesterol-dependent interaction with the membrane lipid bilayer, we analyzed the location of this mutation in the context of the potential membrane-interaction site(s) within the toxin. Mapping of the Ala425Val mutation onto the VCC oligomeric structure confirms its location within a potential membrane interacting loop (Tyr420-Tyr421-Val422-Val423-Gly424-Ala425; Ala425 being the last residue of this 'longest loop' in the VCC membrane-proximal rim domain). The mutation is located in the loop positioned in such a way that would presumably make direct contact with the membrane, partly penetrating the outer leaflet of the membrane lipid bilayer. The location of this mutation also aligns very well with the potential membrane binding site of the *S. aureus* α-hemolysin. More critical analysis of the location of the Ala425Val mutation with respect to the sequence/structure context shows that the mutation is positioned in the loop (Tyr420-Tyr421-Val422-Val423-Gly424-Ala425) that forms the lining of a shallow grove at the membrane-proximal rim domain of VCC. This grove is also lined by the residues from two additional loops of the VCC cytolysin domain: Thr236-Thr237-Leu238 and Asp359-Ala360-Leu361-Trp362. Such grove-like structure is also present within the rim domain of the *S. aureus* α-hemolysin (60), where similar disposition, without any noticeable sequence identity, of the potential membrane-interacting loops is observed. Although distantly related to VCC in terms of sequence identity, overall structural similarity and mechanism of pore formation, the so called "cholesterol-dependent cytolysins" (CDCs) including perfringolysin O and intermedilysin also highlight presence of similar, prominent loop structures (namely, L1-L3 loops) in their membrane-binding domains. More importantly, these L1-L3 loops in the CDCs have been shown to be the critical structural elements responsible for their cholesterol-dependent membrane interaction (23, 77). In particular, a conserved 'Thr-Leu' pair located within the L1-loop of the CDCs has

been conclusively identified as the key element mediating the recognition and binding of the membrane cholesterol (132). Remarkably, this 'Thr-Leu' pair is found to be present in the rim domain of VCC as part of the Thr236-Thr237-Leu238 loop structure, as mentioned above. It is also important to note that the position of the Ala425 residue aligns well with that of a conserved Ala-residue located at the end of the L2-loop (His-Ser-Gly-Ala-Tyr-Val-Ala in case of perfringolysin O, and His-Asp-Gly-Ala-Phe-Val-Ala in case of intermedilysin) in the CDCs (76). Altogether, these observations indicate the notions that the membrane-proximal rim domain of VCC possesses a prominent structural motif constituted by the residues from three distinct loops. Ala425Val mutation in VCC is positioned within this structural motif. Similar structural motifs found in CDCs are implicated in the process of interaction with membrane cholesterol.

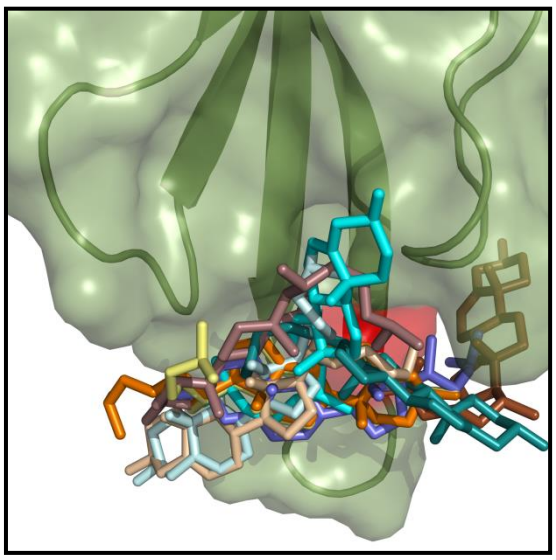

Figure 4.12: Model showing docking of cholesterol molecule with VCC. The docking studies were performed using AutoDock Vina (133).

In this direction, a docking-based modeling strategy also indicated that this structural motif in VCC (constituted by the loops Tyr420-Tyr421-Val422-Val423-Gly424-Ala425, Thr236-Thr237-Leu238 and Asp359-Ala360-Leu361-Trp362) could serve as one of the potential sites within the VCC cytolysin domain where cholesterol could be docked (Figure 4.12). Therefore, based on the result of the modeling, and also consistent with its location in the membrane-proximal rim domain of VCC, the above mentioned structural motif could be speculated as a potential site for recognition and binding of membrane cholesterol. It is important to note that this motif does not show any apparent resemblance to the more prominent 'cholesterol-binding motif' such as the eukaryotic 'cholesterol recognition amino acid consensus' (CRAC) motif (134). A typical CRAC motif has the pattern of Leu/Val-X_{1-5}-

Tyr-X_{1-5}-Arg/Lys, and it is found to be located adjacent to a transmembrane α-helix that allows it's positioning in the juxta-membrane regions, where it can make efficient interactions with the membrane cholesterol.

Nevertheless, analysis of the structure as well as the result of our docking-based modeling indicates presence of a putative structural motif in VCC that could potentially bind to membrane cholesterol. Since Ala425 residue appears to be a prominent component of this structural motif, such notion would also be consistent with our experimental data showing a strong correlation between the Ala425Val mutation and the cholesterol-dependent interaction of the VCC molecule with the membrane lipid bilayer. It is however not clear how exactly the Ala425Val mutation is affecting the cholesterol-dependent membrane interaction of VCC. Detail mutagenesis study targeting this putative 'cholesterol-binding pocket' in VCC would be required to gain more insight regarding the mechanistic basis of this phenomenon.

The present data indicates toward the requirement of cholesterol not only for membrane insertion but also for early VCC-membrane interactions leading to formation of a functional oligomer. Studies have shown that cholesterol is required for the allosteric activation of the cholesterol-dependent cytolysin Streptolysin O for efficient pore-formation. Streptolysin O and VCC have been shown to have stereospecificity toward the 3L-OH group of cholesterol, which plays an important role in toxin oligomerization. It will be interesting to see whether the interaction of VCC with other lipid molecule in the membrane lipid bilayer is also stereospecific.

In our present study we found that the cholesterol-dependent membrane interaction of the VCC protein was severely affected due to the Ala425Val mutation, an alteration that also abolished the functional pore-forming ability of the toxin. As suggested by the earlier studies, the optimal membrane pore formation property of VCC was found to be tightly linked with its efficient interaction with the membrane cholesterol (102). Therefore, we hypothesize that the Ala425Val mutation critically affected the membrane channel-formation process by VCC, presumably by affecting its optimal interaction with the cholesterol molecules anchored in the biomembranes. Interestingly, the Ala425Val mutation affected the cholesterol-dependent intimate association of the VCC protein with the membrane lipid bilayer, without affecting the oligomerization potential of the membrane-bound fraction of the toxin molecules. Earlier studies have suggested the presence of cholesterol in the biomembranes as a critical factor for efficient pore-formation by the VCC toxin (135). Moreover, separate structural motifs present in the cholesterol molecule have been speculated to support the cholesterol-VCC interaction

and VCC-oligomerization (123-124, 135). For example, (i) the α-OH moiety at the C3 position in the A-ring and (ii) the double bond between the C5 and C6 position in the B-ring of the cholesterol have been shown to be critical for the cholesterol-VCC binding (102, 123). It has been speculated that the hydrophobic interaction of the sterol nucleus with VCC could be instrumental in triggering the oligomerization of the toxin in the membrane lipid bilayer. In accordance with such conjecture, and also based on the experimental data presented in the current study, we propose the following hypothesis. It is possible that the Ala425Val mutation disrupted the primary interaction of the VCC molecule with the membrane-bound cholesterol (such interaction could be vaguely defined as the "VCC-cholesterol interaction-I"), thus affecting the cholesterol-mediated targeting of the toxin toward the membrane lipid bilayer. Albeit, it appears that the VCC variant harboring the Ala425Val mutation could still manage to display a basal level binding to the liposome membranes in a cholesterol-independent fashion, presumably via amphipathicity-driven non-specific association with the phospholipid molecules. In case of erythrocyte membranes, such cholesterol-independent binding could also be facilitated by, as yet unknown, receptor(s) or receptor-like molecules. Once bound to the biomembranes, however, the Ala425Val mutant could be acted upon by the membrane cholesterols (via another, as yet undefined, mode of interaction that we vaguely define as "VCC-cholesterol interaction-II") toward forming the SDS-stable oligomeric assembly. As the SDS-stable oligomeric structures formed by the Ala425Val-VCC mutant appeared to be trapped in the form of abortive oligomeric assembly states, and not representing the functional transmembrane channel, we further hypothesize that the "VCC-cholesterol interaction-I" could be instrumental in triggering the conformational fine-tuning in the VCC molecular structure, required for the conversion of the abortive oligomer into the functional transmembrane pore assembly. Future studies will be required, however, to elucidate the structural/molecular details of these interactions between the VCC protein and the membrane cholesterol, as being hypothesized here. Also, additional studies would be required to explore the possibility whether Ala425Val mutation imposes any, as yet unknown, long-range conformational defects, thus interfering with the mechanism of efficient membrane pore-formation process by VCC.

Note:

* This part of the study has been published in the FEBS Journal.

Paul, K. and Chattopadhyay, K. (2012) Single point mutation in *Vibrio cholerae* cytolysin compromises membrane pore-formation mechanism of the toxin. FEBS Journal, 279 (21), 4039-4051.

This part of the thesis has been adapted with permission from "Paul, K. and Chattopadhyay, K. (2012) Single point mutation in *Vibrio cholerae* cytolysin compromises membrane pore-formation mechanism of the toxin. FEBS Journal, 279 (21), 4039-4051" (John Wiley and Sons).

Summary

Bacterial β-barrel pore-forming toxins (β-PFTs) constitute a unique class of protein toxins, which damage the target eukaryotic cell membranes by forming transmembrane oligomeric β-barrel channels. These toxins have been implicated in the virulence mechanisms of many pathogenic bacteria such as *Staphylococcus aureus* (19) and *Aeromonas hydrophila* (15). β–PFTs are secreted by the bacteria as water-soluble monomers, which upon binding to the respective target cell membranes transform into transmembrane oligomeric channels, thus causing colloid-osmotic lysis of the target host cells (32).

Vibrio cholerae cytolysin (VCC) is a prominent member in the β-PFT family. VCC is secreted by most of the *V. cholerae* strains with high pathogenic potential (80, 91). It is secreted as a ~79 kDa inactive precursor (Pro-VCC), which upon proteolytic removal of the ~15 kDa N-terminal Pro-domain, converts into the functionally active mature form of the toxin with the potential to form oligomeric pores in the host cell membranes (136). Consistent with the archetypical β-PFT structural models, central scaffold of the VCC molecule highlights presence of a core cytolysin domain that harbours the so called 'pre-stem' loop (containing two β-strands). In the process of oligomeric membrane pore-formation, pre-stem loop from each toxin protomer participates toward formation of the transmembrane β-barrel segment. Apart from the cytolysin domain, the structure of the VCC molecule also shows presence of additional unique motifs/domains with potential functional implications. The presence of accessory motifs/domains in the VCC architecture makes it different from other PFTs, and yet at the same time, represents it as a suitable model system for addressing the questions related to mechanisms of the toxin-membrane interactions and membrane pore-formation. In this direction, the present study explores the implications of distinct structural motifs/domain in the VCC mode of action, particularly, in the process of its secretion, membrane binding and functional oligomeric membrane pore-formation.

Implications of the Pro-domain in the structure-function mechanism of VCC

We investigated the role of the "Pro" domain by comparing the physicochemical properties of the Pro-VCC and Mature-VCC. Earlier studies have shown that the removal of the Pro-domain from the gene encoding VCC results in the degradation of the toxin in the bacterial periplasmic space. Chemically denatured Pro-VCC recovers complete activity after renaturation. In contrast, Mature-VCC lacking the Pro-domain does not get activated upon renaturation from the unfolded states (97). The Pro-domain also bears sequence similarity

with the Hsp90 family of chaperones. Since the location of the Pro-domain is within the VCC molecule, it has been proposed as an intramolecular chaperone (97), suggesting that the N-terminal Pro-domain might play some role in the secretion/folding of the VCC molecule into its native architecture. However, the exact role of the Pro-domain in the structure-function relationship of VCC needed to be explored in mechanistic detail. We characterised the precursor and the mature form of VCC namely, Pro-VCC and Mature-VCC, respectively, in terms of changes in the tertiary and the secondary structures during the events of protein unfolding. Under the native conditions, both the variants exhibited similar tryptophan environments as revealed by the intrinsic tryptophan fluorescence emission profile. This suggested that both the variants of VCC shared a similar global tertiary structure. However, the variants displayed notable differences in terms of the secondary structural composition when probed by using far-UV circular dichroism (CD). The two variants of VCC were exposed to an array of denaturing conditions, namely, low-pH, chemical denaturants such as urea and high temperature, and were analysed using intrinsic tryptophan fluorescence emission, far-UV circular dichroism (CD) spectroscopy and light scattering measurements. Both the proteins displayed similar changes in their global tertiary structures during low pH-induced unfolding. However, the Pro-VCC molecule displayed a higher tendency toward local changes in the structure owing to an increased exposure of surface hydrophobic patches. Similarly, Pro-VCC displayed a strengthened unfolding propensity toward chemical and high temperature-induced unfolding.

Overall, the precursor Pro-VCC appears to be more susceptible to structural and conformational changes and unfolding than Mature-VCC. It would be a valid argument that the increased unfolding changes observed in Pro-VCC could be due to an increased unfolding tendency of the Pro-domain itself. To test this, we exposed the Pro-domain in isolation to similar denaturing conditions. Surprisingly, the Pro-domain displayed a much decreased tendency to unfold as compared to both Pro-VCC and Mature-VCC. These data suggested that the increased unfolding propensity of Pro-VCC was not contributed by the unfolding tendency of the Pro-domain itself. Rather, it appeared that the presence of the Pro-domain modulated the physicochemical properties of the entire Pro-VCC molecule, presumably via a, not yet characterized, regulatory mechanism. Based on the above results it can be postulated that the presence of the Pro-domain, provides sufficient level of structural plasticity into the Pro-VCC molecule that makes it much more amenable to undergo folding/unfolding processes, thus presumably aiding in the secretion process of the toxin.

Membrane pore formation mechanism of VCC: truncation of the pre-stem region traps the toxin in its membrane-bound pre-pore oligomeric state

One of the steps in the β-PFT mode of action is the formation of a membrane bound non-functional pre-pore oligomeric intermediate, followed by insertion of the pre-stem motif into the membrane lipid bilayer leading to the formation of a functional transmembrane β-barrel pore. The structural analysis of the water-soluble monomeric form of VCC shows presence of a two strand β-structure, known as the pre-stem loop (spanning the residue 281-322) (22). Data from previous studies has shown that the covalent locking of the VCC pre-stem region via engineered disulphide bonds arrests the toxin in an abortive non-functional pre-pore state (119), indicating that the pre-stem loop plays a central role in the formation of a functional transmembrane channel. However, the role of the pre-stem motif in the VCC-membrane interactions and membrane-bound pre-pore oligomer formation needed to be explored. In this direction, we characterized a variant of VCC lacking the pre-stem loop region (ΔPS-VCC). Using this variant, we explored the implications of the pre -stem loop in maintaining the structural integrity of VCC, in binding to target lipid membranes, in the formation of a pre-pore complex, and finally in the process of functional transmembrane pore structure generation. The ΔPS-VCC variant displayed compromised lytic activity toward human erythrocytes indicating that the presence of a β-barrel structure is important for the toxin activity. The mutant variant also showed wild type-like membrane binding toward artificial membrane lipid bilayers and human erythrocytes. However, the ΔPS-VCC lacked the ability to form SDS-stable heptameric assemblies. Covalent crosslinking experiments clearly showed the formation of intermediate pre-pore oligomers when ΔPS-VCC was incubated with Asolectin-cholesterol liposomes. Furthermore, Fluorescence Resonance Energy Transfer (FRET)-based experiments clearly suggested that the truncation of the pre-stem region from VCC leads to the abortive membrane insertion step in the VCC mode of action. Overall, our study suggests that the pre-stem loop within the central cytolysin domain does not play any role in the VCC-membrane interaction step, as well as in the pre-pore oligomer formation stage. However, the presence of this motif is necessary for the formation of a functional transmembrane β-barrel pore structure.

Cholesterol-dependent membrane interaction mechanism of VCC: implication of a single point mutation in the toxin

Earlier studies have suggested a critical requirement for the presence of membrane cholesterol in the VCC mode of action (135, 137). In this direction, we characterized a

variant of VCC (Ala425Val-VCC) harbouring a single point mutation (alanine to valine) at position 425 within the potential membrane-binding region of the toxin. We found that the cholesterol-dependent membrane interaction of VCC was severely affected due to the Ala425Val mutation, an alteration that also abolished the functional pore-forming ability of the toxin. The single point mutation critically affected the membrane pore-forming activity of VCC toward human erythrocytes as well as cholesterol-containing synthetic lipid vesicles/liposomes. Ala425Val-VCC displayed decreased binding toward cholesterol-containing membranes, whereas binding to membranes lacking cholesterol was not affected to any noticeable extent. FRET-based experiments also showed that the Ala425Val-VCC lacked intimate interaction with the membrane lipid bilayer of the cholesterol-containing synthetic lipid vesicles. Further analysis of membrane-binding and oligomerization revealed that the Ala425Val mutation affected the cholesterol-dependent intimate association of the VCC protein with the membrane lipid bilayer, without affecting the oligomerization potential of the membrane-bound fraction of the toxin molecules. Overall, our study suggests that the Ala425Val mutation critically compromises the cholesterol-dependent membrane interaction mechanism of VCC, and it also traps the VCC molecule on the target membranes in the form of an abortive oligomeric assembly state. Our study, for the first time, identifies presence of a potential structural motif within the VCC molecular structure that might have implication for the cholesterol-dependent membrane interaction and functional pore-formation mechanism of the toxin.

References

1. Schiavo G & van der Goot FG (2001) The bacterial toxin toolkit. *Nat Rev Mol Cell Biol* 2(7):530-537.
2. Middlebrook JL & Dorland RB (1984) Bacterial toxins: cellular mechanisms of action. *Microbiological Reviews* 48(3):199-221.
3. Alouf JE & Popoff MR (2005) *The Comprehensive Sourcebook of Bacterial Protein Toxins* (Elsevier Science).
4. Tilley SJ & Saibil HR (2006) The mechanism of pore formation by bacterial toxins. *Current Opinion in Structural Biology* 16(2):230-236.
5. Gonzalez MR, Bischofberger M, Pernot L, van der Goot FG, & Frêche B (2008) Bacterial pore-forming toxins: The (w)hole story? (Translated from English) *Cell. Mol. Life Sci.* 65(3):493-507 (in English).
6. Rojko N, *et al.* (2013) Membrane Damage by an α-Helical Pore Forming Protein Equinatoxin II Proceeds Through Succesion of Ordered Steps. *Journal of Biological Chemistry*.
7. Cascales E, *et al.* (2007) Colicin Biology. *Microbiology and Molecular Biology Reviews* 71(1):158-229.
8. Allured VS, Collier RJ, Carroll SF, & McKay DB (1986) Structure of exotoxin A of Pseudomonas aeruginosa at 3.0-Angstrom resolution. *Proceedings of the National Academy of Sciences* 83(5):1320-1324.
9. Soberón M, *et al.* (2010) Pore formation by Cry toxins. *Proteins Membrane Binding and Pore Formation,* Advances in Experimental Medicine and Biology, eds Anderluh G & Lakey J (Springer New York), Vol 677, pp 127-142.
10. Wallace AJ, *et al.* (2000) E. coli Hemolysin E (HlyE, ClyA, SheA): X-Ray Crystal Structure of the Toxin and Observation of Membrane Pores by Electron Microscopy. *Cell* 100(2):265-276.
11. Fahie M, *et al.* (2013) A non-classical assembly pathway of Escherichia coli pore forming toxin cytolysin A. *Journal of Biological Chemistry*.
12. Collier RJ (1975) Diphtheria toxin: mode of action and structure. *Bacteriological Reviews* 39(1):54-85.
13. Collier RJ (2001) Understanding the mode of action of diphtheria toxin: a perspective on progress during the 20th century. *Toxicon* 39(11):1793-1803.
14. Menestrina G, Dalla Serra M, & Prévost G (2001) Mode of action of β-barrel pore-forming toxins of the staphylococcal α-hemolysin family. *Toxicon* 39(11):1661-1672.

15. Fivaz M, Abrami L, Tsitrin Y, & van der Goot FG (2001) Aerolysin from Aeromonas hydrophila and Related Toxins. *Pore-Forming Toxins,* Current Topics in Microbiology and Immunology, ed van der Goot FG (Springer Berlin Heidelberg), Vol 257, pp 35-52.
16. Degiacomi MT, *et al.* (2013) Molecular assembly of the aerolysin pore reveals a swirling membrane-insertion mechanism. *Nat Chem Biol* 9(10):623-629.
17. Kennedy CL, *et al.* (2009) Pore-Forming Activity of Alpha-Toxin Is Essential for Clostridium septicum-Mediated Myonecrosis. *Infection and Immunity* 77(3):943-951.
18. Hang'ombe MB, Mukamoto M, Kohda T, Sugimoto N, & Kozaki S (2004) Cytotoxicity of Clostridium septicum alpha-toxin: its oligomerization in detergent resistant membranes of mammalian cells. *Microbial Pathogenesis* 37(6):279-286.
19. Dinges MM, Orwin PM, & Schlievert PM (2000) Exotoxins of Staphylococcus aureus. *Clinical Microbiology Reviews* 13(1):16-34.
20. Xiong G, Struckmeier M, & Lutz F (1994) Pore-forming Pseudomonas aeruginosa cytotoxin. *Toxicology* 87(1–3):69-83.
21. Petosa C, Collier RJ, Klimpel KR, Leppla SH, & Liddington RC (1997) Crystal structure of the anthrax toxin protective antigen. *Nature* 385(6619):833-838.
22. Olson R & Gouaux E (2005) Crystal Structure of the Vibrio cholerae Cytolysin (VCC) Pro-toxin and its Assembly into a Heptameric Transmembrane Pore. *Journal of Molecular Biology* 350(5):997-1016.
23. Hotze EM & Tweten RK (2012) Membrane assembly of the cholesterol-dependent cytolysin pore complex. *Biochimica et Biophysica Acta (BBA) - Biomembranes* 1818(4):1028-1038.
24. Gilbert RC (2010) Cholesterol-Dependent Cytolysins. *Proteins Membrane Binding and Pore Formation,* Advances in Experimental Medicine and Biology, eds Anderluh G & Lakey J (Springer New York), Vol 677, pp 56-66.
25. Lakey JH & Slatin SL (2001) Pore-Forming Colicins and Their Relatives. *Pore-Forming Toxins,* Current Topics in Microbiology and Immunology, ed van der Goot FG (Springer Berlin Heidelberg), Vol 257, pp 131-161.
26. Zakharov SD & Cramer WA (2002) Colicin crystal structures: pathways and mechanisms for colicin insertion into membranes. *Biochimica et Biophysica Acta (BBA) - Biomembranes* 1565(2):333-346.
27. Parker MW & Feil SC (2005) Pore-forming protein toxins: from structure to function. *Progress in Biophysics and Molecular Biology* 88(1):91-142.

28. Kurisu G, *et al.* (2003) The structure of BtuB with bound colicin E3 R-domain implies a translocon. *Nat Struct Mol Biol* 10(11):948-954.
29. Anderluh G, Gökçe I, & Lakey JH (2004) A Natively Unfolded Toxin Domain Uses Its Receptor as a Folding Template. *Journal of Biological Chemistry* 279(21):22002-22009.
30. Ghosh P, Mel SF, & Stroud RM (1994) The domain structure of the ion channel-forming protein colicin Ia. *Nat Struct Mol Biol* 1(9):597-604.
31. Slatin SL, Qiu X-Q, Jakes KS, & Finkelstein A (1994) Identification of a translocated protein segment in a voltage-dependent channel. *Nature* 371(6493):158-161.
32. Heuck AP, Tweten RK, & Johnson AE (2001) β-Barrel Pore-Forming Toxins: Intriguing Dimorphic Proteins†. *Biochemistry* 40(31):9065-9073.
33. Bernheimer AW, Avigad LS, & Avigad G (1975) Interactions Between Aerolysin, Erythrocytes, and Erythrocyte Membranes. *Infection and Immunity* 11(6):1312-1319.
34. MacKenzie CR, Hirama T, & Buckley JT (1999) Analysis of Receptor Binding by the Channel-forming Toxin Aerolysin Using Surface Plasmon Resonance. *Journal of Biological Chemistry* 274(32):22604-22609.
35. Van der Goot FG, *et al.* (1992) Spectroscopic study of the activation and oligomerization of the channel-forming toxin aerolysin: identification of the site of proteolytic activation. *Biochemistry* 31(36):8566-8570.
36. Abrami L, *et al.* (1998) The Pore-forming Toxin Proaerolysin Is Activated by Furin. *Journal of Biological Chemistry* 273(49):32656-32661.
37. Nelson KL, Raja SM, & Buckley JT (1997) The Glycosylphosphatidylinositol-anchored Surface Glycoprotein Thy-1 Is a Receptor for the Channel-forming Toxin Aerolysin. *Journal of Biological Chemistry* 272(18):12170-12174.
38. Diep DB, Lawrence TS, Ausio J, Howard SP, & Buckley JT (1998) Secretion and properties of the large and small lobes of the channel-forming toxin aerolysin. *Molecular Microbiology* 30(2):341-352.
39. Gurcel L, Abrami L, Girardin S, Tschopp J, & van der Goot FG (2006) Caspase-1 Activation of Lipid Metabolic Pathways in Response to Bacterial Pore-Forming Toxins Promotes Cell Survival. *Cell* 126(6):1135-1145.
40. Cowell S, Aschauer W, Gruber HJ, Nelson KL, & Buckley JT (1997) The erythrocyte receptor for the channel-forming toxin aerolysin is a novel glycosylphosphatidylinositol-anchored protein. *Molecular Microbiology* 25(2):343-350.

41. Parker MW, *et al.* (1994) Structure of the Aeromonas toxin proaerolysin in its water-soluble and membrane-channel states. *Nature* 367(6460):292-295.
42. Krause K-H, Fivaz M, Monod A, & van der Goot FG (1998) Aerolysin Induces G-protein Activation and Ca2+Release from Intracellular Stores in Human Granulocytes. *Journal of Biological Chemistry* 273(29):18122-18129.
43. Dinarello CA (A Signal for the Caspase-1 Inflammasome Free of TLR. *Immunity* 26(4):383-385.
44. Petit L, Gibert M, & Popoff MR (Clostridium perfringens: toxinotype and genotype. *Trends in Microbiology* 7(3):104-110.
45. Popoff MR (2011) Epsilon toxin: a fascinating pore-forming toxin. *FEBS Journal* 278(23):4602-4615.
46. BULLEN JJ (1952) *Enterotoxaemia of sheep: Clostridium welchii type D in the alimentary tract of normal animals* pp 201-206.
47. Minami J, Katayama S, Matsushita O, Matsushita C, & Okabe A (1997) Lambda-Toxin of Clostridium perfringens Activates the Precursor of Epsilon-Toxin by Releasing Its N- and C-Terminal Peptides. *Microbiology and Immunology* 41(7):527-535.
48. Miyata S, *et al.* (2001) Cleavage of a C-terminal Peptide Is Essential for Heptamerization of Clostridium perfringens ε-Toxin in the Synaptosomal Membrane. *Journal of Biological Chemistry* 276(17):13778-13783.
49. Petit L, Maier E, Gibert M, Popoff MR, & Benz R (2001) Clostridium perfringens Epsilon Toxin Induces a Rapid Change of Cell Membrane Permeability to Ions and Forms Channels in Artificial Lipid Bilayers. *Journal of Biological Chemistry* 276(19):15736-15740.
50. Cole AR, *et al.* (2004) Clostridium perfringens [epsi]-toxin shows structural similarity to the pore-forming toxin aerolysin. *Nat Struct Mol Biol* 11(8):797-798.
51. Knapp O, Maier E, Benz R, Geny B, & Popoff MR (2009) Identification of the channel-forming domain of Clostridium perfringens Epsilon-toxin (ETX). *Biochimica et Biophysica Acta (BBA) - Biomembranes* 1788(12):2584-2593.
52. Chassin C, *et al.* (2007) Pore-forming epsilon toxin causes membrane permeabilization and rapid ATP depletion-mediated cell death in renal collecting duct cells. *American Journal of Physiology - Renal Physiology* 293(3):F927-F937.

53. Miyata S, *et al.* (2002) Clostridium perfringens ε-Toxin Forms a Heptameric Pore within the Detergent-insoluble Microdomains of Madin-Darby Canine Kidney Cells and Rat Synaptosomes. *Journal of Biological Chemistry* 277(42):39463-39468.
54. Shortt SJ, Titball RW, & Lindsay CD (2000) An assessment of the in vitro toxicology of Clostri di urn perfringens type D ε-toxin in human and animal cells. *Human & Experimental Toxicology* 19(2):108-116.
55. Soler-Jover A, *et al.* (2004) Effect of Epsilon Toxin–GFP on MDCK Cells and Renal Tubules In Vivo. *Journal of Histochemistry & Cytochemistry* 52(7):931-942.
56. Peng HL, Novick RP, Kreiswirth B, Kornblum J, & Schlievert P (1988) Cloning, characterization, and sequencing of an accessory gene regulator (agr) in Staphylococcus aureus. *Journal of Bacteriology* 170(9):4365-4372.
57. Novick RP, *et al.* (1993) *Synthesis of staphylococcal virulence factors is controlled by a regulatory RNA molecule* pp 3967-3975.
58. Valeva A, *et al.* (2006) Evidence That Clustered Phosphocholine Head Groups Serve as Sites for Binding and Assembly of an Oligomeric Protein Pore. *Journal of Biological Chemistry* 281(36):26014-26021.
59. Wilke GA & Wardenburg JB (2010) Role of a disintegrin and metalloprotease 10 in Staphylococcus aureus α-hemolysin–mediated cellular injury. *Proceedings of the National Academy of Sciences* 107(30):13473-13478.
60. Song L, *et al.* (1996) Structure of Staphylococcal α-Hemolysin, a Heptameric Transmembrane Pore. *Science* 274(5294):1859-1865.
61. Duesbery NS, *et al.* (1998) Proteolytic Inactivation of MAP-Kinase-Kinase by Anthrax Lethal Factor. *Science* 280(5364):734-737.
62. Vitale G, *et al.* (1998) Anthrax Lethal Factor Cleaves the N-Terminus of MAPKKs and Induces Tyrosine/Threonine Phosphorylation of MAPKs in Cultured Macrophages. *Biochemical and Biophysical Research Communications* 248(3):706-711.
63. Leppla SH (1982) Anthrax toxin edema factor: a bacterial adenylate cyclase that increases cyclic AMP concentrations of eukaryotic cells. *Proceedings of the National Academy of Sciences* 79(10):3162-3166.
64. Klimpel KR, Molloy SS, Thomas G, & Leppla SH (1992) Anthrax toxin protective antigen is activated by a cell surface protease with the sequence specificity and catalytic properties of furin. *Proceedings of the National Academy of Sciences* 89(21):10277-10281.

65. Molloy SS, Bresnahan PA, Leppla SH, Klimpel KR, & Thomas G (1992) Human furin is a calcium-dependent serine endoprotease that recognizes the sequence Arg-X-X-Arg and efficiently cleaves anthrax toxin protective antigen. *Journal of Biological Chemistry* 267(23):16396-16402.
66. Benson EL, Huynh PD, Finkelstein A, & Collier RJ (1998) Identification of Residues Lining the Anthrax Protective Antigen Channel†. *Biochemistry* 37(11):3941-3948.
67. Qa'dan M, Christensen KA, Zhang L, Roberts TM, & Collier RJ (2005) Membrane Insertion by Anthrax Protective Antigen in Cultured Cells. *Molecular and Cellular Biology* 25(13):5492-5498.
68. Lacy DB, Wigelsworth DJ, Melnyk RA, Harrison SC, & Collier RJ (2004) Structure of heptameric protective antigen bound to an anthrax toxin receptor: A role for receptor in pH-dependent pore formation. *Proceedings of the National Academy of Sciences of the United States of America* 101(36):13147-13151.
69. Mogridge J, Mourez M, & Collier RJ (2001) Involvement of Domain 3 in Oligomerization by the Protective Antigen Moiety of Anthrax Toxin. *Journal of Bacteriology* 183(6):2111-2116.
70. Rosovitz MJ, *et al.* (2003) Alanine-scanning Mutations in Domain 4 of Anthrax Toxin Protective Antigen Reveal Residues Important for Binding to the Cellular Receptor and to a Neutralizing Monoclonal Antibody. *Journal of Biological Chemistry* 278(33):30936-30944.
71. Tweten RK (2005) Cholesterol-Dependent Cytolysins, a Family of Versatile Pore-Forming Toxins. *Infection and Immunity* 73(10):6199-6209.
72. Birmingham CL, *et al.* (2008) Listeriolysin O allows Listeria monocytogenes replication in macrophage vacuoles. *Nature* 451(7176):350-354.
73. Martner A, Dahlgren C, Paton JC, & Wold AE (2008) Pneumolysin Released during Streptococcus pneumoniae Autolysis Is a Potent Activator of Intracellular Oxygen Radical Production in Neutrophils. *Infection and Immunity* 76(9):4079-4087.
74. Nagamune H, *et al.* (1996) Intermedilysin, a novel cytotoxin specific for human cells secreted by Streptococcus intermedius UNS46 isolated from a human liver abscess. *Infection and Immunity* 64(8):3093-3100.
75. Schuerch DW, Wilson-Kubalek EM, & Tweten RK (2005) Molecular basis of listeriolysin O pH dependence. *Proceedings of the National Academy of Sciences of the United States of America* 102(35):12537-12542.

76. Dowd KJ & Tweten RK (2012) The Cholesterol-Dependent Cytolysin Signature Motif: A Critical Element in the Allosteric Pathway that Couples Membrane Binding to Pore Assembly. *PLoS Pathog* 8(7):e1002787.
77. Soltani CE, Hotze EM, Johnson AE, & Tweten RK (2007) Structural elements of the cholesterol-dependent cytolysins that are responsible for their cholesterol-sensitive membrane interactions. *Proceedings of the National Academy of Sciences* 104(51):20226-20231.
78. Honda T & Finkelstein RA (1979) Purification and characterization of a hemolysin produced by Vibrio cholerae biotype El Tor: another toxic substance produced by cholera vibrios. *Infection and Immunity* 26(3):1020-1027.
79. De S & Olson R (2011) Crystal structure of the Vibrio cholerae cytolysin heptamer reveals common features among disparate pore-forming toxins. *Proceedings of the National Academy of Sciences* 108(18):7385-7390.
80. Barrett TJ & Blake PA (1981) Epidemiological usefulness of changes in hemolytic activity of Vibrio cholerae biotype El Tor during the seventh pandemic. *Journal of Clinical Microbiology* 13(1):126-129.
81. Kaper JB, Morris JG, & Levine MM (1995) Cholera. *Clinical Microbiology Reviews* 8(1):48-86.
82. De SN (1959) Enterotoxicity of Bacteria-free Culture-filtrate of Vibrio cholerae. *Nature* 183(4674):1533-1534.
83. Finkelstein RA & LoSpalluto JJ (1969) Pathogenesis of experimental cholera: Preparation and Isolation of choleragen and choleragenoid. *The Journal of Experimental Medicine* 130(1):185-202.
84. Dutta NK, Panse MV, & Kulkarni DR (1959) Role of cholera toxin in experimeantal cholera. *Journal of Bacteriology* 78(4):594-595.
85. Di Pierro M, *et al.* (2001) Zonula Occludens Toxin Structure-Function Analysis: Identification of the fragment biologically active on tight junctions and of the zonulin receptor binding domain. *Journal of Biological Chemistry* 276(22):19160-19165.
86. Fasano A, *et al.* (1995) Zonula occludens toxin modulates tight junctions through protein kinase C-dependent actin reorganization, in vitro. *The Journal of Clinical Investigation* 96(2):710-720.
87. Trucksis M, Galen JE, Michalski J, Fasano A, & Kaper JB (1993) Accessory cholera enterotoxin (Ace), the third toxin of a Vibrio cholerae virulence cassette. *Proceedings of the National Academy of Sciences* 90(11):5267-5271.

88. Trucksis M, Conn TL, Fasano A, & Kaper JB (1997) Production of Vibrio cholerae accessory cholera enterotoxin (Ace) in the yeast Pichia pastoris. *Infection and Immunity* 65(12):4984-4988.
89. Acheson DW, *et al.* (1993) Comparison of Shiga-like toxin I B-subunit expression and localization in Escherichia coli and Vibrio cholerae by using trc or iron-regulated promoter systems. *Infection and Immunity* 61(3):1098-1104.
90. Acheson DW, Levine MM, Kaper JB, & Keusch GT (1996) Protective immunity to Shiga-like toxin I following oral immunization with Shiga-like toxin I B-subunit-producing Vibrio cholerae CVD 103-HgR. *Infection and Immunity* 64(1):355-357.
91. Ichinose Y, *et al.* (1987) Enterotoxicity of El Tor-like hemolysin of non-O1 Vibrio cholerae. *Infection and Immunity* 55(5):1090-1093.
92. Zitzer A, Wassenaar TM, Walev I, & Bhakdi S (1997) Potent membrane-permeabilizing and cytocidal action of Vibrio cholerae cytolysin on human intestinal cells. *Infection and Immunity* 65(4):1293-1298.
93. Aim RA, Stroeher UH, & Manning PA (1988) Extracellular proteins of Vibrio cholerae: nucleotide sequence of the structural gene (hlyA) for the haemolysin of the haemolytic El Tor strain 017 and characterization of the hlyA mutation in the non-haemolytic classical strain 569B. *Molecular Microbiology* 2(4):481-488.
94. Yamamoto K, *et al.* (1990) Two-step processing for activation of the cytolysin/hemolysin of Vibrio cholerae O1 biotype El Tor: nucleotide sequence of the structural gene (hlyA) and characterization of the processed products. *Infection and Immunity* 58(12):4106-4116.
95. Nagamune K, *et al.* (1996) In vitro proteolytic processing and activation of the recombinant precursor of El Tor cytolysin/hemolysin (pro-HlyA) of Vibrio cholerae by soluble hemagglutinin/protease of V. cholerae, trypsin, and other proteases. *Infection and Immunity* 64(11):4655-4658.
96. Sathyamoorthy V, S. Huntley J, C. Hall A, & H. Hall R (1997) Biochemical and physiological characteristics of hlya, a pore-forming cytolysin of Vibrio cholerae serogroup O1. *Toxicon* 35(4):515-527.
97. Nagamune K, Yamamoto K, & Honda T (1997) Intramolecular Chaperone Activity of the Pro-region of Vibrio cholerae El Tor Cytolysin. *Journal of Biological Chemistry* 272(2):1338-1343.

98. Yao J, Nellas RB, Glover MM, & Shen T (2011) Stability and Sugar Recognition Ability of Ricin-like Carbohydrate Binding Domains. *Biochemistry* 50(19):4097-4104.

99. Lee X, *et al.* (1998) Structure of the Complex of Maclura pomiferaAgglutinin and the T-antigen Disaccharide, Galβ1,3GalNAc. *Journal of Biological Chemistry* 273(11):6312-6318.

100. Peumans WJ, Hause B, & Van Damme EJM (2000) The galactose-binding and mannose-binding jacalin-related lectins are located in different sub-cellular compartments. *FEBS Letters* 477(3):186-192.

101. Mazumdar B, Ganguly S, Ghosh A, & Banerjee K (2011) The role of C-terminus carbohydrate-binding domain of *Vibrio cholerae* haemolysin/cytolysin in the conversion of the pre-pore b-barrel oligomer to a functional diffusion channel. *The Indian Journal of Medical Research* 133(2):131-137.

102. Zitzer A, Zitzer O, Bhakdi S, & Palmer M (1999) Oligomerization of Vibrio cholerae Cytolysin Yields a Pentameric Pore and Has a Dual Specificity for Cholesterol and Sphingolipids in the Target Membrane. *Journal of Biological Chemistry* 274(3):1375-1380.

103. Dutta S, Mazumdar B, Banerjee KK, & Ghosh AN (2010) Three-Dimensional Structure of Different Functional Forms of the Vibrio cholerae Hemolysin Oligomer: a Cryo-Electron Microscopic Study. *Journal of Bacteriology* 192(1):169-178.

104. Saha N & Banerjee KK (1997) Carbohydrate-mediated Regulation of Interaction of Vibrio cholerae Hemolysin with Erythrocyte and Phospholipid Vesicle. *Journal of Biological Chemistry* 272(1):162-167.

105. Abita JP, Delaage M, Lazdunski M, & Savrda J (1969) The Mechanism of Activation of Trypsinogen. *European Journal of Biochemistry* 8(3):314-324.

106. Dreyer WJ & Neurath H (1955) The activation of chymotrypsinogen: Isolation and identification of a peptide liberated during activation. *Journal of Biological Chemistry* 217(2):527-540.

107. Marciniszyn J, Huang JS, Hartsuck JA, & Tang J (1976) Mechanism of intramolecular activation of pepsinogen. Evidence for an intermediate delta and the involvement of the active site of pepsin in the intramolecular activation of pepsinogen. *Journal of Biological Chemistry* 251(22):7095-7102.

108. Van de Craen M, Declercq W, Van den brande I, Fiers W, & Vandenabeele P (1999) The proteolytic procaspase activation network: an in vitro analysis. (Translated from eng) *Cell Death Differ* 6(11):1117-1124 (in eng).
109. Silen JL & Agard DA (1989) The a-lytic protease pro-region does not require a physical linkage to activate the protease domain in vivo. *Nature* 341(6241):462-464.
110. Zhu X, Ohta Y, Jordan F, & Inouye M (1989) Pro-sequence of subtilisin can guide the refolding of denatured subtilisin in an intermolecular process. *Nature* 339(6224):483-484.
111. Winther JR & Sørensen P (1991) Propeptide of carboxypeptidase Y provides a chaperone-like function as well as inhibition of the enzymatic activity. *Proceedings of the National Academy of Sciences* 88(20):9330-9334.
112. Collaborative (1994) The CCP4 suite: programs for protein crystallography. *Acta Crystallographica Section D* 50(5):760-763.
113. Lee B & Richards FM (1971) The interpretation of protein structures: Estimation of static accessibility. *Journal of Molecular Biology* 55(3):379-IN374.
114. Baker NA, Sept D, Joseph S, Holst MJ, & McCammon JA (2001) Electrostatics of nanosystems: Application to microtubules and the ribosome. *Proceedings of the National Academy of Sciences* 98(18):10037-10041.
115. Schrodinger, LLC (2010) The PyMOL Molecular Graphics System, Version 1.3r1.
116. Chattopadhyay K & Banerjee KK (2003) Unfolding of Vibrio cholerae Hemolysin Induces Oligomerization of the Toxin Monomer. *Journal of Biological Chemistry* 278(40):38470-38475.
117. Iacovache I, van der Goot FG, & Pernot L (2008) Pore formation: An ancient yet complex form of attack. *Biochimica et Biophysica Acta (BBA) - Biomembranes* 1778(7–8):1611-1623.
118. Los FCO, Randis TM, Aroian RV, & Ratner AJ (2013) Role of Pore-Forming Toxins in Bacterial Infectious Diseases. *Microbiology and Molecular Biology Reviews* 77(2):173-207.
119. Löhner S, *et al.* (2009) Pore formation by Vibrio cholerae cytolysin follows the same archetypical mode as β-barrel toxins from gram-positive organisms. *The FASEB Journal* 23(8):2521-2528.
120. Lomize MA, Pogozheva ID, Joo H, Mosberg HI, & Lomize AL (2012) *OPM database and PPM web server: resources for positioning of proteins in membranes* pp D370-376.

121. Berube B & Wardenburg J (2013) Staphylococcus aureus α-Toxin: Nearly a Century of Intrigue. *Toxins* 5(6):1140-1166.
122. Robin Harris J, *et al.* (2002) Interaction of the Vibrio cholerae cytolysin (VCC) with cholesterol, some cholesterol esters, and cholesterol derivatives: a TEM study. *Journal of Structural Biology* 139(2):122-135.
123. Zitzer A, *et al.* (2001) Coupling of Cholesterol and Cone-shaped Lipids in Bilayers Augments Membrane Permeabilization by the Cholesterol-specific Toxins Streptolysin O and Vibrio cholerae Cytolysin. *Journal of Biological Chemistry* 276(18):14628-14633.
124. Zitzer A, Westover EJ, Covey DF, & Palmer M (2003) Differential interaction of the two cholesterol-dependent, membrane-damaging toxins, streptolysin O and Vibrio cholerae cytolysin, with enantiomeric cholesterol. *FEBS Letters* 553(3):229-231.
125. Nelson LD, Johnson AE, & London E (2008) How Interaction of Perfringolysin O with Membranes Is Controlled by Sterol Structure, Lipid Structure, and Physiological Low pH: Insights into the origin of perfringolysin O-lipid raft interaction. *Journal of Biological Chemistry* 283(8):4632-4642.
126. Palmer M, *et al.* (1998) Assembly mechanism of the oligomeric streptolysin O pore: the early membrane lesion is lined by a free edge of the lipid membrane and is extended gradually during oligomerization. *The EMBO Journal* 17(6):1598-1605.
127. Abramoff MD, Magelhaes PJ, & Ram SJ (2004) Image Processing with ImageJ. *Biophotonics International* 11(7):36-42.
128. Arnold K, Bordoli L, Kopp J, & Schwede T (2006) The SWISS-MODEL workspace: a web-based environment for protein structure homology modelling. *Bioinformatics* 22(2):195-201.
129. Kiefer F, Arnold K, Künzli M, Bordoli L, & Schwede T (2009) The SWISS-MODEL Repository and associated resources. *Nucleic Acids Research* 37(suppl 1):D387-D392.
130. Ramachandran S, Kota P, Ding F, & Dokholyan NV (2011) Automated minimization of steric clashes in protein structures. *Proteins: Structure, Function, and Bioinformatics* 79(1):261-270.
131. Zitzer A, Westover EJ, Covey DF, & Palmer M (2003) Differential interaction of the two cholesterol-dependent, membrane-damaging toxins, streptolysin O and Vibrio cholerae cytolysin, with enantiomeric cholesterol. (Translated from eng) *FEBS Lett* 553(3):229-231 (in eng).

132. Farrand AJ, LaChapelle S, Hotze EM, Johnson AE, & Tweten RK (2010) Only two amino acids are essential for cytolytic toxin recognition of cholesterol at the membrane surface. *Proceedings of the National Academy of Sciences*.
133. Trott O & Olson AJ (2010) AutoDock Vina: Improving the speed and accuracy of docking with a new scoring function, efficient optimization, and multithreading. *Journal of Computational Chemistry* 31(2):455-461.
134. Jafurulla M, Tiwari S, & Chattopadhyay A (2011) Identification of cholesterol recognition amino acid consensus (CRAC) motif in G-protein coupled receptors. *Biochemical and Biophysical Research Communications* 404(1):569-573.
135. Zitzer A, *et al.* (2000) Vibrio cholerae cytolysin: assembly and membrane insertion of the oligomeric pore are tightly linked and are not detectably restricted by membrane fluidity. *Biochimica et Biophysica Acta (BBA) - Biomembranes* 1509(1–2):264-274.
136. Finkelstein RA & Hanne LF (1982) Purification and characterization of the soluble hemagglutinin (cholera lectin)(produced by Vibrio cholerae. *Infection and Immunity* 36(3):1199-1208.
137. Krasilnikov OV, *et al.* (2007) Pore formation by Vibrio cholerae cytolysin requires cholesterol in both monolayers of the target membrane. *Biochimie* 89(3):271-277.